THE PLATE PROBLEM FOR
A CANTILEVER SECTOR OF UNIFORM THICKNESS

Thesis by

Max L. Williams, Jr.

In Partial Fulfillment of the Requirements

For the Degree of

Doctor of Philosophy

California Institute of Technology

Pasadena, California

1950

ACKNOWLEDGMENT

The author is pleased to express his appreciation to H. R. Lawrence, Herbert Wagner, and A. T. Zahorski of the Northrop Aircraft Company for suggesting this problem, and for their assistance during its formulation. In addition, he wishes to thank the GALCIT Research staff in general and E. E. Sechler and Y. C. Fung in particular for their helpful comments during the latter stages of the work.

The assistance of G. M. Hrebec in preparing the figures and of Miss Geraldine M. Ellis and Miss Grace Dominic in preparing the manuscript in its final form is also gratefully acknowledged.

SUMMARY

As one approach to the problem of analyzing missile wings of approximately delta configuration for stress and deflection characteristics, a uniformly thin plate of sector planform clamped along one radial edge has been considered.

It is shown that an infinite set of deflection functions, resulting from a product solution to the double Laplacian, may be generated, but practical utility is impeded because the functions are non-orthogonal. It is believed that should the importance of the solution warrant, the deflection of a sector under normal loading may be found by using a combination of the deflection functions, the Trefftz variational method, and high speed computing machinery.

Another section of the report is devoted to a study of the stress along the clamped edge in the vicinity of the corner, and it is shown that the stress varies from zero to a mathematical infinity as the opening angle of the sector increases from zero through ninety degrees with the stress singularity becoming progressively stronger as the opening angle is increased. Experimental data are included that show engineering agreement with the theoretical results, for the case of a delta plate of thirty degree opening angle and varying trailing edge angle.

In conclusion, some remarks are made upon the application of the sector results to swept rectangular plates by means of a hydrodynamic analogy wherein the possibility of obtaining approximate overall stress distributions is indicated.

TABLE OF CONTENTS

I INTRODUCTION

One of the more important problems arising in the field of high speed aeronautics is connected with the structural design of swept wings. Recently a considerable amount of effort has been expended in this direction with the modes of approach being directed along one of the following three lines.

The most practical solution has been to build and test experimentally a scale model of the desired full-scale wing, and, in so far as the particular specimen is concerned, the answers obtained have justified this method. Unfortunately, however, and aside from the great cost of an experimental program, it frequently happens that the structural configuration changes during the manufacture of the aircraft and there is no one frozen design which the structural engineer feels safe in testing. Such a fact leads one to look for some design parameters, in this case associated with the sweep angle, which will permit at least a qualitative answer to such questions as the variation of the root stress with sweep angle. With such information at his disposal, the designer feels a bit more secure in extrapolating experimental results in case the design is changed slightly from the initial configuration.

For the particular problem of the swept wing, some solutions have already been presented in the form of beam equations, which have proved satisfactory for the zero sweep case, with a more or less empirical correction factor dependent upon sweep. Such solutions, which are certainly desirable from an engineer's point of view, are

usually restricted to the range for which the results have been substantiated experimentally. It would therefore be very useful to have an exact solution against which empirical formulas would be compared. The deviation between the exact solution and the actual behavior of the specimen would thus be reduced to a question of the validity of the assumptions used in arriving at the solution.

As a first step, an investigation has been made to determine what simplifying, though rational, assumptions can be applied to a complex wing structure of an aircraft or missile which would permit an idealization of the structure amenable to precise mathematical treatment, without destroying or arbitrarily eliminating effects which are important to the problem. As the present interest is confined to wings of high solidity and low thickness ratio, it would seem reasonable to consider a solid or homogeneous wing such as the type with a double wedge cross section. Such an analysis leads directly to simulating the actual wing by a cantilever plate of variable thickness and taper. As is well known, the solution of this problem involves at least a fourth order partial differential equation with boundary conditions for which solutions are known only in isolated cases. It further appears that as yet there exist no solutions which take account of variable thickness, and hence the idealization which still retains some semblance of the actual structure and yet promises some hope of solution is a cantilever plate of constant thickness.

Having an idealized structure, one must next examine the boundary conditions. Here again it is found that a rigorous solution

for the actual boundary conditions at the supported edge is too difficult for the present. Actual wing-fuselage joints vary widely in form, and while it is theoretically possible to simulate the boundary conditions by an elastic support, only the simpler case of a fixed edge will be treated here. The philosophy is to find one solution first, if possible, and then to introduce the additional complications. The idealized boundary conditions are thus zero deflection and slope along the support, and unloaded boundaries elsewhere.

With the problem formulated in this way, one planform has already been treated. The deflection of a rectangular plate of constant chord for arbitrary sweep angle is given in References 1 and 2. This solution is most useful for aircraft wings, as distinguished from missile wings. In order to examine the latter type of planform in which there is also some interest, it is proposed to investigate a constant thickness plate of sector planform supported along one of its radial edges. It will be shown that while the deflection may in principle be represented satisfactorily by a series of eigen functions which seems to converge satisfactorily, the non-orthogonal character of the functions requires lengthly, though simple, computations which impede their utility. On the other hand, these same functions permit the character of a stress singularity in the angle between a free and fixed edge to be determined very quickly. This latter phenomenon is of course related to the build-up of stress along the rear spar of a swept back wing.

Finally, a solution using three eigen functions for a sector

under uniform load is included to indicate the method and probable convergence, and the paper is concluded by some remarks on other approximations, and by posing a mathematical problem upon the completeness of the eigen functions.

II THE EIGEN VALUE PROBLEM

According to the classical theory for the bending of thin plates[3], the governing partial-differential equation in polar coordinates for the deflection $w(r,\theta)$ of a plate in a planform region R subject to a loading $q(r,\theta)$ normal to its surface is

$$\Delta\Delta\, w(r,\theta) \equiv \left[\frac{\partial^2}{\partial r^2} + \frac{1}{r}\frac{\partial}{\partial r} + \frac{1}{r^2}\frac{\partial^2}{\partial\theta^2}\right]^2 w(r,\theta) = \frac{1}{D}\, q(r,\theta)$$

where $D = \dfrac{E\,t^3}{12(1-\nu^2)}$ is the flexural rigidity.

In order to apply the solution of this equation to a particular problem, two conditions must be prescribed along the boundary C of the region. (Figure 1)

Because of the linear nature of the thin plate theory it is permissible within certain limits to superimpose the effects of various simpler loadings and boundary conditions to attain the desired result. The deflection function may therefore be separated into two parts; one the complementary solution to the homogeneous problem, and the other the particular solution for the given loading. As the latter solution presents no particular difficulty, only the homogeneous or complementary loading (i.e., $q(r,\theta) = 0$) will be considered. This, of course, implies that the boundary conditions over C are not homogeneous also, or else only the trivial solution of zero deflection under zero load would result.

As the first step toward finding a solution for the problem of a general cantilever plate of arbitrary planform R, it is proposed to consider here the case of a uniformly thin plate whose planform is the

sector of a unit circle. This type of normalization is arbitrary and is introduced merely for convenience. Furthermore, it is assumed that (Figure 1) the radial edges OA and OB are clamped and free respectively, and some arbitrary shear and moment loading are applied along the circumferential edge AB. Note also that AB may be any continuous boundary, not necessarily restricted to part of an arc as it is in the following development.

Stating the problem in mathematical terms using the notation of Timoshenko[3], it is required to solve

$$\Delta\Delta w(r,\theta) = 0 \qquad \text{in R} \tag{1}$$

subject to the following boundary conditions along C.

Along OA, deflection and slope zero,

$$w(r,0) = 0 \tag{2}$$

$$\frac{\partial w(r,0)}{\partial \theta} = 0 \tag{3}$$

Along OB, moment and shear zero,

$$\Delta w(r,\alpha) - (1-\nu)\frac{\partial^2 w(r,\alpha)}{\partial r^2} = 0 \tag{4}$$

$$\frac{\partial \Delta w(r,\alpha)}{r\partial\theta} + (1-\nu)\frac{\partial}{\partial r}\left[\frac{1}{r}\frac{\partial^2 w(r,\alpha)}{\partial r\,\partial\theta} - \frac{1}{r^2}\frac{\partial w(r,\alpha)}{\partial\theta}\right] = 0 \tag{5}$$

Along AB, given moment and shear,

$$M_r(1,\theta) = -D\left[(1-\nu)\frac{\partial^2}{\partial r^2} + \nu\Delta\right] w(1,\theta) = m_0(\theta) \tag{6}$$

$$V_r(1,\theta) = -D\left\{\frac{\partial\Delta}{\partial r} + (1-\nu)\frac{1}{r}\frac{\partial}{\partial\theta}\left[\frac{1}{r}\frac{\partial}{\partial\theta}\left(\frac{\partial}{\partial r} - \frac{1}{r}\right)\right]\right\} w(1,\theta) = V_0(\theta) \tag{7}$$

In addition, the deflection and slope are to be finite at the origin.

As a first step in the solution, a product type solution is assumed for the deflection function(4). Later on, some additional remarks upon the uniqueness and completeness will be inserted, but for the ensuing development, let it suffice to try as a possibility

$$w_n(r,\theta;\lambda_n) = r^{\lambda_n+1} F_n(\theta) \tag{8}$$

where λ_n is some constant independent of the point coordinates. When this function is substituted into (1), it is found that a fourth order total differential equation in $F_n(\theta)$ results, namely

$$F_n^{IV}(\theta) + [(\lambda_n+1)^2 + (\lambda_n-1)^2] F''(\theta) + (\lambda_n+1)^2(\lambda_n-1)^2 F(\theta) = 0 \tag{9}$$

whose solution is

$$F_n(\theta) = b_1 \sin(\lambda_n+1)\theta + b_2 \cos(\lambda_n+1)\theta + b_3 \sin(\lambda_n-1)\theta + b_4 \cos(\lambda_n-1)\theta \tag{10}$$

As boundary conditions (2) and (3) imply that $F_n(0;\lambda_n) = F_n'(0;\lambda_n) = 0$; and that finite deflection and slope at r = 0 require $\lambda \geq 0$, it is easily found that

$$b_2 = -b_4 \equiv A_n \; ; \quad \frac{b_1}{\lambda_n - 1} = -\frac{b_3}{\lambda_n + 1} \equiv B_n \; ; \quad \lambda_n \neq \pm 1$$

so that the deflection function now becomes

$$w_n(r,\theta;\lambda_n) = r^{\lambda_n+1}\{A_n[\cos(\lambda_n+1)\theta - \cos(\lambda_n-1)\theta] + B_n[(\lambda_n-1)\sin(\lambda_n+1)\theta - (\lambda_n+1)\sin(\lambda_n-1)\theta]\} \tag{11}$$

Turning next to the boundary conditions along the free radial edge where $\theta = \alpha$, the boundary conditions (4) and (5) using (8) are equivalent to

$$r^{\lambda_n - 1}\left[(\lambda_n+1)(1+\nu\lambda_n)F(\alpha) + F''(\alpha)\right] = 0 \tag{12}$$

and

$$r^{\lambda_n - 2}\left\{\left[(\lambda_n+1)^2 + (1-\nu)\lambda_n(\lambda_n-1)\right]F'(\alpha) + F'''(\alpha)\right\} = 0 \tag{13}$$

where the primes again signify differentiation with respect to θ.

Next substituting the expression for $F_n(\theta;\lambda)$, equation (10), into these boundary conditions (12) and (13), there result two equations in A_n and B_n which must hold for all values of r, except possibly the origin

$$r^{\lambda_n - 1}\left[\left\{\left[\lambda_n+1\right]\cos(\lambda_n+1)\alpha - \left[\lambda_n - \frac{3+\nu}{1-\nu}\right]\cos(\lambda_n-1)\alpha\right\}A_n \right. \tag{14}$$
$$\left. + \left\{(\lambda_n+1)(\lambda_n-1)\sin(\lambda_n+1)\alpha - (\lambda_n+1)\left(\lambda_n - \frac{3+\nu}{1-\nu}\right)\sin(\lambda_n-1)\alpha\right\}B_n\right] = 0$$

$$r^{\lambda_n - 2}\left[\left\{(\lambda_n+1)\sin(\lambda_n+1)\alpha - \left[\lambda_n + \frac{3+\nu}{1-\nu}\right]\sin(\lambda_n-1)\alpha\right\}A_n \right. \tag{15}$$
$$\left. - \left\{(\lambda_n+1)(\lambda_n-1)\cos(\lambda_n+1)\alpha - (\lambda_n+1)\left(\lambda_n + \frac{3+\nu}{1-\nu}\right)\cos(\lambda_n-1)\alpha\right\}B_n\right] = 0$$

For there to be other than the trivial solution, the determinant of these latter two equations must be set equal to zero which leads to the characteristic equation of the plate

$$1 + \frac{4(1+\nu)}{(1-\nu)^2} + \frac{3+\nu}{1-\nu}\cos 2\lambda_n\alpha - (1-\cos 2\alpha)\lambda_n^2 = 0 \tag{16}$$

The solution of equation (16) then will determine a value or values of the parameter λ_n, and consequently fix the ratio of A_n to

B_n, but not their absolute values as equations (14) and (15) are homogeneous. With the exception of an arbitrary multiplicative normalizing factor then, all the constants in (11) have been evaluated.

The significance of the subscript n now becomes evident. If there are N values of λ_n which satisfy (16), one may then form a linear combination of the functions (11), and choose the constants so as to satisfy, either exactly or in the mean, the boundary conditions (6) and (7) along the arc. Before turning to this point, which involves questions of the completeness of the set of functions, the number of possible solutions to the characteristic equation will be investigated.

III THE EIGEN VALUES

Two items should be noted in equation (16). First, $f(\lambda_n) = f(-\lambda_n)$; and second, there are only a finite number of real values of the eigen parameter λ_n. (To avoid possible confusion, it might be remarked that the word <u>eigen</u> is used in its broader sense of <u>characteristic</u>, as differentiated slightly from its more frequent and familiar usage in connection with Sturm-Liouville theory.) Now in order to obtain an infinite set of eigen values, which is certainly a necessary condition for a complete set of functions, the eigen values must be considered as complex. This of course does not destroy the even property of the eigen equation but merely means that if $\lambda_n \equiv a_n + ib_n$ is a solution, $\lambda_n = -a_n \pm ib_n$ and $\lambda_n = a_n - ib_n$ are also solutions.

As a trivial illustration of the computation of the eigen values, it is instructive to digress momentarily and consider the case of $\alpha = \pi$, for which the eigen equation takes a particularly simple form, namely,

$$\cos(2\pi\lambda_n) = -2,462 \qquad (\nu = 0.3)$$

In this case there are obviously no real roots, but assuming λ_n complex, say $a_n + ib_n$, there are two simultaneous equations;

$$\cos(2\pi a_n)\cosh(2\pi b_n) = -2.462$$

$$\sin(2\pi a_n)\sinh(2\pi b_n) = 0$$

so if

$$\sin(2\pi a_n) = \sin(n\pi) = 0 \; ; \; \pm n = 0,1,2,3,\ldots$$

then

$$\cos(2\pi a_n) = \cos(n\pi) = (-1)^n$$

but as $\cosh(2\pi b_n) \gg 1$ this requires $\pm n = 1, 3, 5, \ldots$ and thus

$$\cosh(2\pi b_n) = 2.462$$

Hence

$$a_n = \frac{n}{2} \quad ; \quad b_n = \frac{1}{2\pi} \cosh^{-1}(2.462) = 0.2467$$

and therefore

$$\lambda_n = \frac{n}{2} \pm 0.2467i \quad ; \quad \pm n = 1, 3, 5, \ldots$$

or in notation consistent with later development

$$\lambda_n = \frac{n-1}{2} \pm 0.2467i \quad ; \quad n = 2, 4, 6, \ldots$$

For the special case of $\alpha = \pi$, $\nu = 0.3$, the eigen constants are easily found to be

$$\text{Re } A_n = 2.4464\,(n+1)(-1)^{\frac{n}{2}}$$

$$\text{Im } A_n = 6.4389\,(-1)^{\frac{n}{2}}$$

$$\text{Re } B_n = 0$$

$$\text{Im } B_n = 4.8857\,(-1)^{\frac{n}{2}} \qquad n = 2, 4, 6, \ldots$$

Returning now to the more general problem of solving (16), write

$$2\lambda_n \alpha = (\mu_n + n\pi) + i\omega_n \quad ; \quad \pm n = 0, 2, 4, 6, \ldots$$

Then setting the real and imaginary parts of (16) separately equal to zero, there result two simultaneous transcendental equations which are most conveniently solved by an iterative process making use of the

asymptotic values at large n for the initial trial values. The detailed method of calculation is given in Appendix I and the results are summarized in Table I.

Thus having illustrated a procedure by which an infinite set of discrete λ_n values having their limit point at infinity may be obtained, the eigen values are ordered according to their absolute values, including the real roots of (16) in their proper places.

Knowing the eigen values, the next step is to evaluate the constants A_n and B_n specifically. Inasmuch as the problem is homogeneous, only the ratio of A_n to B_n is independent which is immediately apparent from (14) and (15). It develops then that a simple choice of constants using (14) is

$$A_n(\lambda) = (\lambda^2-1)\sin(\lambda+1)\alpha + \left(\frac{3+\nu}{1-\nu} - \lambda\right)(\lambda+1)\sin(\lambda-1)\alpha \tag{17}$$

$$B_n(\lambda) = -(\lambda+1)\cos(\lambda+1)\alpha - \left(\frac{3+\nu}{1-\nu} - \lambda\right)\cos(\lambda-1)\alpha \tag{18}$$

where to simplify the notation, $\lambda = a + ib$ is understood to mean $\lambda_n = a_n + ib_n$.

Separating into real and imaginary parts, the constants become

$$\begin{aligned} Re\,A_n = {} & [a^2-b^2-1][\sin(a+1)\alpha\cosh b\alpha] - 2ab[\cos(a+1)\alpha\sinh b\alpha] \\ & + \left[\left(\frac{3+\nu}{1-\nu} - a\right)(a+1) + b^2\right][\sin(a-1)\alpha\cosh b\alpha] \\ & - \left[b\left(\frac{3+\nu}{1-\nu} - 2a - 1\right)\right][\cos(a-1)\alpha\sinh b\alpha] \end{aligned} \tag{19}$$

$$\begin{aligned} Im\,A_n = {} & 2ab\sin(a+1)\alpha\cosh b\alpha + (a^2-b^2-1)\cos(a+1)\alpha\sinh b\alpha \\ & + \left[\left(\frac{3+\nu}{1-\nu} - a\right)(a+1) + b^2\right][\cos(a-1)\alpha\sinh b\alpha] \\ & + \left[b\left(\frac{3+\nu}{1-\nu} - 2a - 1\right)\right][\sin(a-1)\alpha\cosh b\alpha] \end{aligned} \tag{20}$$

$$\mathrm{Re}\,B_n = -(a+1)\cos(a+1)\alpha\cosh b\alpha - b\sin(a+1)\alpha\sinh b\alpha$$
$$+ b\sin(a-1)\alpha\sinh b\alpha - \left(\frac{3+\nu}{1-\nu} - a\right)\cos(a-1)\alpha\cosh b\alpha \qquad (21)$$

$$\mathrm{Im}\,B_n = -b\cos(a+1)\alpha\cosh b\alpha + (a+1)\sin(a+1)\alpha\sinh b\alpha$$
$$+ b\cos(a-1)\alpha\cosh b\alpha + \left(\frac{3+\nu}{1-\nu} - a\right)\sin(a-1)\alpha\sinh b\alpha \qquad (22)$$

IV THE EIGEN FUNCTIONS

It remains to examine the effect of the complex eigen values upon the representation of the deflection function. The λ_n values obtained apply specifically to a particular $w_n(r,\theta;\lambda_n)$ or eigen function which, as a consequence of the complex eigen value, has itself become complex. Here, however, it must be remembered that only the ratio of A_n to B_n is independent and the function is still subject to multiplication by an arbitrary (complex) constant, say $k_n \equiv \delta_n^{(1)} - i\,\delta_n^{(2)}$.

In the first place,

$$w_n(r,\theta;\lambda_n) = r^{a_n+1+ib_n}\left[Re F_n(\theta;\lambda_n) + i\,Im F_n(\theta;\lambda_n)\right]$$

$$= r^{a_n+1}\left\{Re F_n \cos(b_n \log r) - Im F_n \sin(b_n \log r)\right\}$$

$$+ i\, r^{a_n+1}\left\{Im F_n \cos(b_n \log r) + Re F_n \sin(b_n \log r)\right\}$$

$$= w_n^{(1)}(r,\theta;\lambda_n) + i\, w_n^{(2)}(r,\theta;\lambda_n) \qquad (23)$$

where there exists the obvious relationship

$$w_n^{(1)}(r,\theta;\lambda_n) = r^{a_n+1}\left\{Re F_n \cos(b_n \log r) - Im F_n \sin(b_n \log r)\right\} \qquad (24)$$

$$w_n^{(2)}(r,\theta;\lambda_n) = r^{a_n+1}\left\{Im F_n \cos(b_n \log r) + Re F_n \sin(b_n \log r)\right\} \qquad (25)$$

It may be noted incidentally that if the conjugate values, $\bar{\lambda}_n = a_n - ib_n$, are used one can easily show

$$w_n^{(1)}(r,\theta;\bar{\lambda}_n) = w_n^{(1)}(r,\theta;\lambda_n) \text{ ; i.e., an even function in } b_n \quad (26)$$

$$w_n^{(2)}(r,\theta;\bar{\lambda}_n) = -w_n^{(2)}(r,\theta;\lambda_n) \text{ ; i.e., an odd function in } b_n \quad (27)$$

It is then easily seen that

$$\begin{aligned} k_n w_n(r,\theta;\lambda_n) &= \left[\delta_n^{(1)} - i\delta_n^{(2)}\right]\left[w_n^{(1)} + i w_n^{(2)}\right] \\ &= \left[\delta_n^{(1)} w_n^{(1)} + \delta_n^{(2)} w_n^{(2)}\right] - i\left[\delta_n^{(1)} w_n^{(2)} - \delta_n^{(2)} w_n^{(1)}\right] \end{aligned} \quad (28)$$

and then as the deflection function is real, the corresponding real part is taken, although the imaginary part also satisfies the field equation and boundary conditions. Forming a linear combination over the infinite number of eigen functions then gives the most general solution obtainable under the assumptions.

$$w(r,\theta) = \sum_{n=2,4,6,\ldots}^{\infty} \left\{\delta_n^{(1)} w_n^{(1)}(r,\theta;\lambda_n) + \delta_n^{(2)} w_n^{(2)}(r,\theta;\lambda_n)\right\} \quad (29)$$

Two boundary conditions have yet to be satisfied along the circumferential length AB, but before proceeding to the evaluation of $\delta_n^{(1)}$ and $\delta_n^{(2)}$ in terms of the moment and shear, further remarks as to the form of $\mathrm{Re}F_n(r,\theta;\lambda_n)$ and $\mathrm{Im}F_n(r,\theta;\lambda_n)$, and incidentally their derivatives, are in order. Specifically then, the real and imaginary angular parts of the deflection function, $F_n(\theta)$, and their derivatives, may be summarized in Table II. For each quantity there are in general the eight terms of the first column multiplied by the coefficients in the second, third, etc. columns for F, F', etc., respectively. The table is constructed for the real parts only but the coefficients for the imaginary expressions may be easily obtained by a simple interchange

of the constants as noted.

By use of equations (24) and (25) and Table II, sufficient information has been developed to evaluate the eigen functions.

Completeness

The next problem is to evaluate the constants $\delta_m^{(1)}$ and $\delta_m^{(2)}$ in terms of the arbitrary loadings along the circumferential edge. It is precisely this point which provides the greatest difficulty as for an exact solution the determination of the constants requires a completeness proof for the eigen functions. Such a proof is handicapped because so much of the work in the mathematical literature has been carried out on the basis of Sturm-Liouville equations and real eigen values. It would be presumptive to state that the set is complete even though it possesses certain properties, to be discussed presently, that make it seem intuitively so. On the other hand, the author has been unable to establish the incompleteness of the set. Between these two limits, the most that can be justified is that, using the functions generated in the foregoing analysis, linear combinations using, for example, the method of least squares, can be set down which approximate the desired expansion with the smallest error possible with the given functions.

One such convenient method is due to Hildebrand[5], although it is more complicated for this case than satisfying the moment and shear at arbitrary points and solving a set of simultaneous linear equations. His procedure is somewhat of a variational method coupled with numerical integrations permitting a weighting at important points in the expansion.

No further description is necessary as the reference paper is readily available. It may be noted incidentally that if the functions are complete, this approximation would be better than any other good approximation based on functions which were not part of a complete set.

In lieu of a formal analysis, some points which lead to an intuitive feeling of completeness will be enumerated. First, the eigen values are infinite in number, discrete, and have their limit point at infinity. Secondly, the complex eigen value is asymptotic to a complex number having for its real part an integer and for its imaginary part a value which becomes vanishingly small compared to the real part. If the value at infinity in some sense then approaches a real integer, the eigen functions themselves would approach trigonometric functions which are, of course, known to form a complete set. And finally, the functions when plotted appear to have interlacing zeros. Such considerations at infinity in no way prove the desired result but intuitively might mean that if the behavior is regulated at infinity where, speaking loosely, one essentially loses track of the individual functions, the behavior in the large might be adequate to insure completeness.

From a rigorous mathematical standpoint, there are at least two formal approaches one may make to establish the completeness of a set of functions. One method is to consider the eigen functions themselves, formally orthonormalize them if practicable, and show that the set has the necessary closure and completeness properties. Practically speaking, the calculations are too lengthly and cumbersome to apply in the present case. Another intuitive argument may be presented, however,

by considering the case of $\alpha = \pi$. Here the eigen values have been shown to be $\lambda_n = \frac{n-1}{2} + ib_0$ (n = 2, 4, 6, ...). The eigen functions in θ are then made up of terms containing

$$e^{i\lambda_n\theta} \sim e^{-b_0\theta - i\frac{\theta}{2}} e^{i\frac{n}{2}\theta} \sim e^{im\theta} \qquad (m = 1, 2, 3, \ldots)$$

which ranging over m form a trigonometric (complete) series. However, no rigorous justification is implied.

The other alternative to proving completeness would be to argue directly from the solution to the partial differential equation. It has been proved[6] that the general solution to the double Laplacian (1) for a convex simply connected region R may be written as

$$w(r,\theta) = f_1(r,\theta) + r^2 f_2(r,\theta) \tag{30}$$

where $f_1(r,\theta)$ and $f_2(r,\theta)$ are functions harmonic in R; that is they each satisfy Laplace's equation.

The problem then is to find the two harmonic functions which are analytic in the sector R. Suppose for the moment that each one could be represented by its (complex) power series

$$f_1(r,\theta) = f_1(z) = \sum_n c_n z^n \tag{31}$$

$$f_2(r,\theta) = f_2(z) = \sum_m d_m z^m \tag{32}$$

then the complex deflection would be represented by

$$w(r,\theta) = \sum_{n,m} c_n r^n [\cos n\theta + i \sin n\theta] + d_m r^{m+2} [\cos m\theta + i \sin m\theta]$$

Taking the real part of the deflection function, there remains, upon renaming the constants

$$w(r,\theta) = \sum_{n,m}^{\infty} \{r^n (a_n^{(1)} \cos n\theta + a_n^{(2)} \sin n\theta) + r^{m+2} (a_m^{(3)} \cos m\theta + a_m^{(4)} \sin m\theta)\} \qquad (33)$$

and now for the infinite summation, it appears that there are two ways of grouping the terms, namely by letting n = m or n = m + 2.

$$w(r,\theta) = \sum_{n}^{\infty} \{[a_n^{(1)} r^n + a_n^{(3)} r^{n+2}] \cos n\theta + [a_n^{(2)} r^n + a_n^{(4)} r^{n+2}] \sin n\theta\} \qquad (34)$$

or

$$w(r,\theta) = \sum_{n}^{\infty} r^n [a_n^{(1)} \cos n\theta + a_{n-2}^{(3)} \cos(n-2)\theta + a_n^{(2)} \sin n\theta + a_{n-2}^{(4)} \sin(n-2)\theta] \qquad (35)$$

It is easily seen that the representation is the same in either case, the choice depending primarily upon the ease of application to the given boundary conditions. The first is essentially that given by Prescott[7], while the latter form under the transformation $n = \lambda_n + 1$ is similar to (8). The difference of course lies in the fact that n has been taken to run to infinity through integer values, while it has been found that the λ_n values are non-integers.

The completeness property of the eigen functions would automatically follow then if it could be proved that the harmonic functions in the sector can be represented by the complex power series where the powers do not necessarily run through integers. One method might be to consider the complex power series analytic in the unit circle and

then by conformal mapping to the sector, show that the exponents of the power series become non-integers under the transformation.

There may also be other methods unknown to the author for dealing with the problem, but so far it has proved impossible to insure the completeness of the set with the necessary mathematical rigor. Temporarily, at least, approximate methods of applying these functions to the practical problem will have to suffice.

Inasmuch as each value of λ_n corresponds to a particular or characteristic loading along the arc, which except in fortuitious cases will not be the prescribed $m_o(\theta)$ or $v_o(\theta)$ of (6) and (7) (in which case of course an exact solution will have been obtained), it will be of interest to calculate some of these loadings for particular angles in order to get a feeling for the types of functions and loadings which are under consideration. The combination of two or more eigen functions to obtain approximations to an arbitrary loading will be taken up in a later section.

The Characteristic Loads

By using known relations, the stress conditions can be calculated at any point in the plate from the deflection function. In particular, the radial moment and shear are obtained from

$$M_r(r,\theta) = -D\left[(1-\nu)\frac{\partial^2}{\partial r^2} + \nu\Delta\right]W(r,\theta) \qquad (36)$$

$$V_r(r,\theta) = Q_r - \frac{1}{r}\frac{\partial M_{r\theta}}{\partial \theta}$$

$$= -D\left\{\frac{\partial \Delta}{\partial r} + (1-\nu)\frac{1}{r}\frac{\partial}{\partial \theta}\left[\frac{1}{r}\frac{1}{\partial \theta}\left(\frac{\partial}{\partial r} - \frac{1}{r}\right)\right]\right\} w(r,\theta) \tag{37}$$

Substituting (11)* and writing for the n^{th} term,

$$V_{r_n}(r,\theta;\lambda_n) = \lambda(1-\nu)r^{\lambda-2}\left[(\lambda+1)^2 A\cos(\lambda+1)\theta - (\lambda-1)(\lambda-\frac{5-\nu}{1-\nu})A\cos(\lambda-1)\theta\right.$$

$$+(\lambda+1)^2(\lambda-1)B\sin(\lambda+1)\theta$$

$$\left.-(\lambda^2-1)(\lambda-\frac{5-\nu}{1-\nu})B\sin(\lambda-1)\theta\right] \tag{38}$$

$$M_{r_n}(r,\theta;\lambda_n) = -\lambda(1-\nu)r^{\lambda-1}\left[(\lambda+1)A\cos(\lambda+1)\theta - (\lambda+\frac{1+3\nu}{1-\nu})A\cos(\lambda-1)\theta\right.$$

$$+(\lambda^2-1)B\sin(\lambda+1)\theta$$

$$\left.-(\lambda+1)(\lambda+\frac{1+3\nu}{1-\nu})B\sin(\lambda-1)\theta\right] \tag{39}$$

These latter two equations may then be written in terms of their real and imaginary parts corresponding to the deflections of (24) and (25), respectively.

$$V_{r_n}^{(1)} = Dr^{a-2}\left[\{k_1 ImF + [a(2-\nu)-1]ImF'' + k_2 ReF\right.$$

$$\left.+b(2-\nu)ReF''\}\sin(b\log r)\right. \tag{40}$$

$$\left.+\{k_2 ImF + b(2-\nu)ImF'' - k_1 ReF\right.$$

$$\left.-[a(2-\nu)-1]ReF''\}\cos(b\log r)\right]$$

---

* In this and following sections, the subscript n will frequently be omitted for convenience where no confusion will result.

$$M_{r(m)}^{(1)} = D r^{a-1}\{(K_3 \mathrm{Im}F + K_4 \mathrm{Re}F + \nu \mathrm{Im}F'')\sin(b\log r) - (K_3 \mathrm{Re}F - K_4 \mathrm{Im}F + \nu \mathrm{Re}F'')\cos(b\log r)\} \tag{41}$$

where

$$K_1 = (a-1)[(a+1)^2 - b^2] - 2(a+1)b^2$$

$$K_2 = b[2(a^2-1) + (a+1)^2 - b^2]$$

$$K_3 = (a+\nu)(a+1) - b^2$$

$$K_4 = (2a+1+\nu)b$$

$\mathrm{Re}F_n$, $\mathrm{Im}F_n$, $\mathrm{Re}F_n''$, $\mathrm{Im}F_n''$ are found from Table II. $V_{r_n}^{(2)}$ and $M_{r_n}^{(2)}$ are obtained by replacing $\mathrm{Re}F_n$ by $\mathrm{Im}F_n$ and $\mathrm{Im}F_n$ by $-\mathrm{Re}F_n$ in (40) and (41), respectively. The derivatives are interchanged by the same rule.

As in equations (24) and (25), the superscript (1) stands for the shear and moment obtained from $w_n^{(1)}$ and the superscript (2) for the corresponding quantities obtained from $w_n^{(2)}$. At the circumferential edge, r = 1, the equations take the simple form

$$\frac{1}{D} V_{r_n}^{(1)}(1,\theta) = K_2 \mathrm{Im}F(\theta) + (2-\nu)b\,\mathrm{Im}F''(\theta) - K_1 \mathrm{Re}F(\theta) - [(2-\nu)a - 1]\mathrm{Re}F''(\theta) \tag{42}$$

$$\frac{1}{D} M_{r_n}^{(1)}(1,\theta) = -K_3 \mathrm{Re}F(\theta) + K_4 \mathrm{Im}F(\theta) - \nu \mathrm{Re}F''(\theta) \tag{43}$$

$$\frac{1}{D} V_{r_n}^{(2)}(1,\theta) = -K_2 \operatorname{Re} F(\theta) - (2-\nu)\, b \operatorname{Re} F''(\theta) \qquad (42a)$$
$$-K_1 \operatorname{Im} F(\theta) - [a(2-\nu) - 1] \operatorname{Im} F''(\theta)$$

$$\frac{1}{D} M_{r_n}^{(2)}(1,\theta) = -K_3 \operatorname{Im} F(\theta) - K_4 \operatorname{Re} F(\theta) - \nu \operatorname{Im} F''(\theta) \qquad (43a)$$

Concentrated Load

In addition to the distributed loading previously described, there is in general a concentrated load at B(1,α) given by

$$2M_{r\theta_n}(r,\theta) = 2(1-\nu)D\left[\frac{1}{r}\frac{\partial}{\partial\theta}\left(\frac{\partial}{\partial r} - \frac{1}{r}\right)\right] W_n(r,\theta) \qquad (44)$$

or in complex form

$$2M_{r\theta_n}(r,\theta) = -2(1-\nu)\lambda r^{\lambda-1}\left\{A_n[(\lambda+1)\sin(\lambda+1)\theta - (\lambda-1)\sin(\lambda-1)\theta]\right. \qquad (45)$$
$$\left. -(\lambda^2-1)B_n[\cos(\lambda+1)\theta - \cos(\lambda-1)\theta]\right\} D$$

when written in terms of real and imaginary parts,

$$2M_{r\theta_n}^{(1)}(r,\theta) = -2(1-\nu)D r^{a-1}\left\{[b \operatorname{Re} F'(\theta) + a \operatorname{Im} F'(\theta)]\sin(b \log r)\right. \qquad (46)$$
$$\left. -[a \operatorname{Re} F'(\theta) - b \operatorname{Im} F'(\theta)]\cos(b \log r)\right\}$$

$$2M_{r\theta_n}^{(2)}(r,\theta) = -2(1-\nu)D r^{a-1}\left\{[b \operatorname{Im} F'(\theta) - a \operatorname{Re} F'(\theta)]\sin(b \log r)\right.$$
$$\left. -[a \operatorname{Im} F'(\theta) + b \operatorname{Re} F'(\theta)]\cos(b \log r)\right\} \qquad (46a)$$

The above equations are easily specialized to the point B(1,α).

$$2M^{(1)}_{r\theta_n}(1,\alpha) = 2(1-\nu)D\left[a\,\mathrm{Re}F_n'(\alpha) - b\,\mathrm{Im}F_n'(\alpha)\right]$$

$$2M^{(2)}_{r\theta_n}(1,\alpha) = 2(1-\nu)D\left[a\,\mathrm{Im}F_n'(\alpha) + b\,\mathrm{Re}F_n'(\alpha)\right]$$

Support Loads

From an aeronautical point of view, one of the most interesting quantities to investigate is the reaction at the support or in the case of a wing, the root reaction. The two quantities of interest, namely, the shear V_θ and the moment M_θ, are easily obtained from

$$\begin{aligned} V_\theta(r,\theta) &= Q_\theta - \frac{\partial M_{r\theta}}{\partial r} \\ &= -D\left[\frac{1}{r}\frac{\partial \Delta}{\partial \theta} + (1-\nu)\frac{\partial}{\partial r}\left(\frac{1}{r}\frac{\partial^2}{\partial r \partial \theta} - \frac{1}{r^2}\frac{\partial}{\partial \theta}\right)\right] w(r,\theta) \end{aligned} \tag{47}$$

$$M_\theta(r,\theta) = -D\left[\Delta - (1-\nu)\frac{\partial^2}{\partial r^2}\right] w(r,\theta) \tag{48}$$

With the usual substitution, the complex forms become

$$\begin{aligned} \frac{1}{D}V_\theta(r,\theta) = \lambda(1-\nu)(\lambda-1)r^{\lambda-2}\Big\{&\left[(\lambda+1)\sin(\lambda+1)\theta - \left(\lambda + \frac{3+\nu}{1-\nu}\right)\sin(\lambda-1)\theta\right]A \\ &-\left[(\lambda^2-1)\cos(\lambda+1)\theta \right. \\ &\left. -(\lambda+1)\left(\lambda+\frac{3+\nu}{1-\nu}\right)\cos(\lambda-1)\theta\right]B\Big\} \end{aligned} \tag{49}$$

$$\frac{1}{D} M_\theta(r,\theta) = -(1-\nu)\lambda r^{\lambda-1}\Big\{\Big[(\lambda+1)\cos(\lambda+1)\theta - (\lambda - \tfrac{3+\nu}{1-\nu})\cos(\lambda-1)\theta\Big]A + \Big[(\lambda^2-1)\sin(\lambda+1)\theta - (\lambda+1)(\lambda-\tfrac{3+\nu}{1-\nu})\sin(\lambda-1)\theta\Big]B\Big\} \tag{50}$$

When written in terms of their real and imaginary parts corresponding to the deflections of (24) and (25) respectively, in the same manner as in the previous case of the radial shear and moment,

$$\frac{1}{D} V_{\theta_n}^{(1)}(r,\theta) = r^{a-2}\Big\{\Big[K_9\, Im F'(\theta) + K_{10}\, Re F'(\theta) + Im F'''(\theta)\Big]\sin(b\log r) - \Big[K_9\, Re F'(\theta) - K_{10}\, Im F'(\theta) + Re F'''(\theta)\Big]\cos(b\log r) \tag{51}$$

$$\frac{1}{D} M_{\theta_n}^{(1)}(r,\theta) = \nu r^{a-1}\Big\{\Big[K_5\, Im F(\theta) + K_6\, Re F(\theta) + \frac{1}{\nu} Im F''(\theta)\Big]\sin(b\log r) - \Big[K_5\, Re F(\theta) - K_6\, Im F(\theta) + \frac{1}{\nu} Re F''(\theta)\Big]\cos(b\log r) \tag{52}$$

where

$$K_5 = (a+\tfrac{1}{\nu})(a+1) - b^2$$

$$K_6 = (2a+1+\tfrac{1}{\nu})\, b$$

$$K_9 = (a+1)^2 - b^2 + (1-\nu)(a-1)(a-b^2)$$

$$K_{10} = 2b(a+1) + (1-\nu)(a^2-1)\, b$$

As before, $V_{\theta_n}^{(2)}$ and $M_{\theta_n}^{(2)}$ are obtained by replacing ReF_n by ImF_n and ImF_n by $-ReF_n$ in (51) and (52) respectively, with the same rule applying to the derivatives.

At the support, the shear and moment equations take a particularly simple form as for $\theta = 0$; $ReF(0) = ImF(0) = ReF'(0) = ImF'(0) = 0$ which leaves

$$\frac{1}{D} V_{\theta_n}^{(1)}(r;0) = r^{a-2}[ImF''(0)\sin(b\log r) - ReF'''(0)\cos(b\log r)] \quad (53)$$

$$\frac{1}{D} M_{\theta_n}^{(1)}(r;0) = r^{a-1}[ImF''(0)\sin(b\log r) - ReF''(0)\cos(b\log r)] \quad (54)$$

$$\frac{1}{D} V_{\theta_n}^{(2)}(r;0) = r^{a-2}[-ReF'''(0)\sin(b\log r) - ImF'''(0)\cos(b\log r)] \quad (53a)$$

$$\frac{1}{D} M_{\theta_n}^{(2)}(r;0) = r^{a-1}[-ReF''(0)\sin(b\log r) - ImF''(0)\cos(b\log r)] \quad (54a)$$

These quantities which have been calculated are graphed for a range of opening angles and eigen values and presented in Figures 16 through 43. Six quantities have been shown; the deflection, applied shear and applied moment along the arc, the deflection along the free radial edge, and the reacting shear and moment at the root.

It should be emphasized that regardless of any completeness considerations, if any of the loadings given correspond to a distribution actually desired, the eigen function gives an exact solution. The problem arises in deciding how to combine the loads to obtain some other edge loading not given uniquely by one or more of the functions.

V THE UNIFORM LOAD OVER THE SECTOR PLATE

The Particular Solution

While the eigen functions in themselves are interesting from a mathematical point of view, it would be much more useful for practical purposes to obtain a solution for some sort of distributed load over the plate. The root reactions would then be more typical of conditions to be expected from air loads. For this reason, the solution for a uniform load over the sector plate will be derived.

It is relatively easy to find a particular solution of the plate equation in this case; one such solution to

$$D \Delta \Delta w(r,\theta) = q(r,\theta) = q_0 = \text{constant}$$

being

$$w(r,\theta) = \frac{1}{24} \frac{q_0}{D} r^4 \cos^4\theta \tag{55}$$

In this case, however, it is important to select a solution which fits as many of the boundary conditions as possible. If, for instance, it were possible to pick a solution which satisfied the boundary conditions of zero deflection and slope along $\theta = 0$ and also zero shear and moment along $\theta = \alpha$, one would have only to calculate the shear and moment variation along θ for r = 1 due to this solution, and then add the same shear and moment with a negative sign expressed in a proper combination of the previously-developed eigen functions. Such a superposition is the principal virtue of this new set as it essentially permits a relaxation or a certain arbitrariness of the

boundary conditions along the circumferential edge AB. As a consequence, then, one may set out to find a particular solution for the case of a uniform load which satisfies boundary conditions at least along $\theta = 0$ and $\theta = \alpha$.

As a first step, let

$$w_p^*(r,\theta) = \frac{1}{24}\frac{q_0}{D} r^4 \sin^4\theta \tag{56}$$

which certainly satisfies the conditions of zero deflection and slope along $\theta = 0$. Then, from equations (36) and (37), compute the radial moment and shear which become

$$\frac{1}{D} M_{\theta_p}^*(r,\alpha) = -\frac{q_0 r^2}{2D}\left[1-(1-\nu)\sin^2\alpha\right]\sin^2\alpha \tag{57}$$

$$\frac{1}{D} V_{\theta_p}^*(r,\alpha) = -\frac{q_0 r}{2D}\left[1+(1-\nu)\sin^2\alpha\right]\sin 2\alpha \tag{58}$$

In passing, note that the particular solution (56) is already the desired result if the sector is of opening angle $\alpha = \pi$, as $V_{\theta_p}^*(r,\pi) = M_{\theta_p}^*(r,\pi) = 0$. This is a fortuitous happening that does not, in general, extend to other angles. For these cases, additional analysis is necessary.

It is possible, however, to extend the method used in deriving the original eigen functions by introducing a slight variation. Equation (12)

$$w_n(r,\theta) = r^{\lambda_n+1}\left\{A_n\left[\cos(\lambda_n+1)\theta - \cos(\lambda_n-1)\theta\right]\right. \tag{12}$$

$$\left. + B_n\left[(\lambda_n-1)\sin(\lambda_n+1)\theta - (\lambda_n+1)\sin(\lambda_n-1)\theta\right]\right\}$$

also satisfies the conditions along $\theta = 0$ and contains the two undetermined coefficients A_n and B_n. If, now, instead of requiring these constants to be such as to satisfy zero moment and shear along $\theta = \alpha$, A_n and B_n are chosen so that the moment and shear along $\theta = \alpha$ are respectively the negative of those given in (57) and (58), there will be defined a deflection function which, when added to (56), results in a particular solution, namely,

$$w_p(r,\theta) = \frac{1}{24}\frac{q_o}{D} r^4 \sin^4\theta + r^4\{A[\cos 4\theta - \cos 2\theta] + B[2\sin 4\theta - 4\sin 2\theta]\} \qquad (59)$$

which gives a uniform load over the plate and satisfies the boundary conditions along both radial edges $\theta = 0$ and $\theta = \alpha$.

The details are as follows: Equating the moments M_r following from (12) to the negative of (57),

$$(1-\nu)\lambda r^{\lambda-1}\{A[(\lambda+1)\cos(\lambda+1)\alpha - (\lambda - \tfrac{3+\nu}{1-\nu})\cos(\lambda-1)\alpha$$

$$+ B[(\lambda^2-1)\sin(\lambda+1)\alpha - (\lambda+1)(\lambda - \tfrac{3+\nu}{1-\nu})\sin(\lambda-1)\alpha]\}$$

$$= \frac{q_o r^2}{2D}[1-(1-\nu)\sin^2\alpha]\sin^2\alpha$$

it follows that $\lambda = 3$, which simplifies the above equation to

$$A[4\cos 4\alpha - (3 - \tfrac{3+\nu}{1-\nu})\cos 2\alpha] + B[8\sin 4\alpha - 4(3 - \tfrac{3+\nu}{1-\nu})\sin 2\alpha] \qquad (60)$$

$$= \frac{q_o \sin^2\alpha}{6(1-\nu)D}[1-(1-\nu)\sin^2\alpha]$$

Similarly from the shears, where the assumption $\lambda = 3$ is consistent,

$$A\left[-4\sin 4\alpha + \left(3+\frac{3+\nu}{1-\nu}\right)\sin 2\alpha\right] + B\left[8\cos 4\alpha - 4\left(3+\frac{3+\nu}{1-\nu}\right)\cos 2\alpha\right]$$

$$= -\frac{q_0 \sin 2\alpha}{12(1-\nu)D}\left[1 + (1-\nu)\sin^2\alpha\right] \tag{61}$$

These latter two equations may be solved for the constants $A(\alpha, \nu)$ and $B(\alpha, \nu)$.

The final step is evident. There remains only to calculate the moment, shear, and concentrated load along the circumferential edge due to (59) and subtract it out by a suitable combination of the eigen functions. If the set had been proved complete, or if it becomes possible to establish this fact, an exact mathematical solution for the uniform loading, including root reactions, will have been obtained. Otherwise approximations will have to suffice. These are considered in the subsequent section.

Approximate Methods for Finding the Deflection Function

For a wide variety of problems in elasticity, the classical approach for obtaining the unknown coefficients of the linear expansion of a function, here taken as the deflection, is to employ the principle of minimum energy in one form or another.

There are, broadly speaking, two methods of attack. One either choses a set of functions which satisfy the boundary conditions of the problem and not necessarily the governing differential equation, or vice versa, the functions satisfy the differential equation and not the boundary conditions. A linear combination of a finite number, say

N, of the functions in the set are written down and the unknown coefficients determined by requiring that variation of the energy with respect to each coefficient be zero. In general there results from this procedure a set of N equations in N unknowns from which the coefficients of the expansion or combination can be determined. Of the two alternatives outlined above, the first is commonly referred to as the Rayleigh-Ritz method, while the second procedure is known as the Courant-Trefftz method. Inasmuch as both have been treated at length (1, 8), no discussion will be introduced here. Suffice to note that as the eigen-functions satisfy the partial differential equation, an application of energy methods to the sector plate will naturally lead to the Courant-Trefftz method.

The theorem of minimum potential energy requires that the difference between internal strain energy and the work done by the external forces be a minimum, i.e., the variation of the potential energy, V, may be written as

$$\delta V = \iint_R \left(\Delta\Delta w - \frac{q}{D}\right) w r\,dr\,d\theta - \int_6 M_r(1,\theta)\,\frac{\partial w(1,\theta)}{\partial r}\,d\theta \tag{62}$$

$$+ \int_6 V_r(1,\theta)\, w(1,\theta)\,d\theta + 2M_{r\theta}(1,\alpha)\, w(1,\alpha) = 0$$

where the last three terms are energies due to the externally applied loads and the variation function has been taken as the solution itself, $w(r,\theta)$, in accordance with the usual procedure.

Now as the eigen functions and the particular solution satisfy the partial differential equation over the surface and the boundary

conditions on the two radial edges exactly, only the line integrals over the arc remain. While the vanishing of the surface integral is a great advantage eliminating as it does two integrations, the apparent simplicity of the remaining integrals is misleading because, as indicated previously, the eigen functions are not orthogonal and although there is in principle no difficulty involved in carrying out the integrations, in practice the amount of computation involved is great enough to warrant investigation of other approximations. The results of a three term expansion for a 45 degree sector under a uniform loading using the non-orthogonal functions are indicated, however, for comparison with other solutions (Figure 2). A five term expansion appears to be the largest number of functions that can be handled conveniently with desk calculators. Because of the improbability of their use, none of the formulas for evaluating the energy integrals will be included.

Another way of approximating the deflection would be to satisfy the boundary conditions at a certain number of discrete points along the arc. This method was tried for the case of $\theta = 0$, 15°, 30°, and 45° using

$$w(r,\theta) = w_p(r,\theta) + \sum_{m=1,2,3,\ldots}^{N=11} \gamma_m \varphi_m(r,\theta) \tag{63}$$

where $\varphi_m(r,\theta)$ are the ordered eigen functions. The results were unsatisfactory and any extension of this method, if attempted, should be based on Hildebrand's procedure.

The final method which might be tried is to use equation (11),

assuming λ_n belongs to a set of integers, and insert it into the energy expression where, of course, there will be two additional integrations to perform along the radial line $\theta = \alpha$ because the boundary conditions have not been satisfied there. Inasmuch as the functions along $r = 1$ are now orthogonal except for the interval of integration, the computations may be simpler although probably not enough so as to justify carrying them out at present.

In concluding this section, it may be said that if the importance of the deflection problem for sectors warrants, the energy method using the eigen functions as originally proposed may be used, particularly if adapted to high speed automatic calculating equipment.

VI THE STRESS SINGULARITY IN A CORNER

Basic Considerations

One of the most interesting and practically useful results of this investigation concerns the magnitude of stresses in the vicinity of a corner bounded by fixed and free edges. While the development is for the most part given in reference (9), the important features will be repeated here so that there will be sufficient background to interpret the experimental data which will be presented.

It will be recalled that the method used in obtaining the eigen functions consisted of satisfying the partial differential equation governing the behaviour of thin plates in bending and the Kirchhoff boundary conditions along the two radial edges, with the possible exclusion of the origin itself where $r = 0$ (equations 14 and 15). Then, in so far as the mathematics represents the actual physical situation, one would expect to have a fairly correct solution in the neighborhood of the origin providing the circumferential boundary at the unit radius was not too close to the origin or that there were no highly irregular or discontinuous loadings in this vicinity.

Furthermore, it will be remembered that not only was there one solution which satisfied these two radial boundary conditions, but an infinite set of them. Suppose for the moment that the set is complete and that any deflection function may be expressed in an infinite series of these eigen functions, and further, let the series be differentiable as required. It will, therefore, be possible to compute the stress anywhere in the plate and, in particular, near the origin. For the

sake of presenting this intuitive argument, consider the case of the support stress, where $\theta = 0$.

Since, for constant thickness plates, M_θ, the reacting moment, and σ_θ, the reacting surface stress, are proportional,

$$\sigma_\theta = \frac{6M_\theta}{t^2} \quad ,$$

the series for the stress along the root will be made up of terms of the form (see 54, 54a).

$$\sigma_\theta(r,0) = K r^{a-1}\left[C_1 \sin(b \log r) + C_2 \cos(b \log r)\right] \tag{64}$$

For small values of r, that is for the stress near the origin or corner, the term in brackets is bounded by some constant, say $\bar{M}$. A bound on the series for the root stress may now be written, where $K_n^{(i)}$ is an arbitrary, real constant

$$|\sigma_\theta(r,0)| \leq K_2^{(1)} |\sigma_{\theta_2}^{(1)}| + K_2^{(2)} |\sigma_{\theta_2}^{(2)}| + K_r |\sigma_{\theta_r}| + K_4^{(1)} |\sigma_{\theta_4}^{(1)}| + K_4^{(2)} |\sigma_{\theta_4}^{(2)}| + \cdots$$

$$\leq K_2^{(1)} r^{a_2-1} \bar{M}_2^{(1)} + K_2^{(2)} r^{a_2-1} \bar{M}_2^{(2)} + K_r r^{a_r-1} \bar{M}_r + \cdots$$

$$\leq r^{a_2-1}\left[K_2^{(1)} \bar{M}_2^{(1)} + K_2^{(2)} \bar{M}_2^{(2)} + K_r \bar{M}_r r^{a_r-a_2}\right.$$

$$\left. + (K_4^{(1)} \bar{M}_4^{(1)} + K_4^{(2)} \bar{M}_4^{(2)}) r^{a_4-a_2} + \cdots\right]$$

Then, inasmuch as the eigen values have been ordered, $0 < (a_r - a_2) < (a_4 - a_2) < \cdots$, the behavior of the absolute value of the root stress near the corner is of the order

$$|\sigma_\theta(r \to 0, \theta)| \sim K r^{a_2 - 1} \tag{65}$$

where a_2 is the lowest eigen value for a given opening angle. The same type of behavior with r may be shown for any value of θ, although the constant of proportionality will be different.

It is next interesting to examine the significance of the previous expression and in particular the values of the exponent of r. In the vicinity of the corner, it appears possible to obtain a bound on the stresses which tends to zero, a constant, or infinity depending upon whether a_2 is greater than, equal to, or less than unity, although it should be remembered that σ is defined as a stress per unit length. Inasmuch as it can be shown that the eigen equation (16) is continuous in both the real and imaginary parts of λ, it is permissible to construct the curve shown in Figure 3, where a_2, the minimum eigen value, is plotted versus the opening angle, α. It is seen that a_2 is continuous through unity and hence the postulated states of stress may occur.

Upon reflection, one's intuition may not be too badly offended because the unit value for a_2 occurs very close to 90°, and it does not seem too unreasonable to expect finite stresses at the root if the opening angle is acute, and on the other hand to expect a high stress for an obtuse angle. This latter effect shows up in the fact that the stress singularity becomes stronger as the opening angle is increased, which again seems reasonable.

Before proceding further with a discussion of the singularity,

there are some items of mathematical and physical interest which will be brought out. It has been emphasized previously that the origin may possibly be a singular point — and indeed, for cases of $a_2 < 2$, the eigen equation (16) makes no sense exactly at the origin, inasmuch as (14) and (15) become infinite in the limit as $r \to 0$. Nevertheless, for all finite values of $r \geq \epsilon > 0$, however small, (64) is perfectly valid and gives the true character of the singularity, while (65) gives the bound.

The trigonometric variation in the stress, or the deflection also for that matter, is somewhat unusual inasmuch as the value of the stress, or deflection, passes through zero an arbitrary number of times, depending upon ϵ. A close examination of this oscillatory character and an investigation of the zeros and maximums of $\begin{matrix}\sin \\ \cos\end{matrix}$ (b log r) will show, however, that for the lowest eigen functions, the first zero will occur at $r \lesssim 1/10$ for $\pi/2 \leq \alpha \leq \pi$ and the second zero at $r \lesssim 1/100$, so that the aggravated oscillatory character does not manifest itself until very near the origin where the solution must be restricted anyhow because of the singular point.

Some concern naturally arises as to the amount of root reaction which is taken out near the corner. It develops that the positive and negative sections of the trigonometric variation cancel out in such a way that there is no resultant contribution at the origin. This fact may be shown by considering the integrated root reaction. Using (64)

$$\frac{\int_0^r \sigma_\theta(r,0)\,dr}{\int_0^1 \sigma_\theta(r,0)\,dr} = \frac{r^a\{[ac_1+bc_2]\sin(b\log r)+[ac_2-bc_1]\cos(b\log r)\}}{ac_2-bc_1}$$

$$\leq K' r^a$$

and as $a > 0$, the percentage reaction near the origin referred to the total root reaction is less than $K'\epsilon^a \to 0$.

Furthermore, additional analysis shows that in nearly all cases, the behavior of (64) closely approaches the bound given by (65) which, for practical purposes, permits the absolute value signs to be removed from (65).

While it is physically impossible to obtain an infinite or unbounded stress, it is believed that its occurrence merely reflects plastic flow or some other phenomenon which is no longer represented accurately at the origin by the mathematics of the problem. A somewhat similar case occurs in hydrodynamics. The incompressible flow around a sharp corner gives an infinite velocity whereas actually the velocity is finite when the mathematical formulation of the problem is extended to include the effects of viscosity. It should also be mentioned that it is somewhat disturbing that the unit value of a_2 does not occur at exactly 90°, particularly as the deviation, which

amounts to approximately a half a degree, is a function of Poisson's ratio, ν . This matter is not altogether understood, but as will be shown, experimental data taken to check the stress singularity and its variation agree too well with the predicted character of the singularity to discard the result on what may turn out to be a physical or mathematical triviality.

Before turning to a practical application of (65), a similar behavior in the shear should be pointed out. In a similar manner as before, as the shear is essentially the third derivative of the deflection, it may be shown that

$$V_\theta \sim C r^{a_2-2} \tag{66}$$

The singularity is stronger and occurs at approximately 60° and here it must be admitted that so far not even an intuitive explanation as to why such a phenomenon should occur at this acute angle can be presented, although it should be remembered that V_θ is defined as the shear per unit length.

It furthermore appears at first glance that the integral of the shear is not even finite for $\alpha > 60^\circ$. If so, this would contradict the laws of statics and it was deemed advisable to consider the equilibrium of vertical forces for the complete sector. No difficulty was found in this respect, however, when due consideration was given to the trigonometric terms.

Before concluding these general remarks upon the mode of stress singularity, it is desired to include a comment upon the effect of load distribution upon the singularity. So far, one is to expect that

(65) will give the character of the singularity provided that the loading is regular or smoothly varying. If w_p is the particular solution for a given loading, then for the root stresses,

$$\sigma_\theta (r \to 0, 0) \leq \sigma_{\theta_p} (r \to 0, 0) + K r^{a_2 - 1} \tag{67}$$

If $\sigma_{\theta_p}(r \to 0, 0)$ has a stronger singularity than the second term, then the stress will be strongly affected by the load. In the particular case of a uniformly loaded plate it was shown that $w_p \sim r^4$, and hence $\sigma_{\theta_p} (r \to 0, 0) \to 0$. Consequently, the order of the stress singularity for uniform loads is of the order

$$\sigma_\theta (r \to 0, 0) \sim K r^{a_2(\alpha) - 1}$$

Such considerations give one a better appreciation of the effect of type of loading and some idea of the relation between a "regular" and uniform load.

A Practical Application

In order to apply the above to a practical case, for example a swept rectangular plate of constant chord (Figure 4), one may attempt to extend the representation for the root stress in many ways. One originally proposed[9] was of the form

$$\sigma(r, 0) = K \left(\frac{r}{c}\right)^{a_2(\alpha_1) - 1} \left[1 - \left(\frac{r}{c}\right)\right]^{a_2(\alpha_2) - 1} \tag{68}$$

which satisfies the singular behavior properly near $0_1 (r \to 0)$ and $0_2 (r \to c)$. The constant of proportionality, K, was found to be

$$K = \frac{6M_o}{ct^2} \frac{\Gamma[a_2(\alpha_1)+a_2(\alpha_2)]}{\Gamma[a_2(\alpha_1)]\Gamma[a_2(\alpha_2)]} = \frac{6M_o}{ct^2} B^{-1}[a_2(\alpha_1), a_2(\alpha_2)]$$

by equating the applied moment about the root to the integrated root reaction. M_o is the applied moment of the load on the plate about the root and c is the root length $0_1 0_2$.

The root stress variation has been calculated according to (68) for a constant chord rectangular plate at various angles of sweep and the results presented in Figure 6 along with some experimental data for the case of 60 degree sweep. The deviation in magnitude of the two curves is due to the fact that (68) is based upon the bounding stress with the constant determined from the total applied load. The test data show a reverse curvature with negative area near the leading edge which permits a higher concentration of positive area near the corner in the actual case which in turn raises the stress concentration factor above that predicted. The main value of (68) is that this particular formula is very easy to use and may be easily extended to delta configurations, such as shown in Figure 5, inasmuch as the only parameters which enter are the opening angles and the applied moment.

While it is again to be emphasized that the formula is intended to give bounds for regular loadings (a concentrated load near the center of the root would, of course, not be admissible), it is interesting to show a comparison with some experimental data[13] taken for a triangular plate with a 60 degree swept leading edge and various trailing edge angles when the load is concentrated at the tip. It should be

mentioned that this root stress data was taken, not exactly along the root ($\theta = 0$) line, but along a parallel line 1/10 inch outboard. The experimental data has therefore been extended to the root line by following the method outlined in Appendix II, and hence no experimental points are shown on the curve. This comparison of the theoretical and experimental data is presented in Figures 7 through 13 shows surprisingly good agreement considering the simplicity of the formula. As was to be expected, the mode shapes are predicted best in the immediate vicinity of the two corners.

For design purposes, an infinite, increasingly large value of the stress can not be tolerated, and the question arises as to the way of applying the theoretical results. One method which may be used is to first compute the design stress concentration factor $k^* = \frac{\sigma_d c t^2}{6 M_0}$ where σ_d is the design stress for the given plate with root chord c and thickness t under the applied moment M_0 about the root. This value of k* will establish an upper bound above which the material is assumed ineffective, and the area above this value of k* and under the curve of k vs $\frac{r}{c}$ will represent the amount of stress which must be taken into the support elsewhere. This area is labeled A_1 in Figure 14. The suggested design criterion is to replace A_1 with an equivalent area beneath the k* bound as indicated in A_2 of Figure 15.

Such a requirement leads to

$$k^* \frac{r_0}{c} = \int_0^{\frac{r_0}{c}} \frac{\sigma c t^2}{6 M_0} \, d\left(\frac{r}{c}\right)$$

From which, using (68), it is found that

$$K^*\left(\frac{r_o}{c}\right) = B^{-1}[a_2(\alpha_1), a_2(\alpha_2)] \int_0^{\frac{r_o}{c}} \left(\frac{r}{c}\right)^{a_2(\alpha_1)-1} \left(1-\frac{r}{c}\right)^{a_2(\alpha_2)-1} d\left(\frac{r}{c}\right)$$

and approximating the integral for small values of $\frac{r}{c}$

$$K^*\frac{r_o}{c} = B^{-1}[a_2(\alpha_1), a_2(\alpha_2)] \frac{1}{a_2(\alpha_1)} \left(\frac{r_o}{c}\right)^{a_2(\alpha_1)}$$

from which, $\frac{r_o}{c} << 1$

$$\frac{r_o}{c} = \left[\frac{1}{K^* a_2(\alpha_1) B[a_2(\alpha_1), a_2(\alpha_2)]}\right]^{\frac{1}{1-a_2(\alpha_1)}} \tag{69}$$

A typical design curve is shown as the heavy line on Figure 15. For the case of the constant chord rectangular plate swept 60 degrees and a design stress of σ_d = 20000 psi, $\frac{r_o}{c}$ is found to be 0.056 for $k^* = 4.17$.

Another type of approximation from which it appears possible to obtain a closer fit over the entire range of the root has been tried. In this connection note again that the experimental data in Figure 13 shows a reverse curvature that the previous formula can not hope to match. For this reason the complete eigen expressions for the root stress, equation (53), which retains the trigonometric variations may be used. By requiring continuous $D^{(1)}$ behavior of both the shear and moment and fulfilling the laws of statics for a linear combination of say the lowest three eigen functions, it is possible to approach the mode shapes somewhat closer with reasonable computation. In view of the extreme simplicity of the previous formula, however, further work upon this extension does not seem warranted at this time.

Another application of the singularity which seems to possess some merit is its possible utility in computing deflection modes of

triangular plates. As the deflection is essentially two integrations of the stress, one merely assumes that the deflection of each free edge is proportional to $r^{a_2(\alpha)+1}$ where α is the angle the free edge makes with the root. One of the constants of proportionality is fixed by requiring the deflection of the two edges to be the same at the tip of the triangle and the other is determined by the loading condition. Even a linear interpolation between the two free edges has been found to match experimental data within 15 to 20 per cent for some favorable cases. This application to approximate deflection patterns is not intended to be complete but rather to suggest a possible approach particularly for qualitative answers.

The Swept Rectangular Plate

As a final remark upon the connection between the sector results and approximate work, an interesting similarity to a hydrodynamic analogy has been observed. In Figure 3, a second (dashed) curve of $\frac{\pi}{2\alpha}$ versus α has been presented, and it is seen that it lies fairly close to the curve of $a_2(\alpha)$ versus α, especially for the larger included angle. Indeed, the correspondence is exact at $\alpha = \pi$. It develops that this $\frac{\pi}{2\alpha}$ variation is the exponent of conformal transformation between rectilinear flow and the flow around a corner of 2α included angle. A new approach to the bending of a swept rectangular plate is immediately suggested and while again it is not within the scope of the sector study to investigate this new field, it is felt that some ideas are perhaps new enough to be included at this time.

Consider for the moment an unswept cantilever rectangular plate

(Figure 15) with the usual assumptions postulated in thin plate work. Suppose in addition the moment per unit length in the x direction, M_y, is arbitrarily taken to be zero.

$$M_y = D\left(\frac{\partial^2 w}{\partial y^2} + \nu \frac{\partial^2 w}{\partial x^2}\right) = 0$$

which of course implies

$$\frac{\partial^2 w}{\partial y^2} = -\nu \frac{\partial^2 w}{\partial x^2}$$

and hence

$$M_x = D(1-\nu^2)\frac{\partial^2 w}{\partial x^2} \tag{70}$$

from which the deflection may be calculated. It also follows directly that

$$\Delta M_x = \left(\frac{\partial^2}{\partial x^2} + \frac{\partial^2}{\partial y^2}\right) M_x = q(x,y) \tag{71}$$

which, for the homogeneous case, means the bending moment must satisfy the Laplacian equation in the region. It so happens then that the beam equation

$$M_x = DcP(l-x) \tag{72}$$

satisfies the differential equation and the boundary conditions, where it is to be noted that $\frac{\partial M_x}{\partial y}$ along the root is zero which implies that the stress distribution is uniform or, what is the same thing, that the stress concentration factor is unity.

The lines of principal stress are now parallel to the coordinate system and the direction of maximum principal stress is the flow or streamline in the hydrodynamic analogy. It is desired to find the variation of M_x or streamline spacing along the line O_1O_2 when it is

not perpendicular to the free edges. This will give the stress distribution, or with proper normalization, the stress concentration factor for a swept plate. Now such a procedure as outlined, perhaps on a somewhat intuitive basis, required the conformal mapping formula of the rectangular plate into a swept rectangular plate and while the transformation is the well-known Swartz-Christoffel one, its analytic representation in convenient form is impossible for most practical purposes. It may be briefly noted, however, that at least one example, the flow in a channel about a 270 degree corner has been graphed numerically by Bergman[14].

As the basic desire is for a rapid — and probably approximate — solution for stress distribution, suppose an approximate mapping is considered in which one assumes the flow in the immediate vicinity of the corner is determined solely by that corner. The mapping is then given very quickly and easily by the simple incompressible flow from infinity around a corner of 2α degrees in an infinite medium. Using the notation indicated in Figure 15, where the $z = x + iy = re^{i\theta}$ system is used in the rectilinear plane and $w = u + iv = \rho e^{i\varphi}$ in the transformed plane, the connection between the two is given by

$$z = w^{\frac{\pi}{2\alpha}} \tag{73}$$

and hence

$$x = \rho^{\frac{\pi}{2\alpha}} \cos\frac{\pi\varphi}{2\alpha} \qquad r = \rho^{\frac{\pi}{2\alpha}}$$

$$y = \rho^{\frac{\pi}{2\alpha}} \sin\frac{\pi\varphi}{2\alpha} \qquad \theta = \frac{\pi\varphi}{2\alpha}$$

Because of the symmetry of the flow, or principal stress, lines around the corner, the variation of M_x with ρ along the root or $\theta = \alpha$ line is very easily found as

$$\frac{\partial M_x}{\partial \rho} = -\frac{\pi P}{2\alpha} \frac{1}{\left[1 + \tan^2 \frac{\pi \varphi}{2\alpha}\right]^{\frac{1}{2}}} \rho^{\frac{\pi}{2\alpha} - 1}$$

which is essentially of the form

$$\frac{\partial M_x}{\partial \rho} = K \rho^{\frac{\pi}{2\alpha} - 1} \tag{74}$$

The similarity of (74) to the previous result, equation (65), is immediately apparent where $\frac{\pi}{2\alpha}$ is to be associated with $a_2(\alpha)$. Remembering the agreement as indicated in Figure 3, the analogy is substantiated, with the deviation between the exponents probably due to the fact that the conformal mapping is approximate as is the initial assumption of $M_y = 0$. This latter formula would also be expected to hold only in that region near the corner.

There is one added advantage which is gained by considering the flow analogy in that one can get a fairly clear physical picture as to the regions of influence of the singularities. In Figure 15, an attempt has been made to show this characteristic which is born out by experimental data, namely, that the line of principal stress, SS, which bisects the perpendicular distance between the leading and trailing edges at the tip, when carried in to the root, separates the trailing edge effect from the rest of the plate.

In conclusion, it is felt that the flow analogy may be quite useful in gaining a physical feeling for the stress behavior in swept plates and that further work with this analogy might well lead to approximate formulas appropriate to representing the stress and distributions sufficiently well for engineering accuracy and preliminary studies of overall characteristics.

VII CONCLUSIONS

In summarizing the work presented herein, there are only two points which should be emphasized.

First of all, an exact solution for the bending of a cantilever sector has not been established because the infinite set of non-orthogonal eigen functions has not been proved complete. Even had the completeness been established, there would still remain the necessity of calculating the deflection for a practical case. As previously noted, this is difficult to do. Notwithstanding the failure, however, it is believed that if the importance of the problem warrants, the deflection could be obtained if automatic computing equipment were available. For ordinary applications, however, relaxation methods are recommended.

Secondly, inasmuch as the eigen functions seem intuitively correct for describing the phenomenon, because of their method of derivation if for no other reason, one feels justified in taking advantage of their characteristic behavior as a basis for approximate solutions. In particular the eigen function associated with the lowest eigen value has proved extremely valuable as a guide to predicting root stress, and possibly deflection, distributions. One's intuition in the matter of the minimum eigen values and their importance has been substantiated and reinforced by both experimental data and a theoretical analogy, and it is believed that the possibility of expressing the mode of stress singularity in a corner may prove of wider utility than the contemplated use for the analysis of swept missile wings of

high solidity.

In conclusion, it should be pointed out that there is no reason why the same method of developing both the set of eigen functions and their approximate behavior could not be extended to corners of thin plates under different boundary conditions. For instance, the case of the stress in a corner bounded by two clamped edges, which is quite easy to set up, may well be of interest in other fields of applied elasticity.

REFERENCES

1. Fung, Y. C.: Theoretical and Experimental Effect of Sweep Upon the Stress and Deflection Distribution in Aircraft Wings of High Solidity. Part I - Elastostatic and Aeroelastic Problems Relating to Thin Wings of High-Speed Airplanes. Air Force Technical Report 5761. Aug., 1948.

2. Fung, Y. C.: Theoretical and Experimental Effect of Sweep Upon the Stress and Deflection Distribution in Aircraft Wings of High Solidity. Part II - Stress and Deflection Analysis of Swept Plates. Air Force Technical Report 5761. June, 1949.

3. Timoshenko, S.: Theory of Plates and Shells. McGraw-Hill Book Co., Inc., N. Y., 1940.

4. Zahorski, A. T. Mathematical Analysis of Cantilever Plates. Northrop Aircraft, Inc., GM 313. Project MX 775. Jan., 1949.

5. Hildebrand, F. B.: Least Square Procedure for the Solution of the Lifting Line Integral Equation. N.A.C.A. T.N. No. 925, Feb., 1944.

6. Frank, and von Mises: Differentialgleichungen der Physik, Vol. I, p. 848, Vieweg and Sohn, Braumschweig.

7. Prescott, John: Applied Elasticity. Dover Publications, N. Y., 1946. p. 354.

8. Sokolnikoff, I. S.: Mathematical Theory of Elasticity. McGraw-Hill Book Co., Inc., N. Y., 1946.

9. Williams, M. L.: A Simple Formula for the Root Stresses of Swept Triangular and Rectangular Cantilever Plates of Constant Thickness. Northrop Aircraft, Inc., GM 320, Oct., 1949.

10. Williams, M. L.; Garrett, J.; and Henry, W. E.: Theoretical and Experimental Effect of Sweep Upon the Stress and Deflection Distribution in Aircraft Wings of High Solidity. Part VII - An Experimental Investigation of the Stresses and Deflections in a Series of Cantilever Sectors of Uniform Thickness. Air Force Technical Report 5761. June, 1950.

11. Sechler, E. E.;and Dixon, H. H.: Theoretical and Experimental Effect of Sweep Upon the Stress and Deflection Distribution in Aircraft Wings of High Solidity. Part XIII - Review of Analysis Methods for Swept Wing Aircraft Including a Bibliography and Abstracts of Pertinent Theoretical and Experimental References. Air Force Technical Report 5761. July, 1950.

12. Williams, M. L.: The Plane Stress Problem for a Sector with Fixed Radial Edge. Northrop Aircraft, Inc. GM 321, Oct., 1949.

13. Hrebec, G. M.: Theoretical and Experimental Effect of Sweep Upon the Stress and Deflection Distribution in Aircraft Wings of High Solidity. Part VIII - Some Experimental Data for the Deflection and Root Stresses in a Cantilever 30 Degree Triangular Plate of Constant Thickness with Varying Trailing Edge Sweep Angle. Air Force Technical Report 5761. June, 1950.

14. Stein, G. M.: Conformal Maps Involving Multiply Connected Regions and Their Technical Applications. Page 14 of a paper presented at the Symposium on the Construction and Applications of Conformal Maps, University of California at Los Angeles, June, 1949.

15. DeGroff, H. M.: Theoretical and Experimental Effect of Sweep Upon the Stress and Deflection Distribution in Aircraft Wings of High Solidity. Part III - Experimental Investigation of the Effect of Sweep Upon the Stress and Deflection Distribution in Cantilever Plates of Constant Chord and Thickness. Air Force Technical Report 5761. June, 1949.

LIST OF TABLES

TABLE I

TABULATION OF EIGEN VALUES AND EIGEN CONSTANTS

n	λ_n	A_n	B_n
		$\alpha = \pi/4$	
2	2.354499 + 0.683027i	12.4467 + 1.39478i	2.19947 + 3.14238i
r	4.039488	-8.83285	3.94296
4	7.607251 + 1.967820i	69.1666 + 166.785 i	-21.4282 + 12.5273 i
6	11.701552 + 2.56760 i	-435.195 − 532.804 i	40.4176 − 43.2778 i
8	15.752630 + 2.95919 i	1279.90 + 1125.00 i	-60.7954 + 89.4504 i
10	19.786392 + 3.25409 i	-2785.00 -1960.11 i	82.2925 − 150.742 i
		$\alpha = \pi/2$	
2	1.068698 + 0.438577i	1.22732 + 5.73029i	-1.88434 + 1.21378i
r	2.464069	2.031205	.8085373
4	3.820109 + 0.671848i	10.2262 + 14.9684 i	-3.39200 + 4.15628i
6	5.867961 + 1.03110 i	-90.5779 − 71.9258 i	9.23233 − 17.9341 i
8	7.890812 + 1.24177 i	285.152 + 173.058 i	-15.8195 + 39.4442 i
10	9.905466 + 1.39552 i	-638.915 − 322.643 i	22.9984 − 68.5093 i
		$\alpha = 3\pi/4$	
2	0.675693 + 0.322071i	-5.45876 + 3.27590i	-2.09664 − 2.63408i
4	2.032537 + 0.224968i	7.94766 − 1.38555i	-0.110682 + 1.81462i
r	3.094715	-8.365542	3.634729
r	3.805568	-11.362894	-2.405319
r	4.033395	-7.292452	-4.270026
8	5.275094 + 0.410728i	36.5097 − 6.19664i	4.15161 + 6.02625i
10	6.617925 + 0.557198i	-86.3311 + 6.13405i	-4.81010 − 14.0958 i
		$\alpha = \pi$	
2	0.500000 + 0.246824	-7.33205 − 1.20648	− 4.88856i
4	1.500000 + 0.246824	12.2201 + 1.20648	− 4.88856i
6	2.500000 + 0.246824	-17.1081 − 1.20648	− 4.88856i
8	3.500000 + 0.246824	21.9961 + 1.20648	− 4.88856i
10	4.500000 + 0.246824	-26.8842 − 1.20648	− 4.88856i

TABLE II

COEFFICIENTS FOR DEFLECTION, SLOPE AND CURVATURE IN THE CIRCUMFERENTIAL DIRECTION

Note: $F'(\theta) = \frac{dF(\theta)}{d\theta}$	$-\frac{1}{2}$ Re F (θ)	$-\frac{1}{2}$ Re F' (θ)	$-\frac{1}{2}$ Re F" (θ)	$-\frac{1}{2}$ Re $F^{(n)}(\theta)$	$-\frac{1}{2}$ Re $F^{(n+1)}(\theta)$
$\sin\theta \sin a\theta \sinh b\theta$	$-a\,\mathrm{Im}B - b\,\mathrm{Re}B$	$a\,\mathrm{Im}A + b\,\mathrm{Re}A$	$(a^2-3b^2-1)\,a\,\mathrm{Im}B + (3a^2-b^2-1)\,b\,\mathrm{Re}B$	$Y_1^{(r)}$	$bY_2^{(r)} - aY_3^{(r)} - Y_5^{(r)}$
$\sin\theta \sin a\theta \cosh b\theta$	$\mathrm{Re}A$	$(a^2-b^2-1)\,\mathrm{Re}B - 2ab\,\mathrm{Im}B$	$(b^2-a^2-1)\,\mathrm{Re}A + 2ab\,\mathrm{Im}A$	$Y_2^{(r)}$	$bY_1^{(r)} - aY_4^{(r)} - Y_6^{(r)}$
$\sin\theta \cos a\theta \sinh b\theta$	$-\mathrm{Im}A$	$-(a^2-b^2-1)\,\mathrm{Im}B - 2ab\,\mathrm{Re}B$	$-(b^2-a^2-1)\,\mathrm{Im}A + 2ab\,\mathrm{Re}A$	$Y_3^{(r)}$	$aY_1^{(r)} + bY_4^{(r)} - Y_7^{(r)}$
$\sin\theta \cos a\theta \cosh b\theta$	$b\,\mathrm{Im}B - a\,\mathrm{Re}B$	$a\,\mathrm{Re}A - b\,\mathrm{Im}A$	$(a^2-3b^2-1)\,a\,\mathrm{Re}B - (3a^2-b^2-1)\,b\,\mathrm{Im}B$	$Y_4^{(r)}$	$aY_2^{(r)} + bY_3^{(r)} - Y_8^{(r)}$
$\cos\theta \sin a\theta \sinh b\theta$	0	0	$2(b\,\mathrm{Re}A + a\,\mathrm{Im}A)$	$Y_5^{(r)}$	$bY_6^{(r)} - aY_7^{(r)} + Y_1^{(r)}$
$\cos\theta \sin a\theta \cosh b\theta$	$\mathrm{Re}B$	$\mathrm{Re}A$	$-(b^2-a^2+1)\,\mathrm{Re}B - 2ab\,\mathrm{Im}B$	$Y_6^{(r)}$	$bY_5^{(r)} - aY_8^{(r)} + Y_2^{(r)}$
$\cos\theta \cos a\theta \sinh b\theta$	$-\mathrm{Im}B$	$-\mathrm{Im}A$	$(b^2-a^2+1)\,\mathrm{Im}B - 2ab\,\mathrm{Re}B$	$Y_7^{(r)}$	$aY_5^{(r)} + bY_8^{(r)} + Y_3^{(r)}$
$\cos\theta \cos a\theta \cosh b\theta$	0	0	$2(a\,\mathrm{Re}A - b\,\mathrm{Im}A)$	$Y_8^{(r)}$	$aY_6^{(r)} + bY_7^{(r)} + Y_4^{(r)}$

$-\frac{1}{2}\,\mathrm{Re}\,F(\theta) = (-a\,\mathrm{Im}B - b\,\mathrm{Re}B)\sin\theta \sin a\theta \sinh b\theta + \mathrm{Re}A \sin\theta \sin a\theta \cosh b\theta + \ldots\ldots$

$\ldots\ldots - \mathrm{Im}B \cos\theta \cos a\theta \sinh b\theta.$

$-\frac{1}{2}\,\mathrm{Re}\,F'(\theta) = (a\,\mathrm{Im}A + b\,\mathrm{Re}A)\sin\theta \sin a\theta \sinh b\theta + \ldots\ldots - \mathrm{Im}A \cos\theta \cos a\theta \sinh b\theta.$

$-\frac{1}{2}\,\mathrm{Re}\,F''(\theta) = [(a^2-3b^2-1)\,a\,\mathrm{Im}B + (3a^2-b^2-1)\,b\,\mathrm{Re}B]\sin\theta \sin a\theta \sinh b\theta + \ldots\ldots$

To obtain the coefficients of $-\frac{1}{2}\,\mathrm{Im}\,F(\theta)$, $-\frac{1}{2}\,\mathrm{Im}\,F'(\theta)$, $-\frac{1}{2}\,\mathrm{Im}\,F''(\theta)$; replace Re A by Im A, Im A by - Re A, Re B by Im B, and Im B by - Re B in the above table.

LIST OF FIGURES

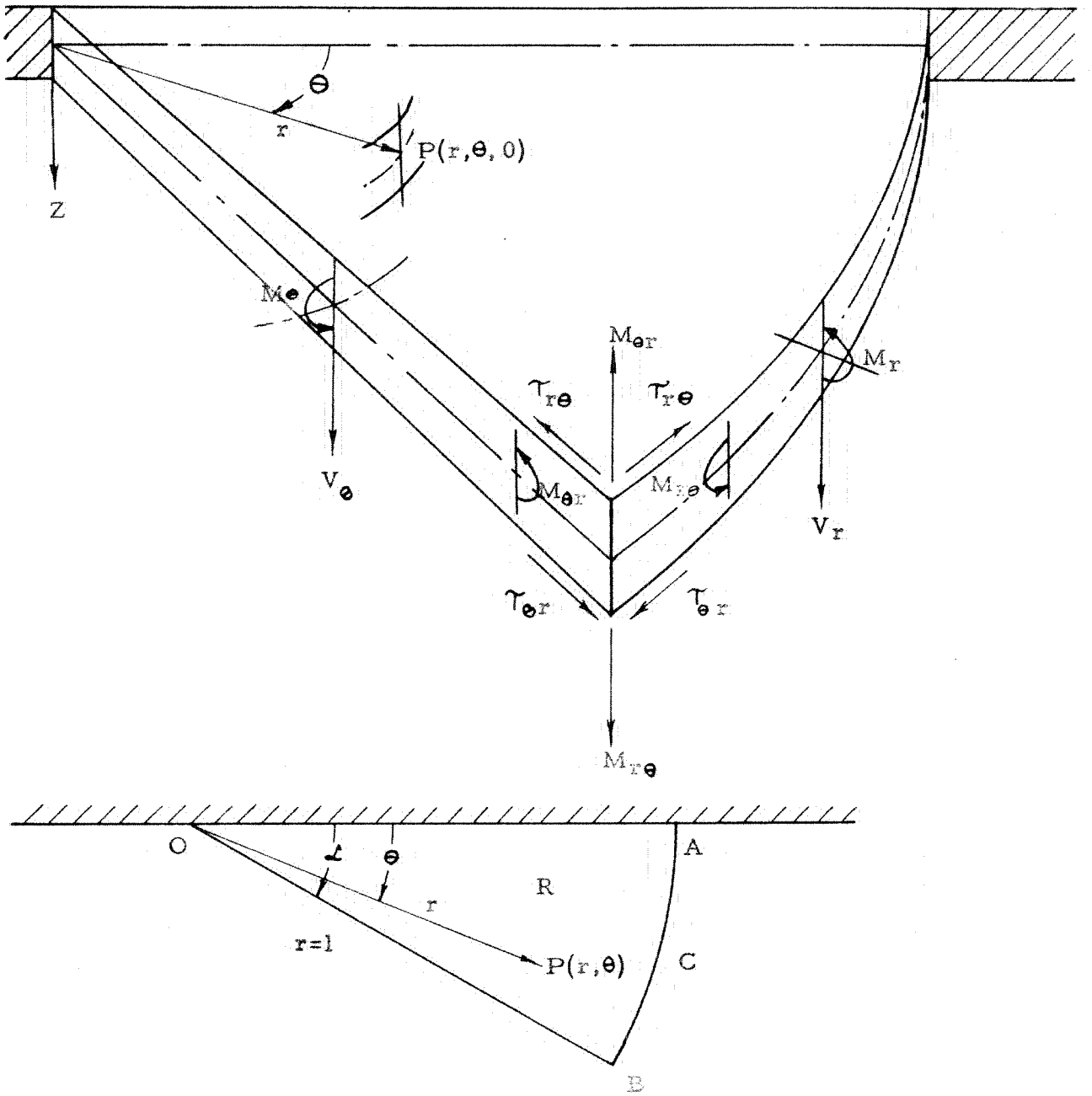

FIGURE 1

SECTOR PLANFORM AND NOTATION

RESULTS OF A THREE TERM EXPANSION IN THE EIGEN FUNCTIONS FOR THE CASE OF A UNIFORM LOAD, $\alpha = 45$ DEGREES, SHOWING THE ERROR IN THE APPROXIMATION AS INDICATED BY THE DEVIATION OF THE SUMMATION OF THE SHEARS, MOMENTS, AND CONCENTRATED LOAD FROM ZERO. FOR THE TRUE SOLUTION,

$$\frac{M_p(\theta)}{q_0} + \sum \gamma_n \frac{M_n(\theta)}{q_0} \equiv 0 \text{ , ETC.}$$

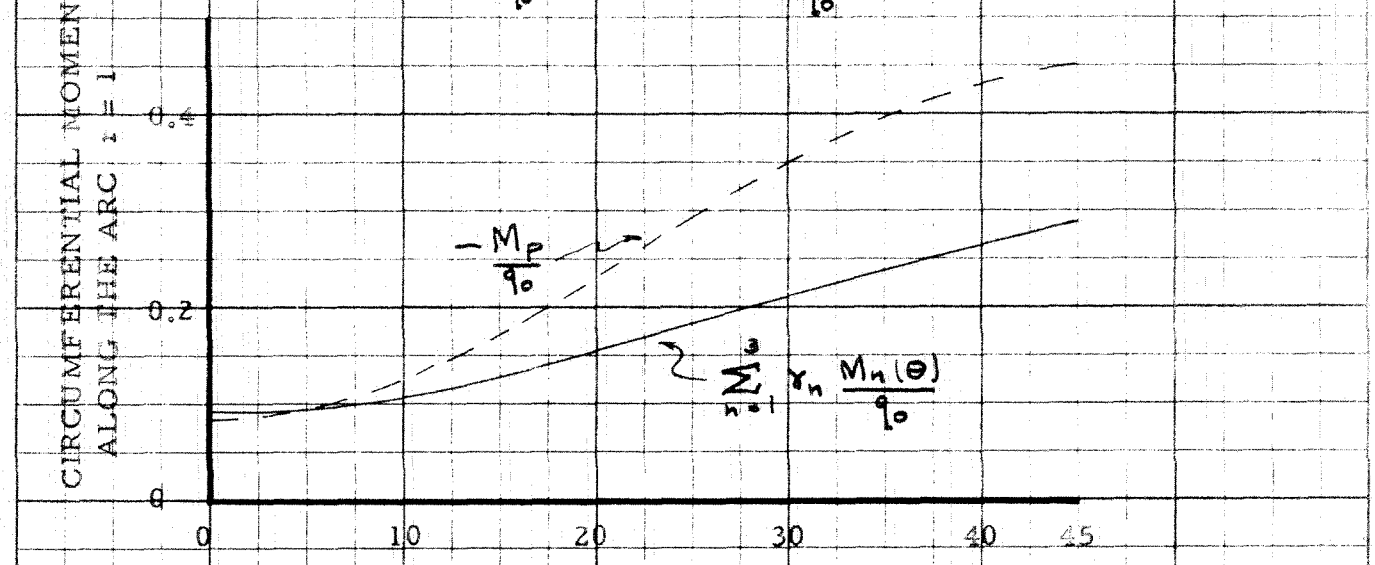

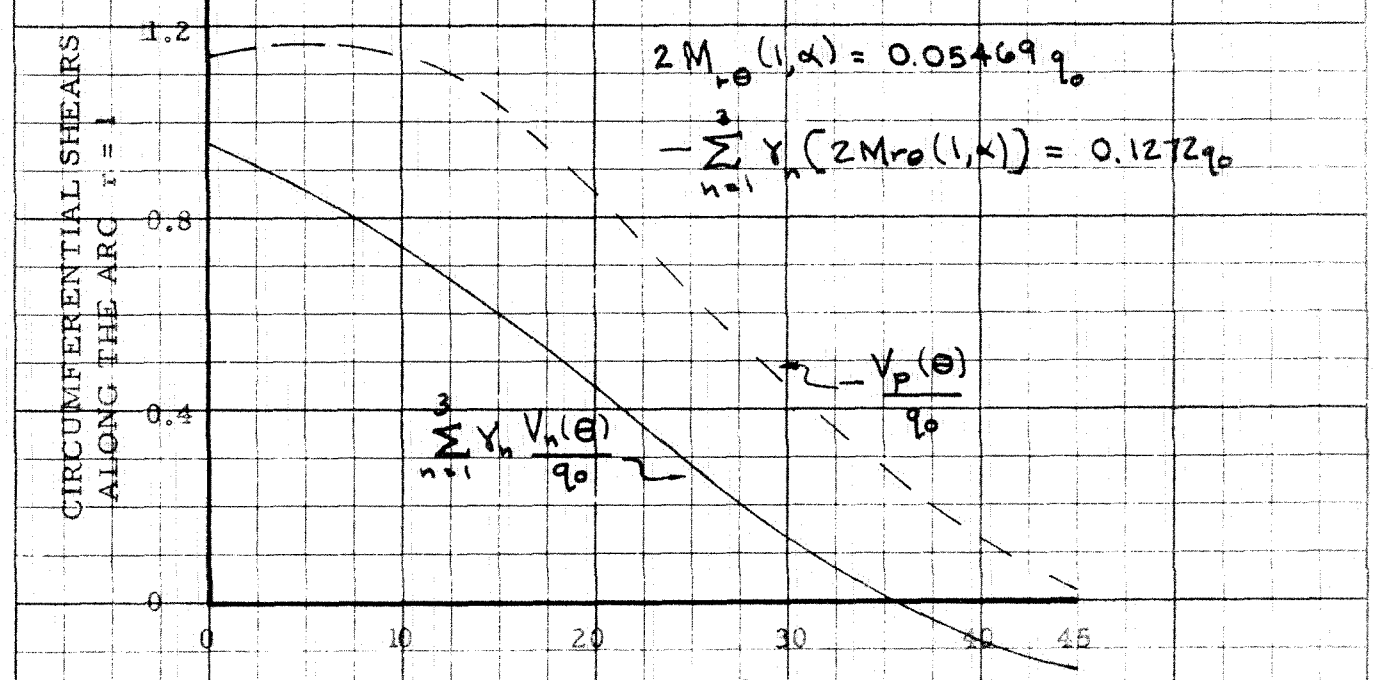

FIGURE 2

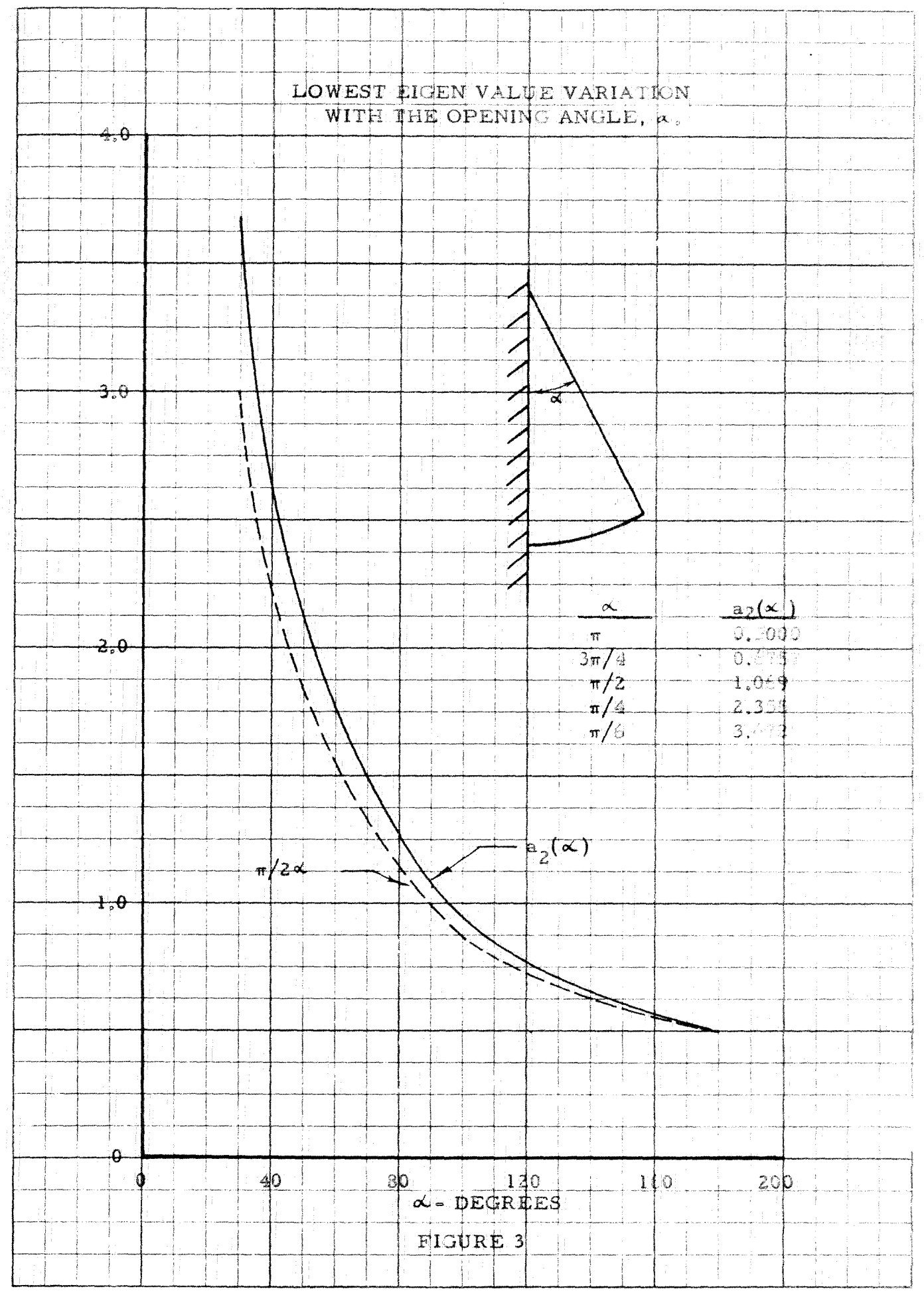
LOWEST EIGEN VALUE VARIATION
WITH THE OPENING ANGLE, α.
4.0
3.0
2.0
1.0
0
α
α a2(α)
π 0.5000
3π/4 0.7[illegible]
π/2 1.0[illegible]
π/4 2.35[illegible]
π/6 3.[illegible]
a2(α)
π/2α
0
40
80
120
160
200
α - DEGREES

FIGURE 3

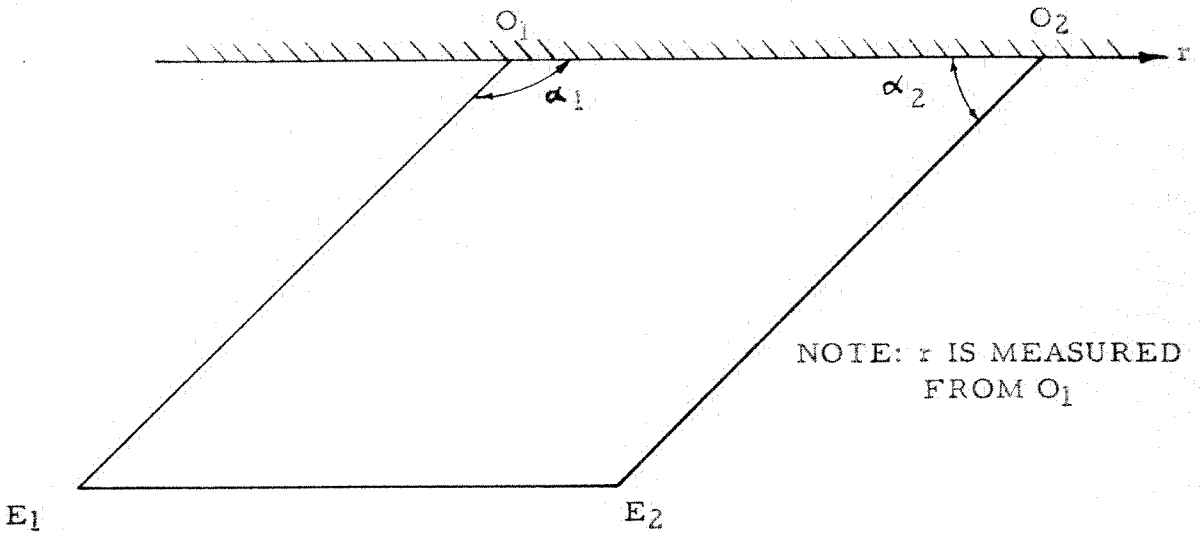

FIGURE 4

NOTATION FOR A SWEPT RECTANGULAR PLATE

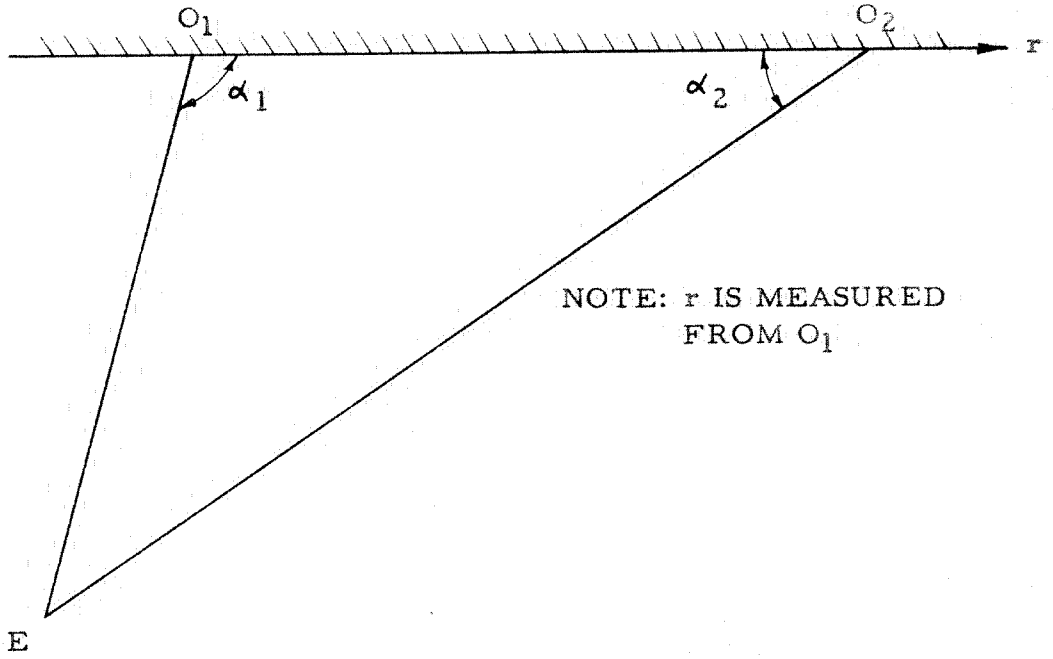

FIGURE 5

NOTATION FOR A TRIANGULAR PLATE

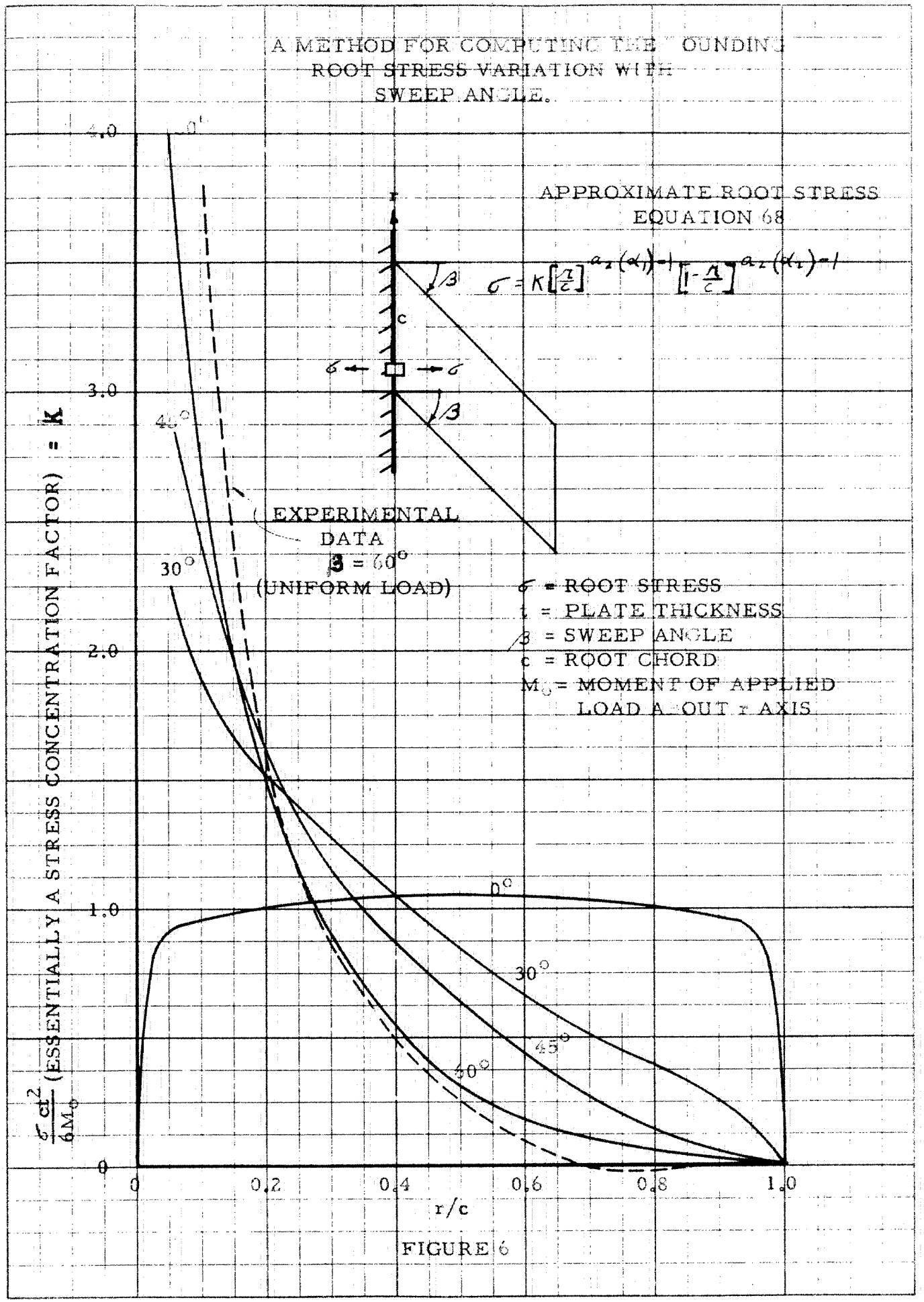
A METHOD FOR COMPUTING THE BOUNDING ROOT STRESS VARIATION WITH SWEEP ANGLE.
APPROXIMATE ROOT STRESS EQUATION 68
$\sigma = K\left[\frac{t}{c}\right]^{a_2(\alpha_1)-1}\left[1-\frac{r}{c}\right]^{a_2(\alpha_1)-1}$
EXPERIMENTAL DATA
$\beta = 60^\circ$
(UNIFORM LOAD)
σ = ROOT STRESS
t = PLATE THICKNESS
β = SWEEP ANGLE
c = ROOT CHORD
M_o = MOMENT OF APPLIED LOAD A OUT r AXIS
$\frac{\sigma ct^2}{6M_o}$ (ESSENTIALLY A STRESS CONCENTRATION FACTOR) = K
r/c
0°
30°
45°
60°
0
0.2
0.4
0.6
0.8
1.0
2.0
3.0
4.0

FIGURE 6

THEORETICAL EFFECT OF TRAILING EDGE SWEEP ANGLE UPON ROOT STRESS VARIATION.

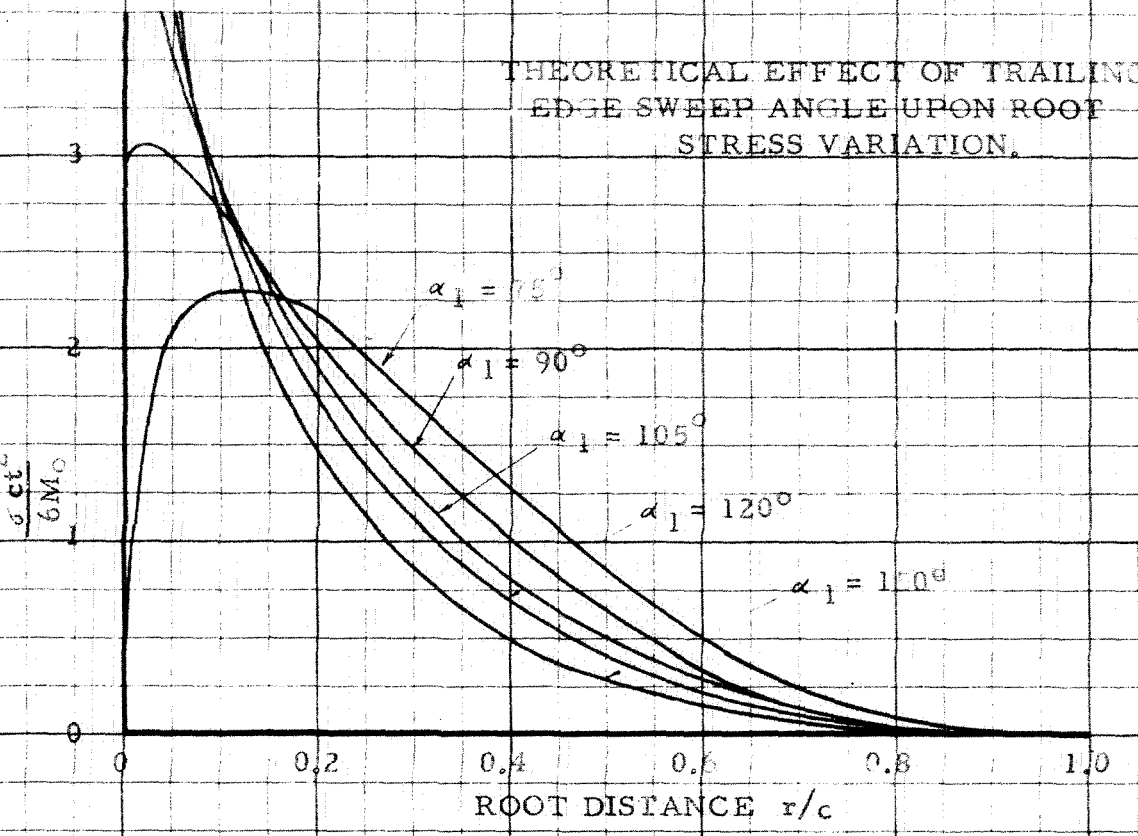

FIGURE 7

EXPERIMENTAL EFFECT OF TRAILING EDGE SWEEP ANGLE UPON ROOT STRESS VARIATION FOR TIP LOAD. (TAKEN FROM REF. 13)

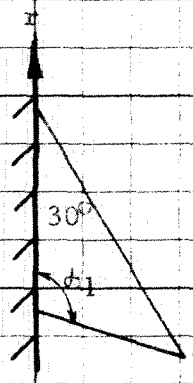

FIGURE 8

COMPARISON OF EXPERIMENTAL AND THEORETICAL ROOT STRESS VARIATION FOR TIP LOAD, $\alpha_1 = 75°$

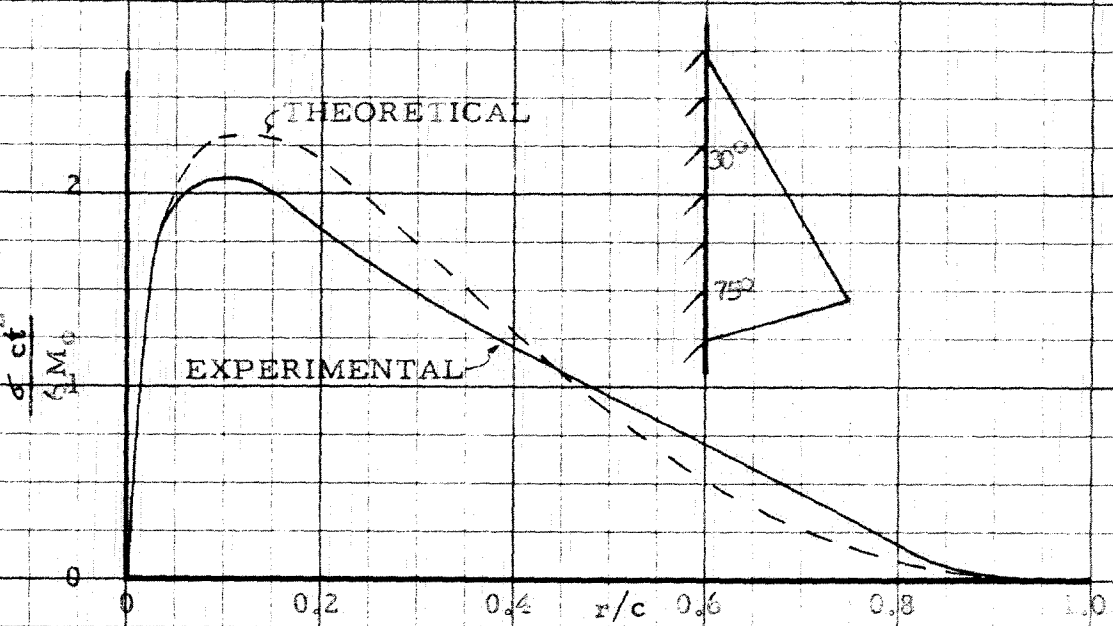

FIGURE 9

COMPARISON OF EXPERIMENTAL AND THEORETICAL ROOT STRESS VARIATION FOR TIP LOAD, $\alpha_1 = 90°$

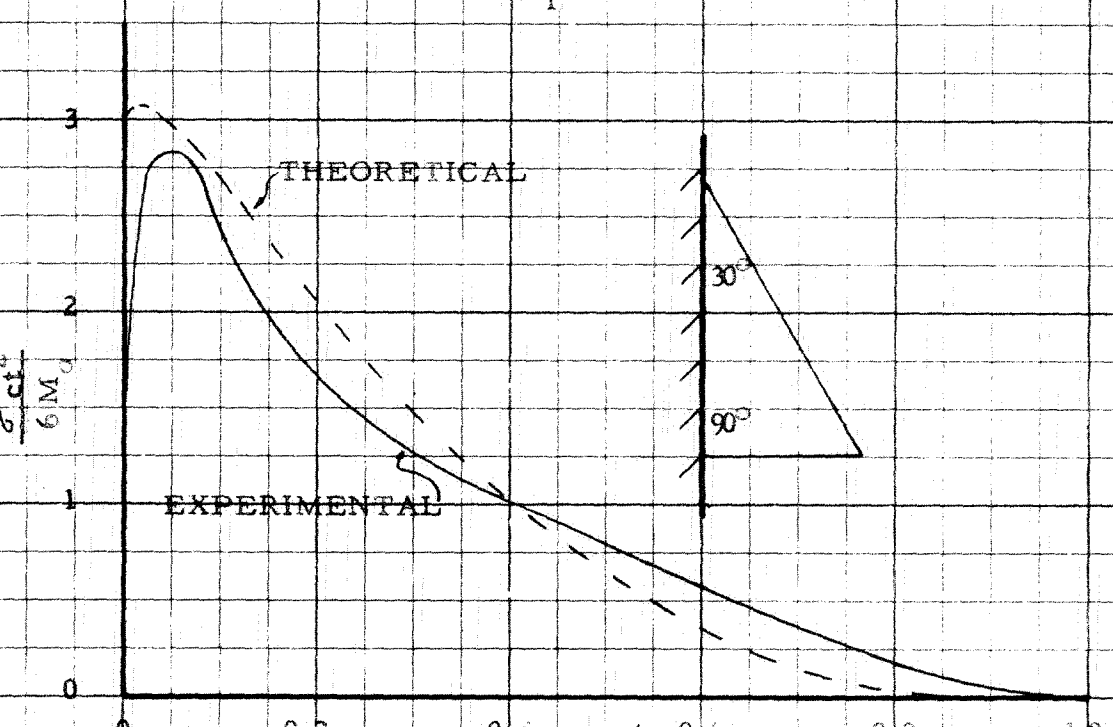

FIGURE 10

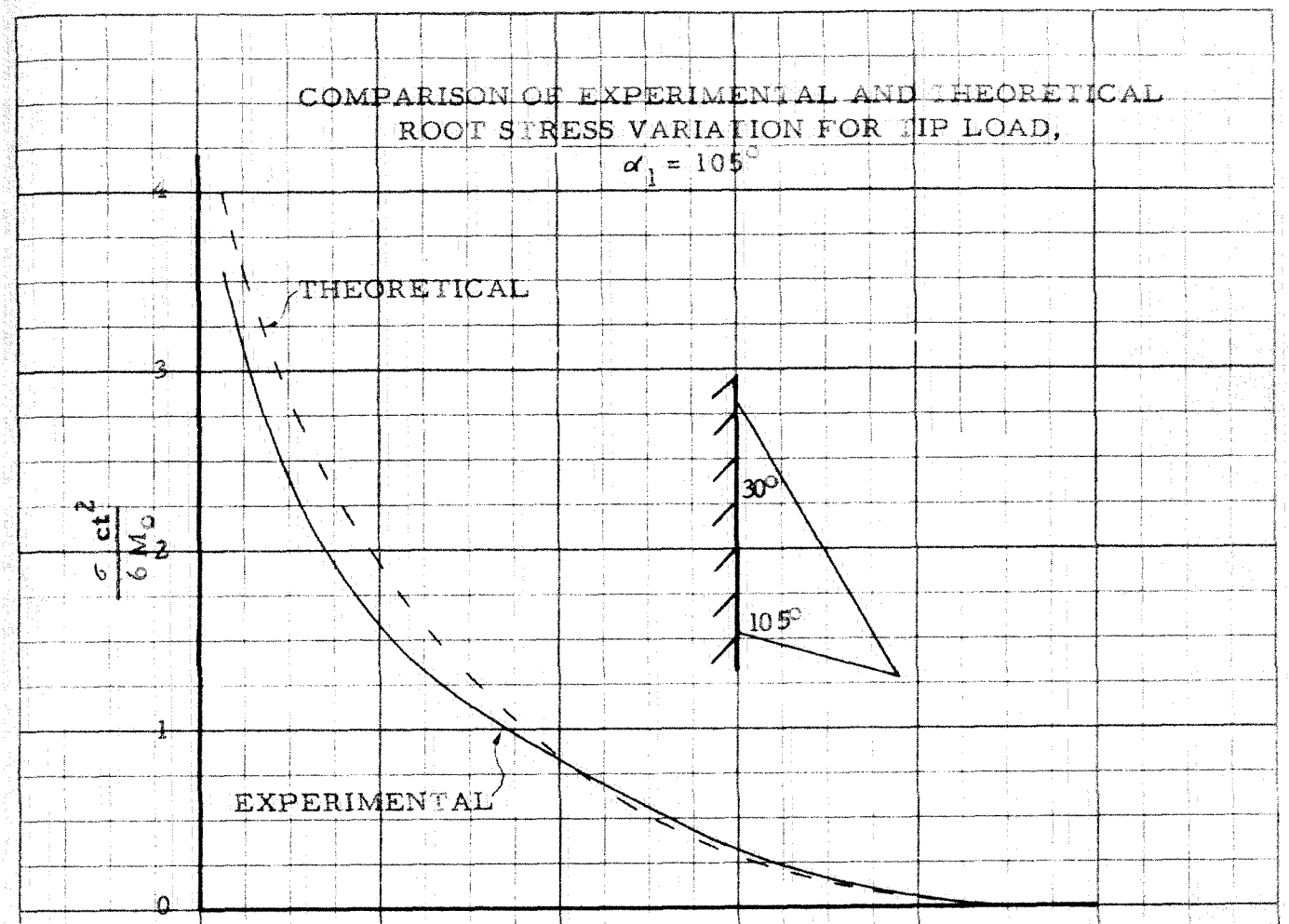

FIGURE 11

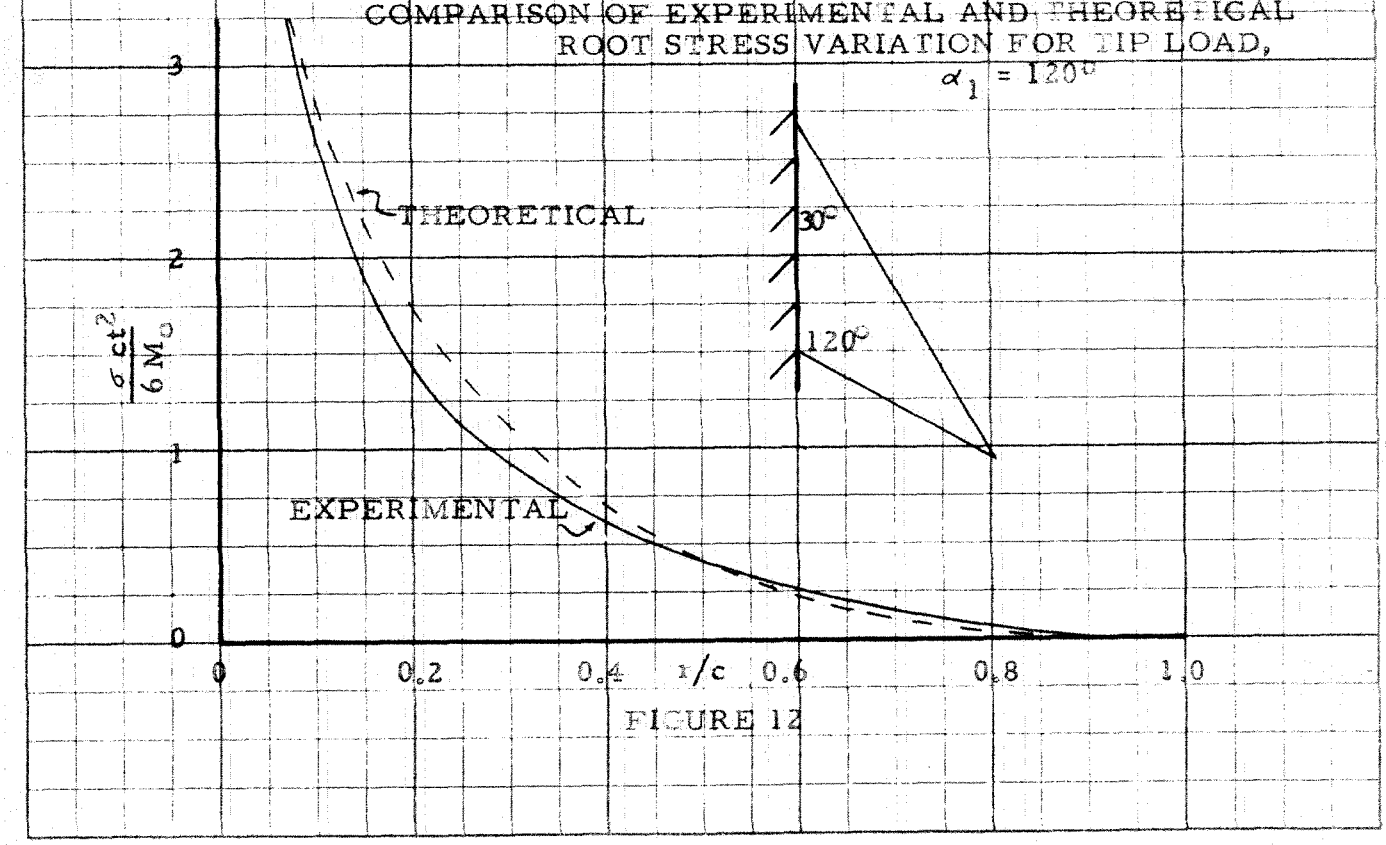

FIGURE 12

COMPARISON OF EXPERIMENTAL AND THEORETICAL ROOT STRESS VARIATION FOR TIP LOAD, $\alpha_1 = 150^\circ$

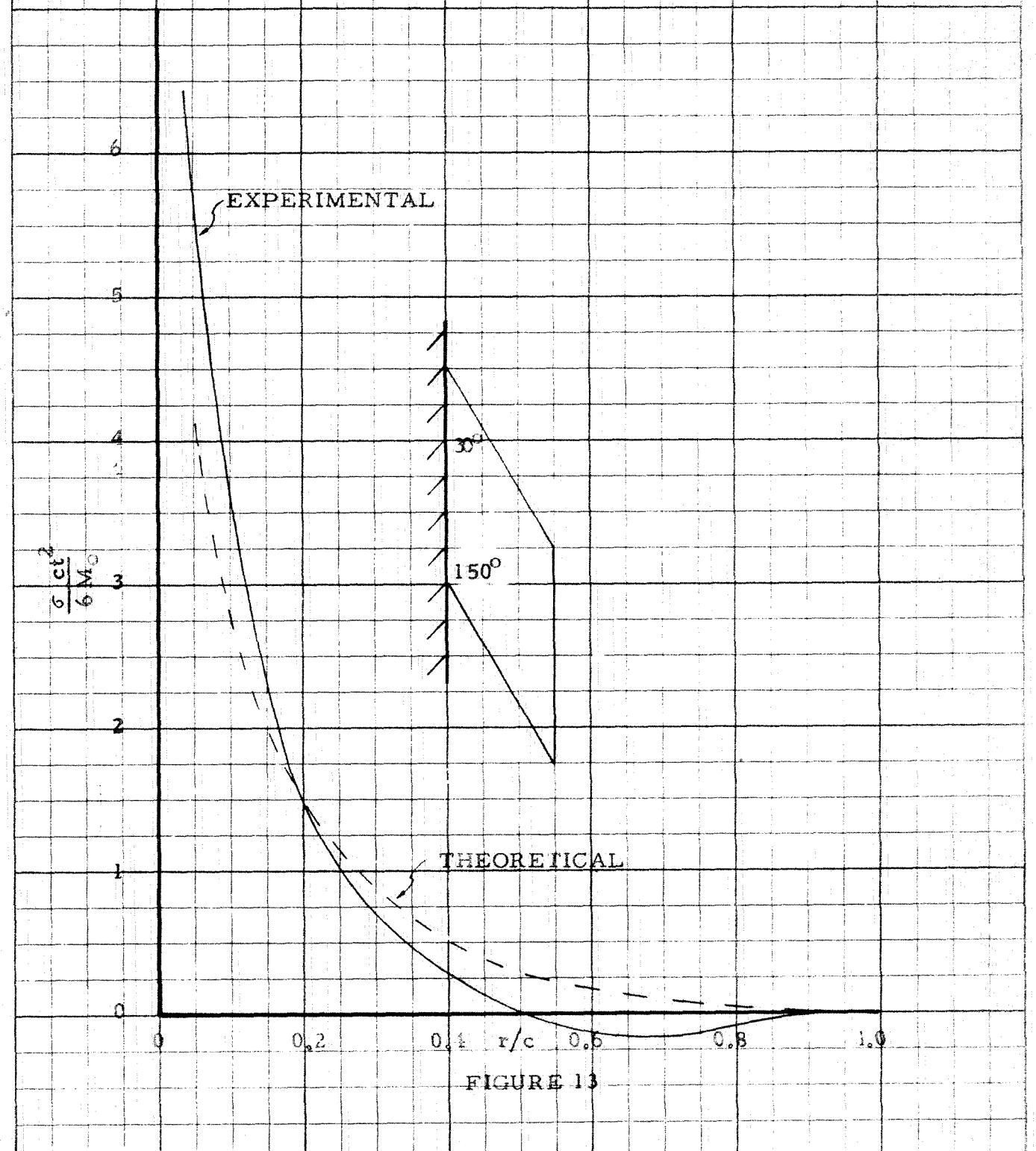

FIGURE 13

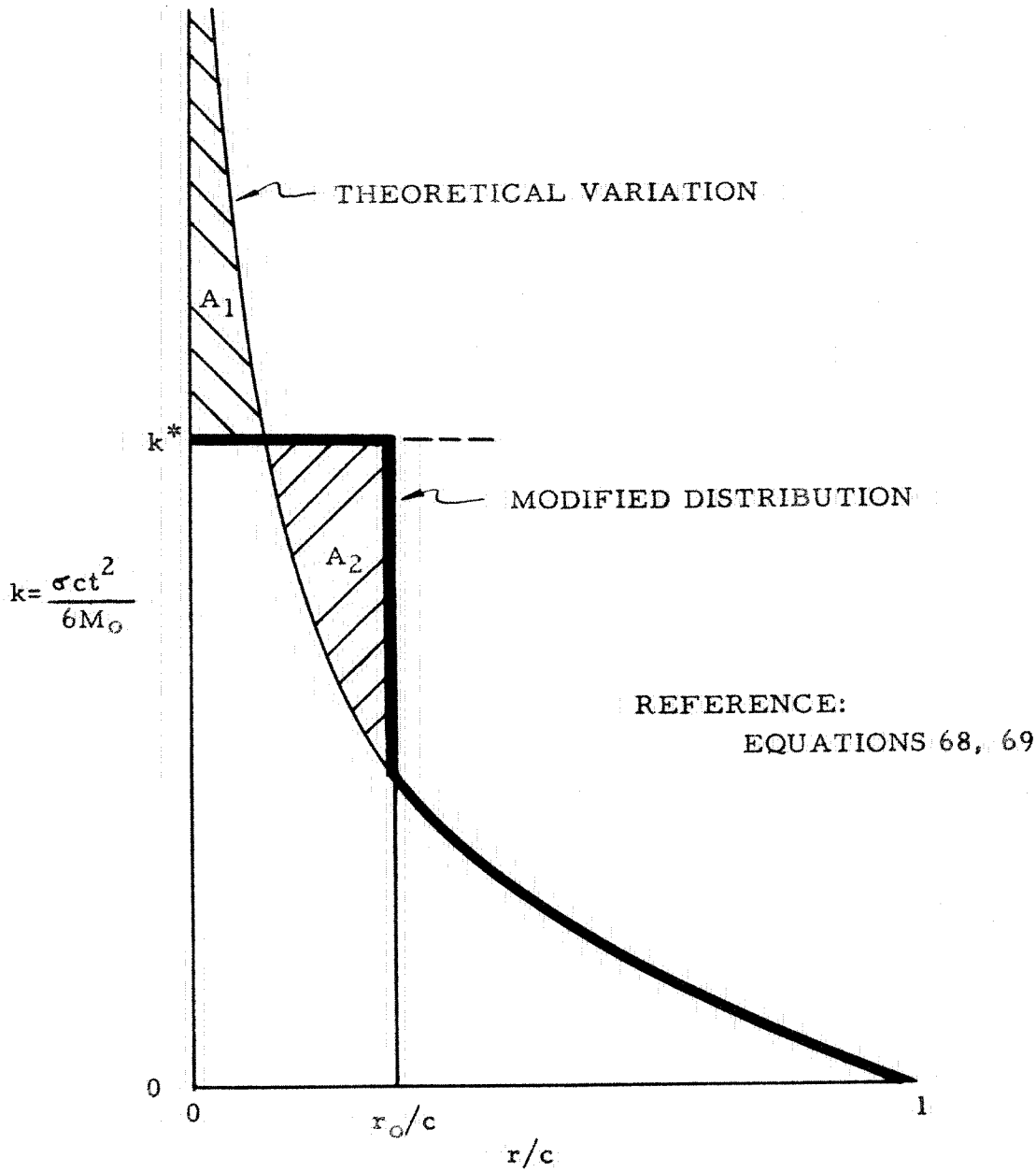

FIGURE 14

MODIFIED DESIGN CURVE

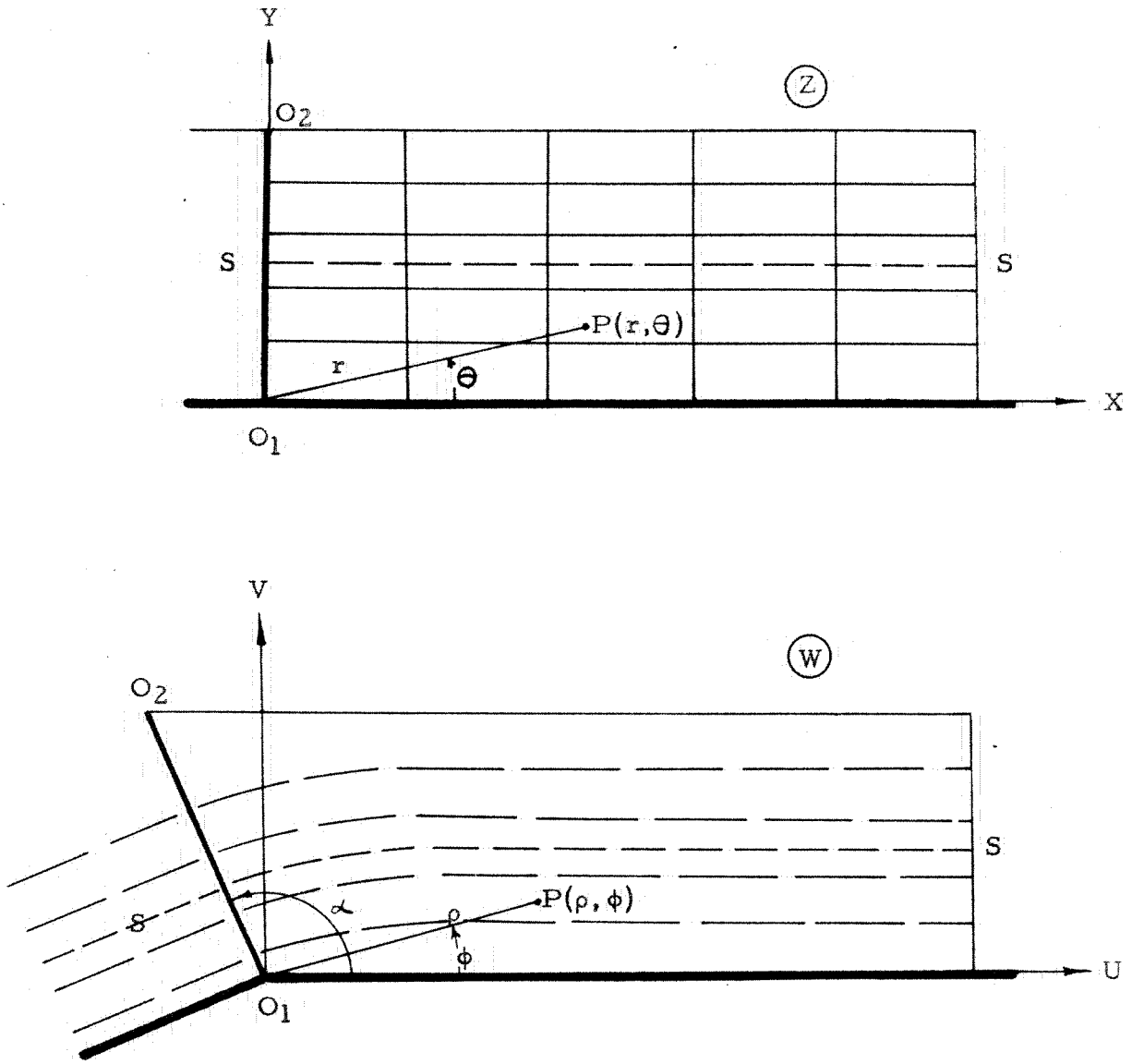

FIGURE 15

COORDINATE SYSTEM FOR THE FLOW ANALOGY

EXPLANATORY NOTE FOR FIGURES 16 THROUGH 42

The figures which follow present the plate deflections and characteristic and support loads for selected values of the opening angle. As an illustration of the typical eigen deflections and load distribution along the supported edge OA (Figure 1) and the circumferential edge AB (Figure 1), a few calculations have been made, taking the value of Poisson's Ratio $\upsilon = 0.3$, for values of the opening angle, namely, $\alpha = \pi/4, \pi/2, 3\pi/4$, and π.

The first few eigen values λ_n and the corresponding eigen constants A_n and B_n have been tabulated in Table I.

The quantities shown in the following graphs, along with the applicable reference equation are as follows:

Quantity	Reference Equation
Deflection along AB	24, 25
Shear $V_r(\theta)$ along AB	42, 42a
Moment $M_r(\theta)$ along AB	43, 43a
Deflection along OB	24, 25
Root Shear $V_\theta(r)$ along OA	53, 53a
Root Moment $M_\theta(r)$ along OA	54, 54a
Concentrated load $2M_{r\theta}(1,\theta)$ at B	46, 46a

The quantities shown in the subsequent curves are intended for qualitative use only, as it has been found that for quantitative purposes much greater accuracy is required than is possible to present satisfactorily on graphs.

FIGURES 16-22

DEFLECTIONS AND LOADING CONDITIONS FOR THE

EIGEN FUNCTIONS FOR VARIOUS OPENING ANGLES

FOR THE CASE OF $\alpha' = \pi/4$

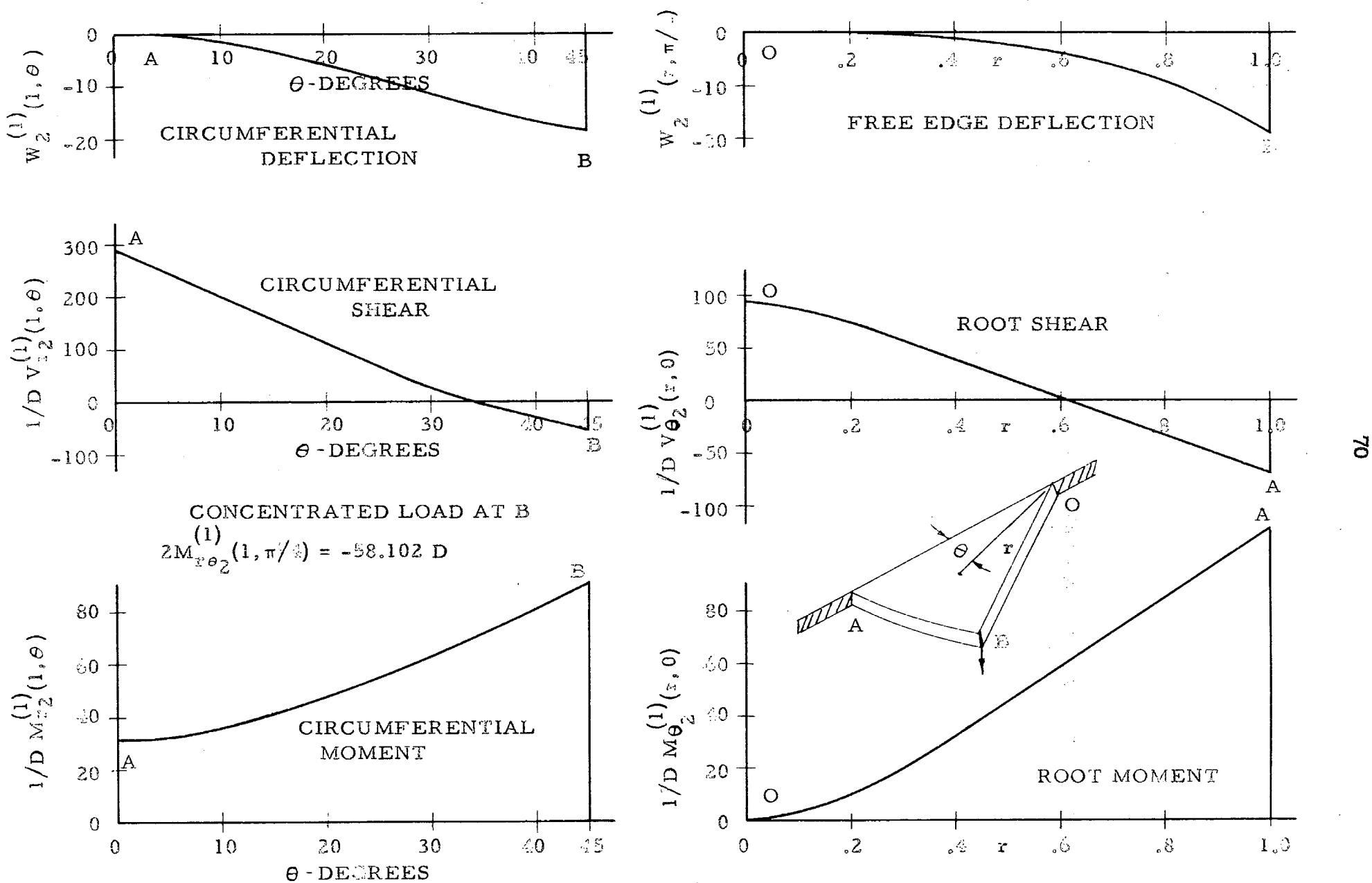

FIGURE 16

LOADING AND DEFLECTION FOR $W_2^{(1)}(r,\theta)$

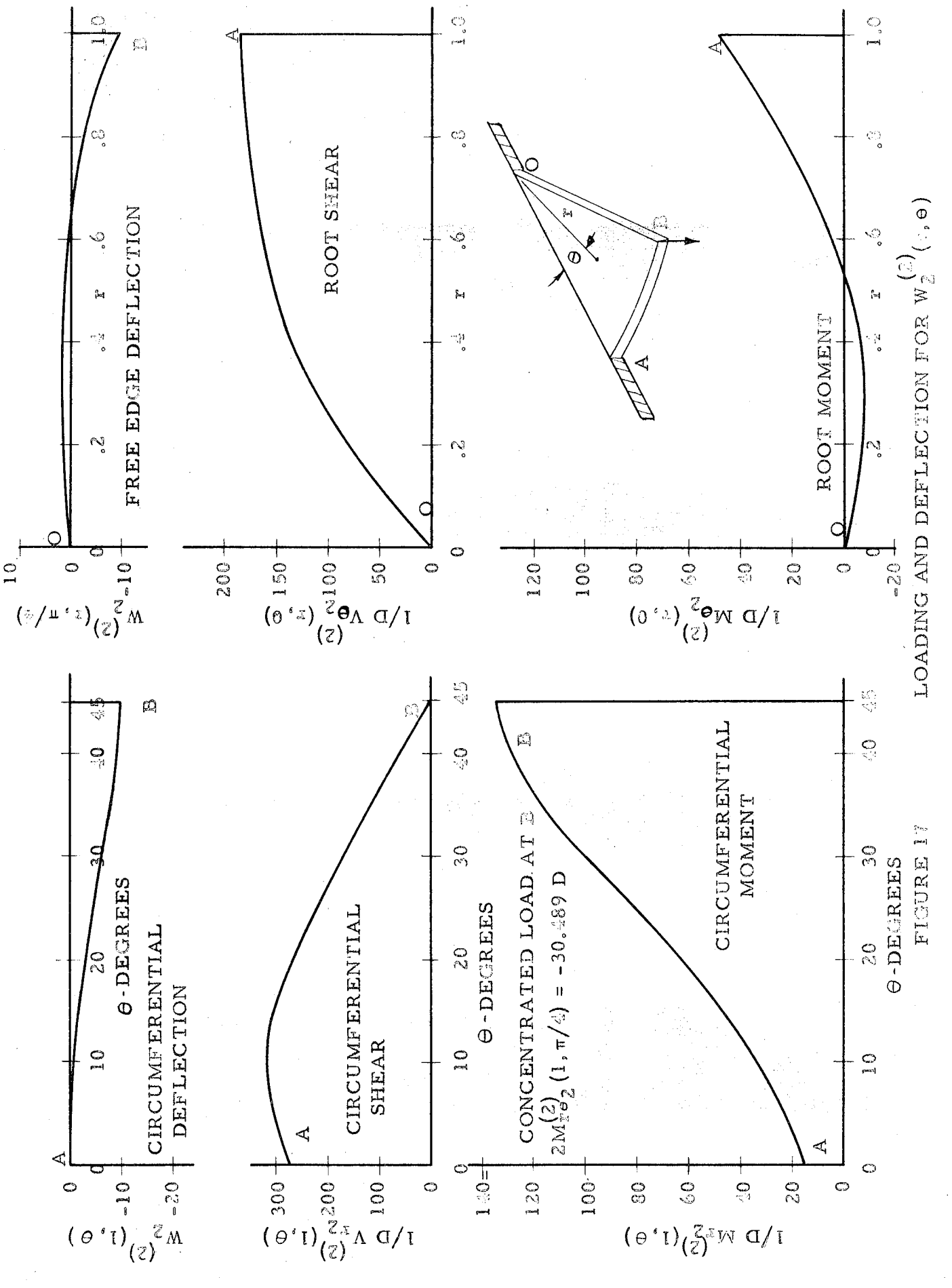

FIGURE 17 LOADING AND DEFLECTION FOR $W_2^{(2)}(\cdot,\theta)$

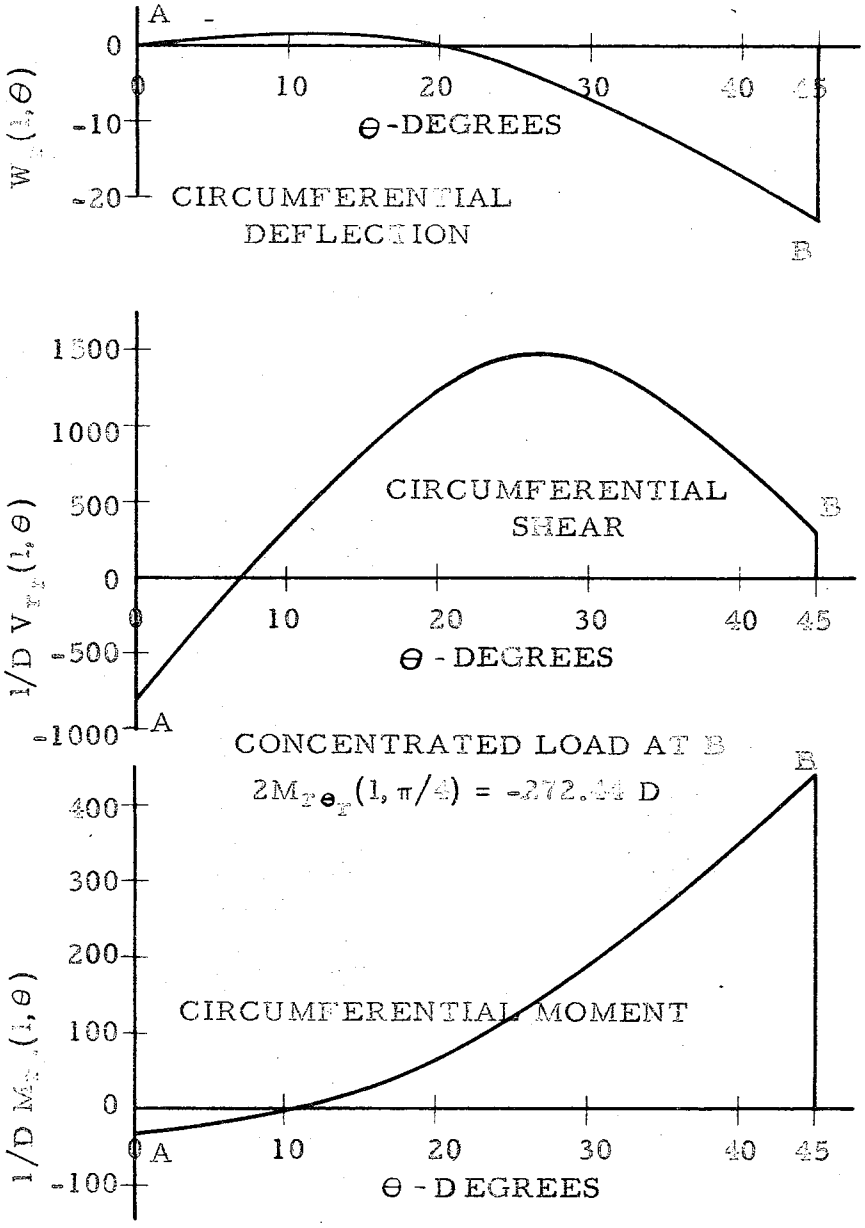

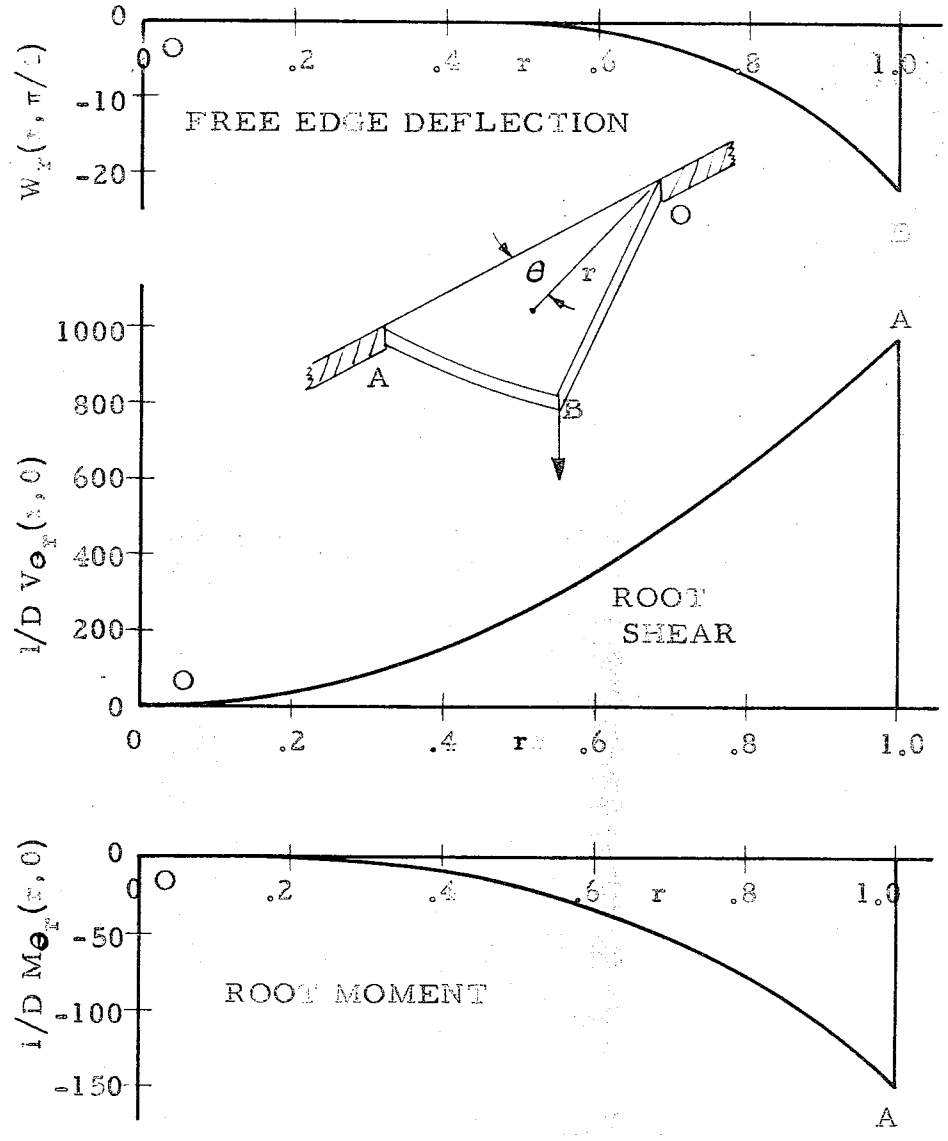

FIGURE 18

LOADING AND DEFLECTION FOR $W_r(r, \theta)$

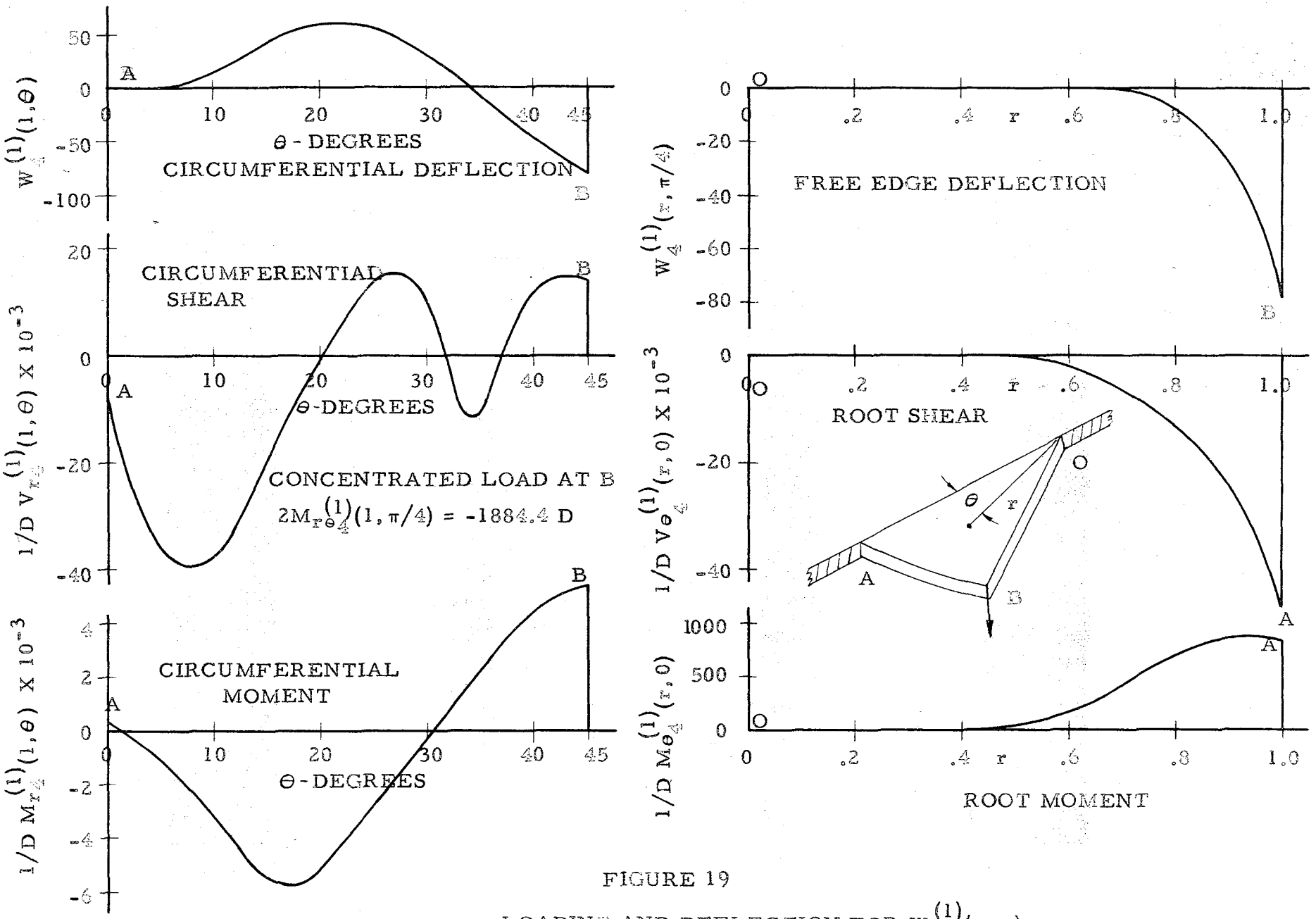

FIGURE 19

LOADING AND DEFLECTION FOR $W_4^{(1)}(r,\theta)$

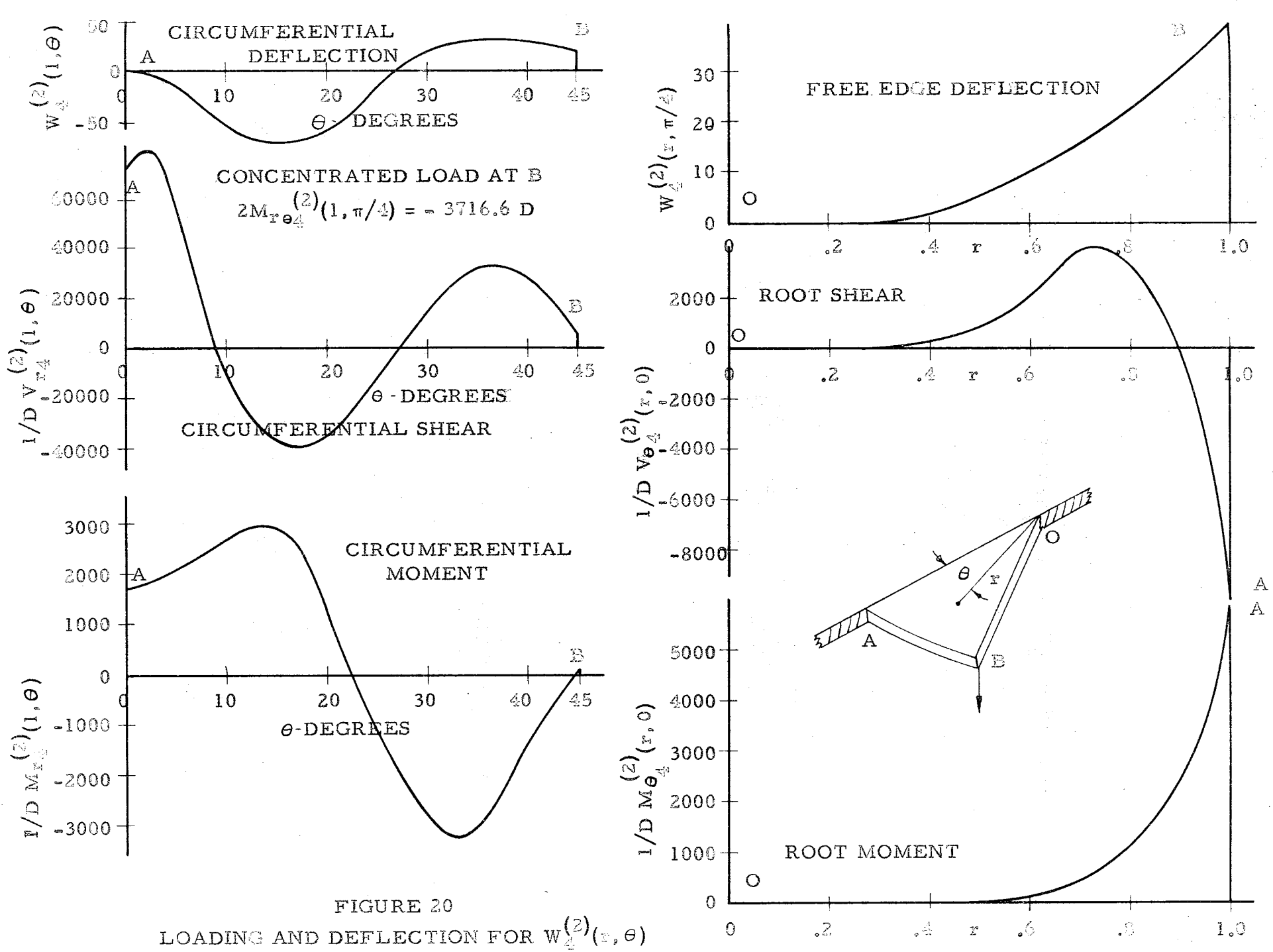

FIGURE 20

LOADING AND DEFLECTION FOR $W_4^{(2)}(r,\theta)$

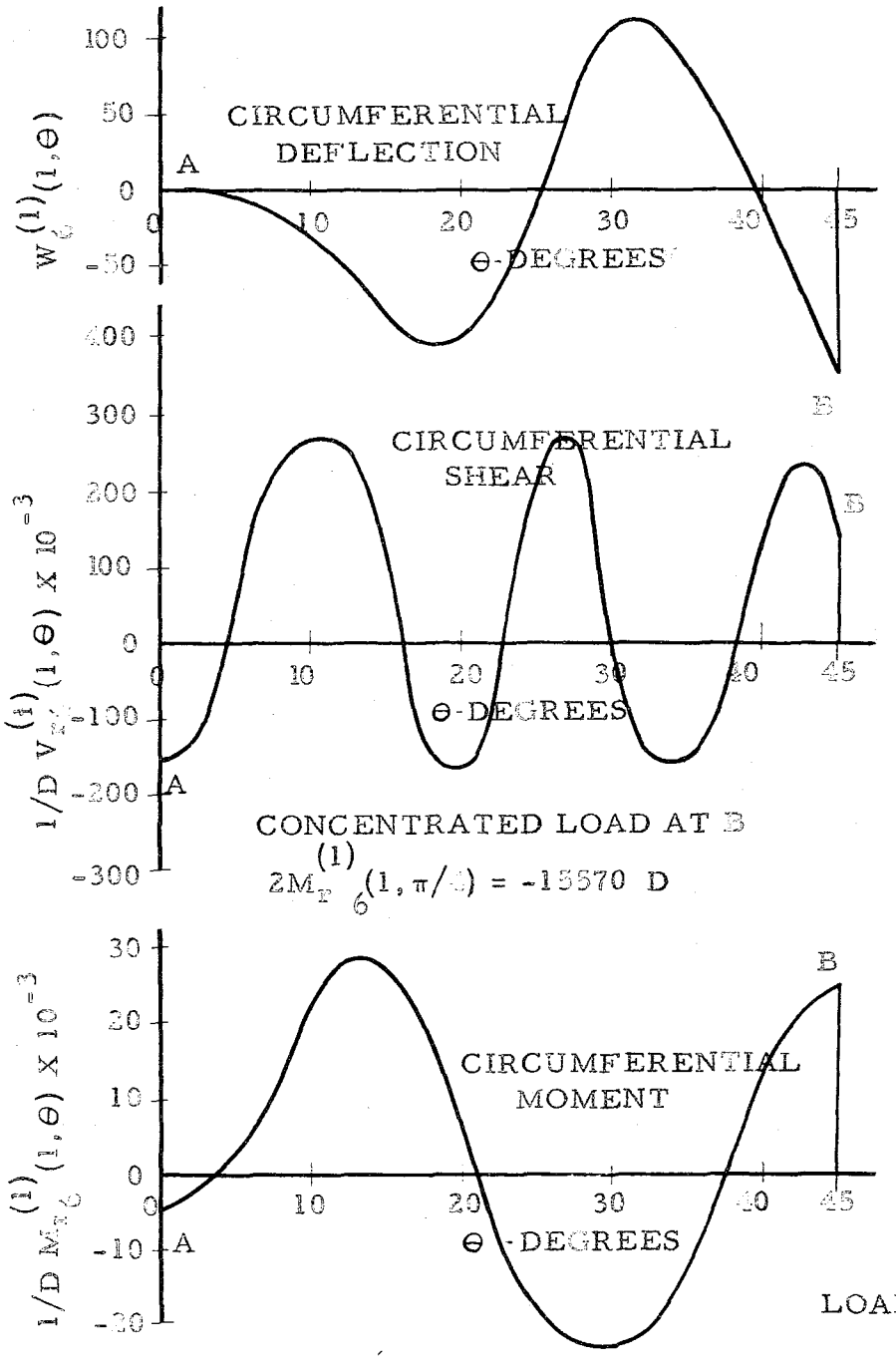

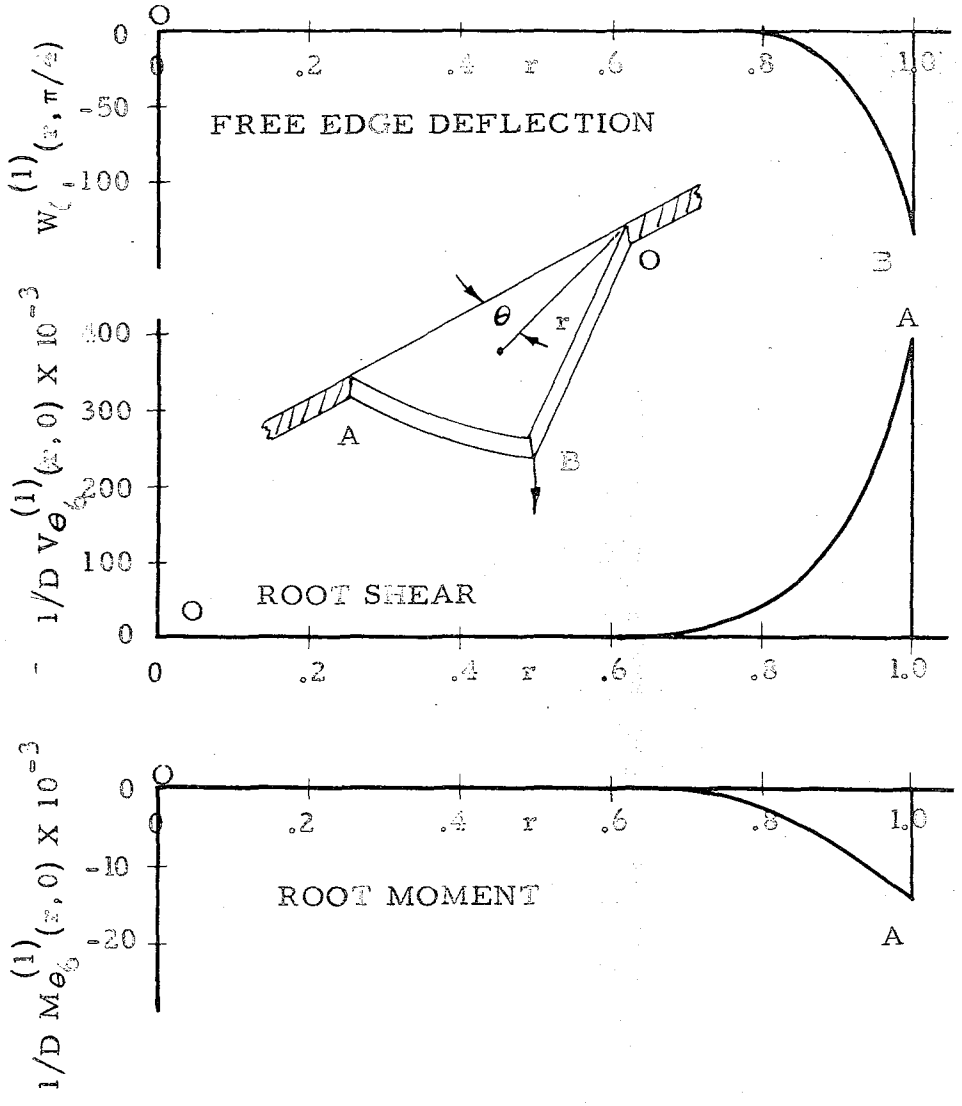

FIGURE 21

LOADING AND DEFLECTION FOR $W_6^{(1)}(r,\theta)$

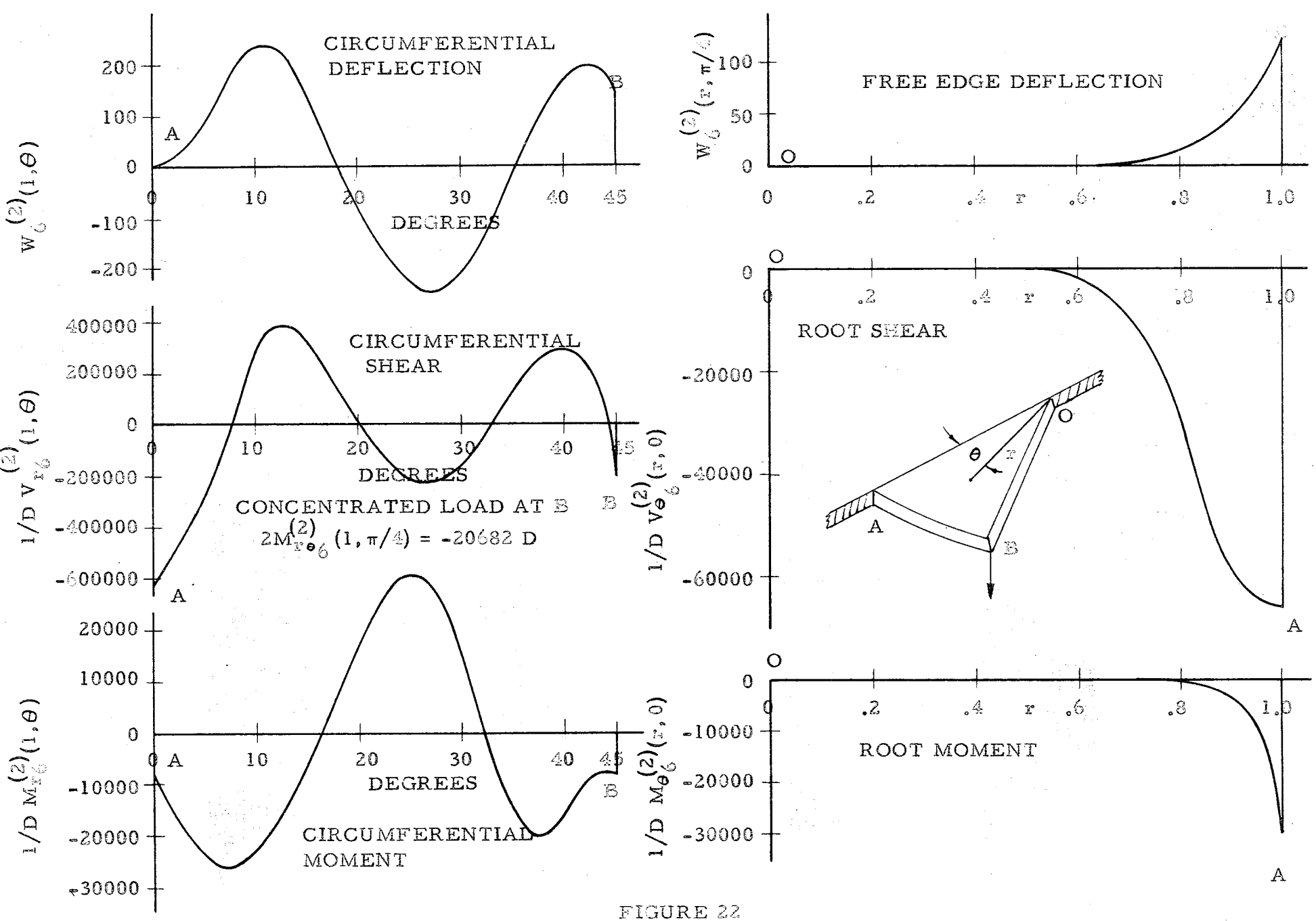

FIGURE 22

LOADING AND DEFLECTION FOR $W_6^{(2)}(r,\theta)$

FIGURES 23-29

DEFLECTIONS AND LOADING CONDITIONS FOR THE

EIGEN FUNCTIONS FOR VARIOUS OPENING ANGLES

FOR THE CASE OF $\alpha = \pi/2$

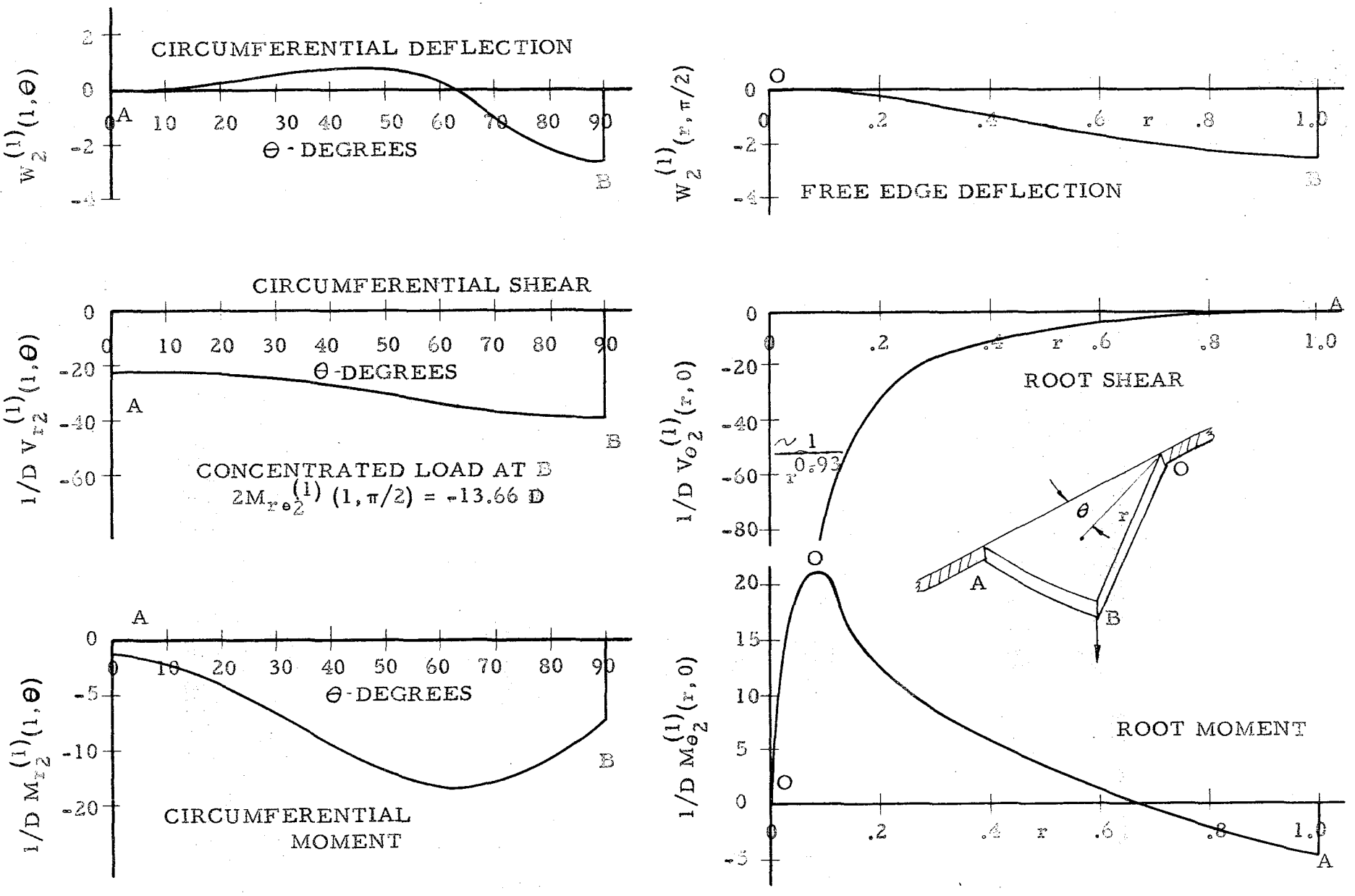

FIGURE 23

LOADING AND DEFLECTION FOR $W_2^{(1)}(r,\theta)$

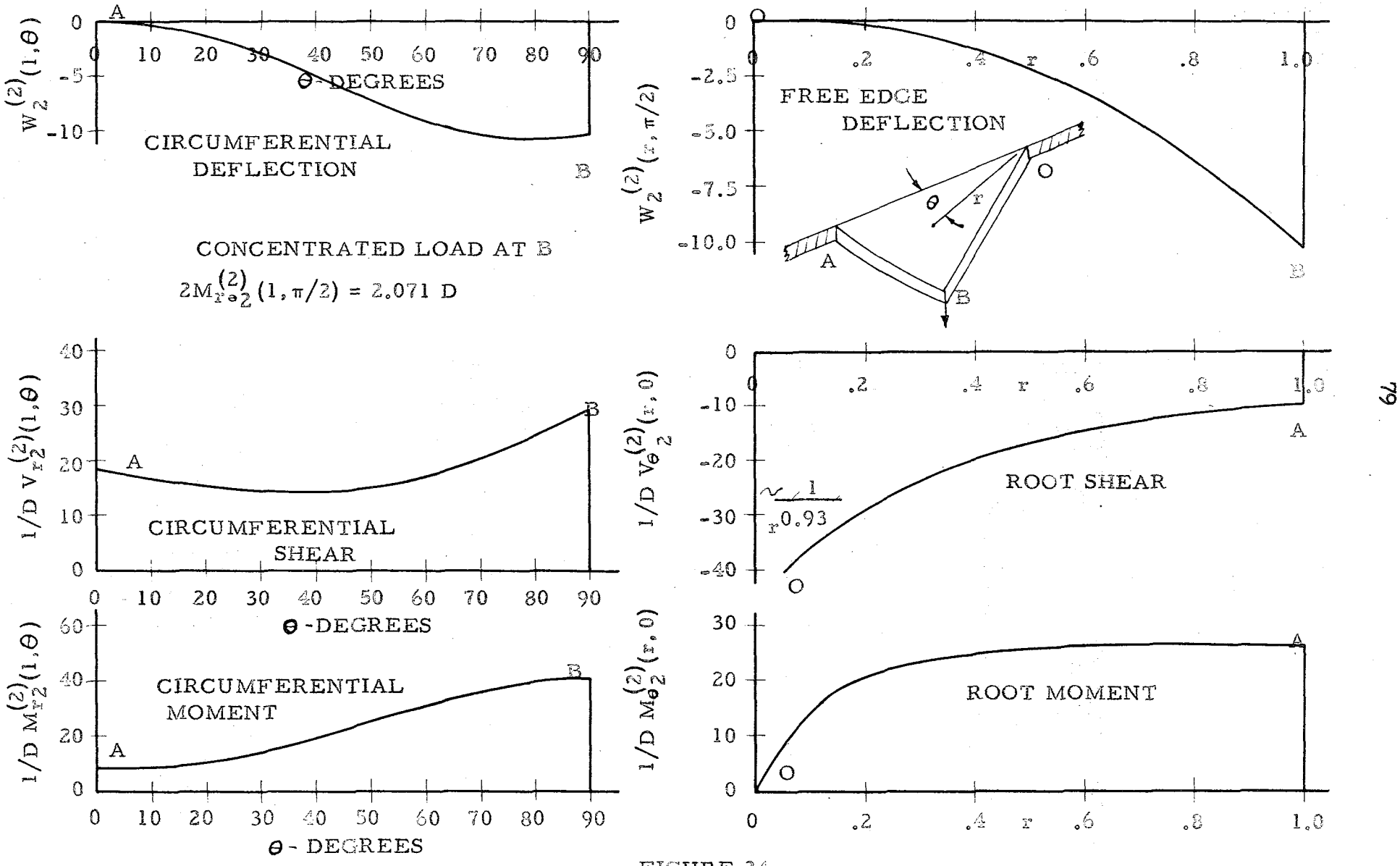

FIGURE 24

LOADING AND DEFLECTION FOR $W_2^{(2)}(r,\theta)$

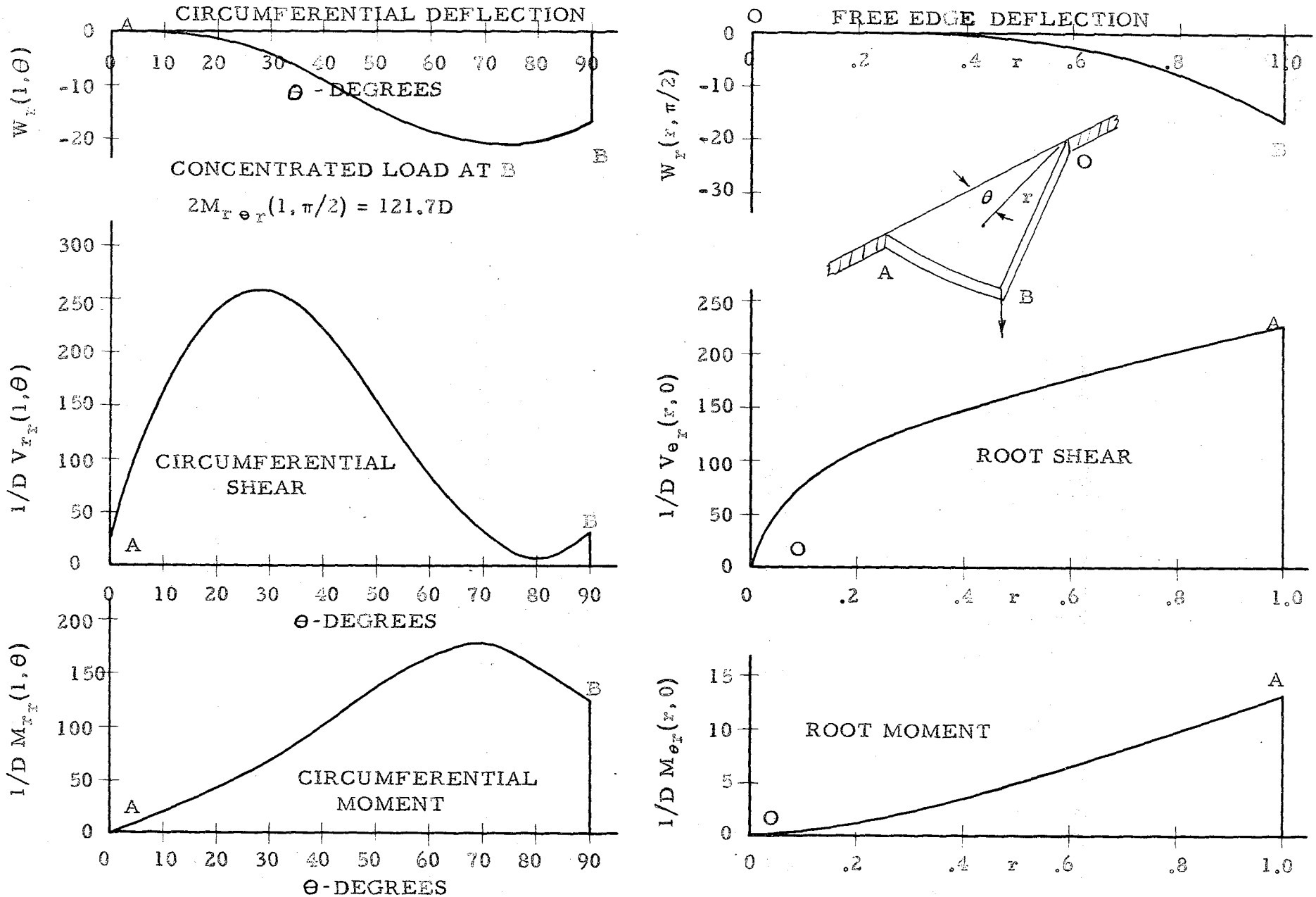

FIGURE 25

LOADING AND DEFLECTION FOR $W_r(r,\theta)$

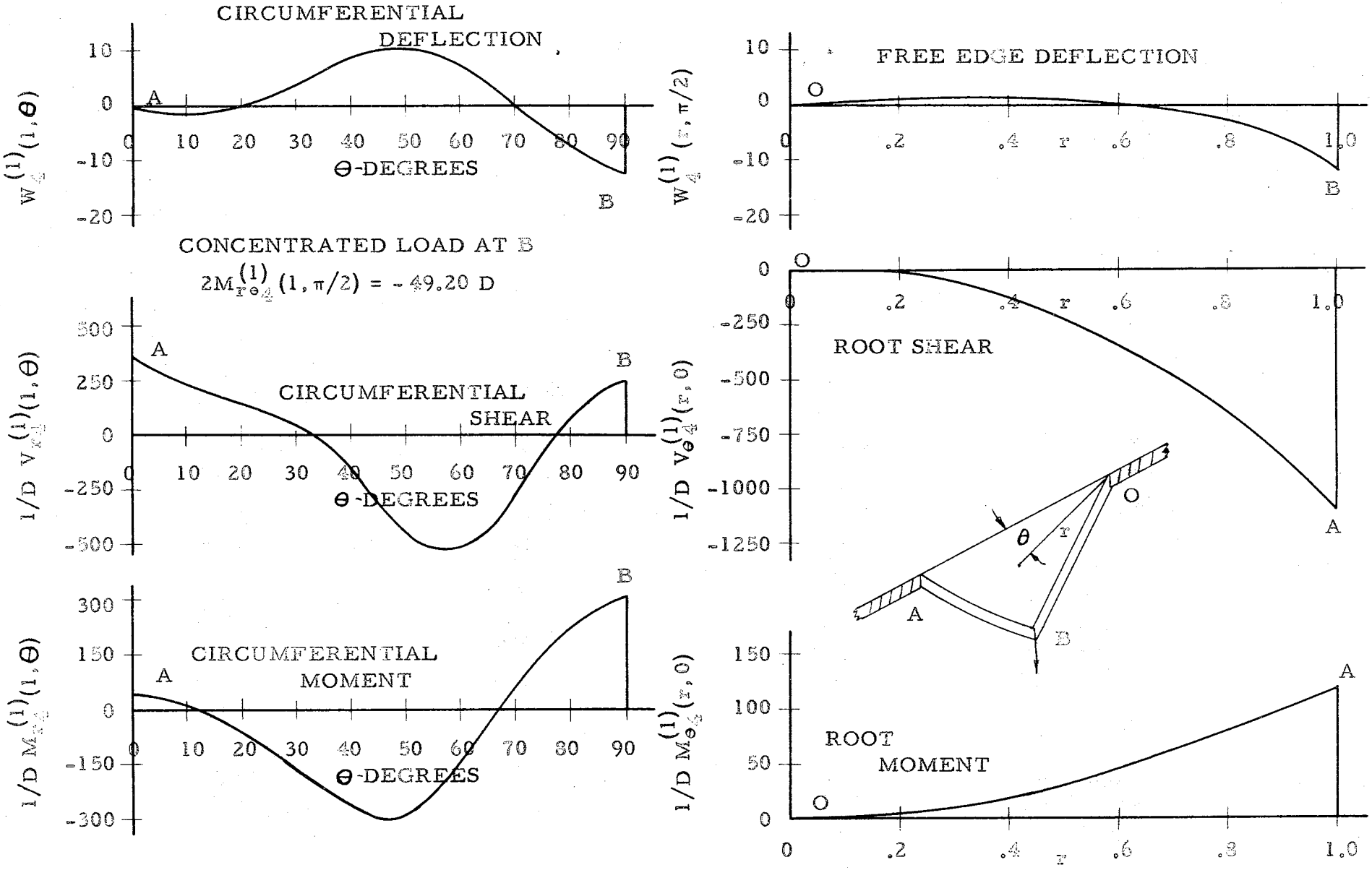

FIGURE 26

LOADING AND DEFLECTION FOR $W_{\frac{1}{4}}^{(1)}(r,\theta)$

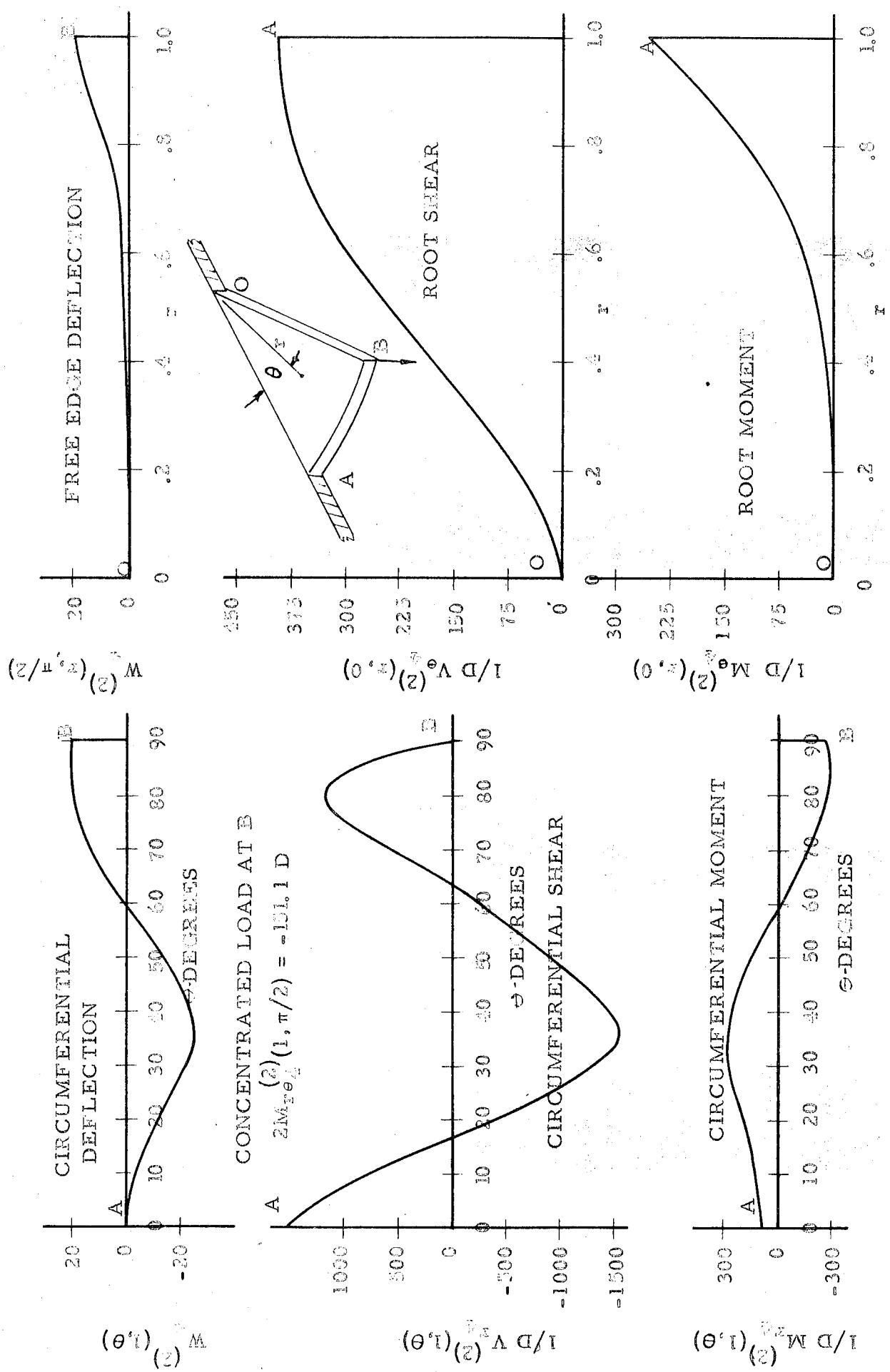

FIGURE 27

LOADING AND DEFLECTION FOR $W_2^{(2)}(r,\theta)$

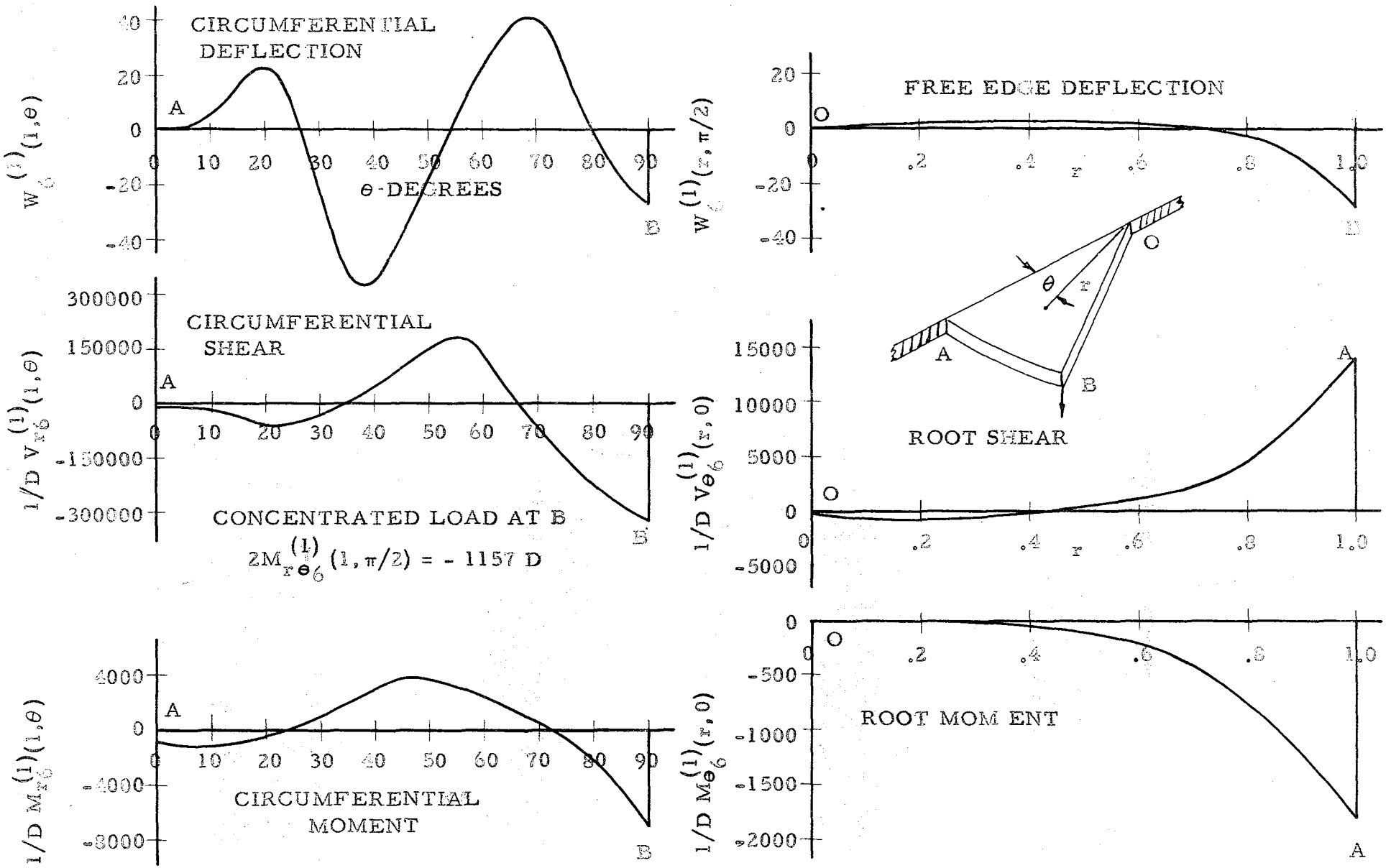

FIGURE 28

LOADING AND DEFLECTION FOR $W_6^{(1)}(r,\theta)$

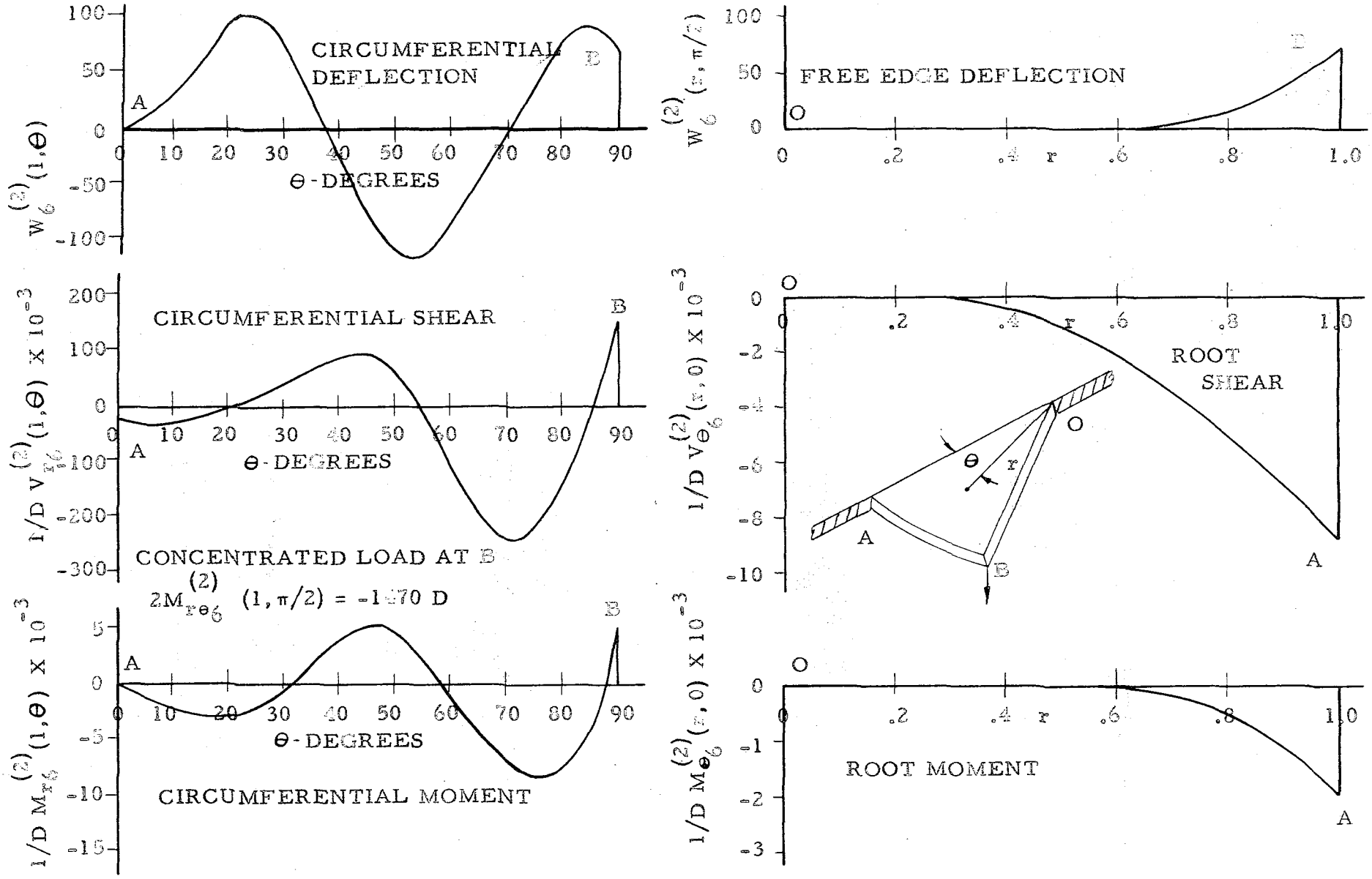

FIGURE 29

LOADING AND DEFLECTION FOR $W_6^{(2)}(r,\theta)$

FIGURES 30-36

DEFLECTIONS AND LOADING CONDITIONS FOR THE

EIGEN FUNCTIONS FOR VARIOUS OPENING ANGLES

FOR THE CASE OF $\alpha = 3\pi/4$

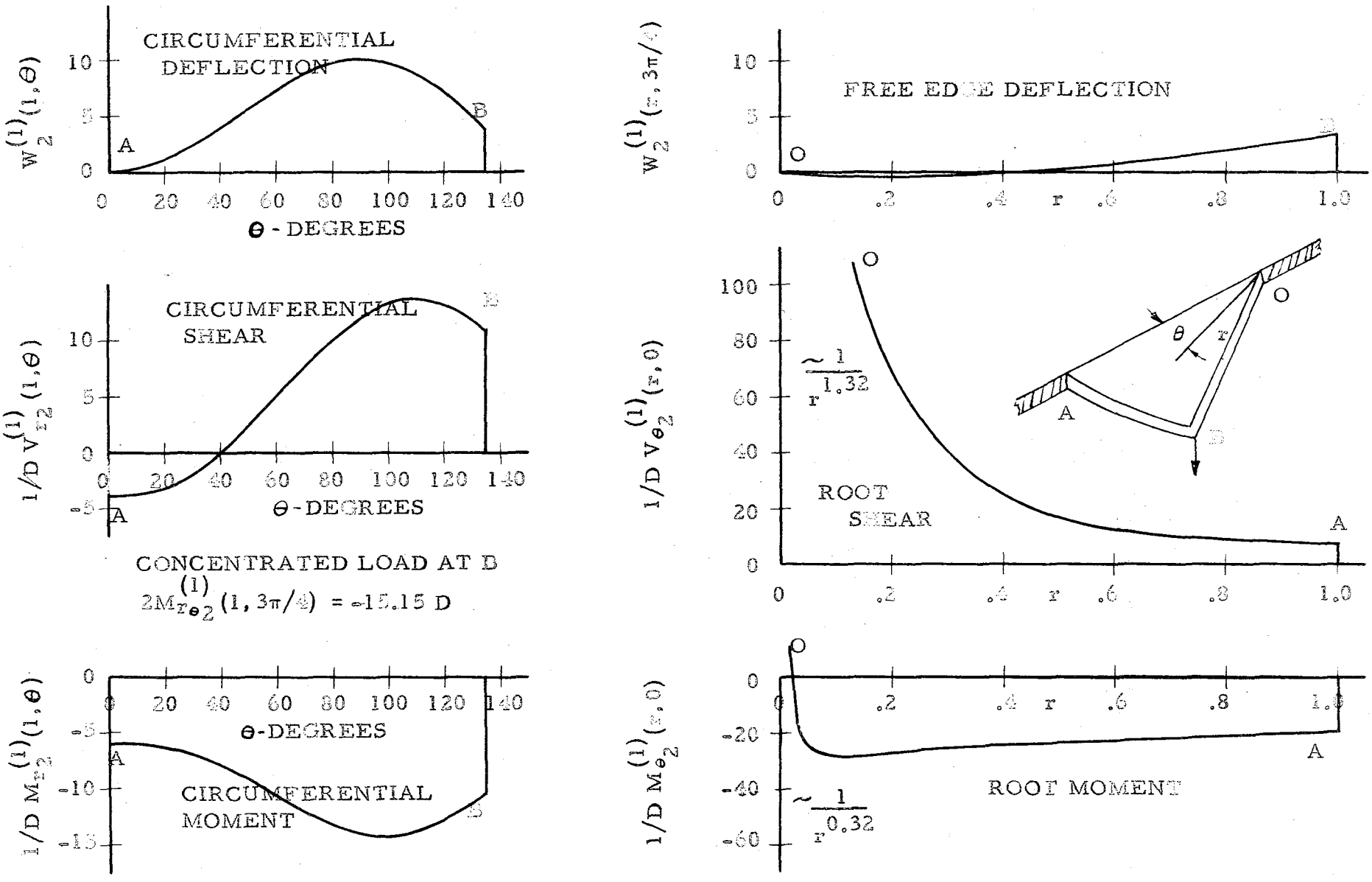

FIGURE 30

LOADING AND DEFLECTION FOR $W_2^{(1)}(r,\theta)$

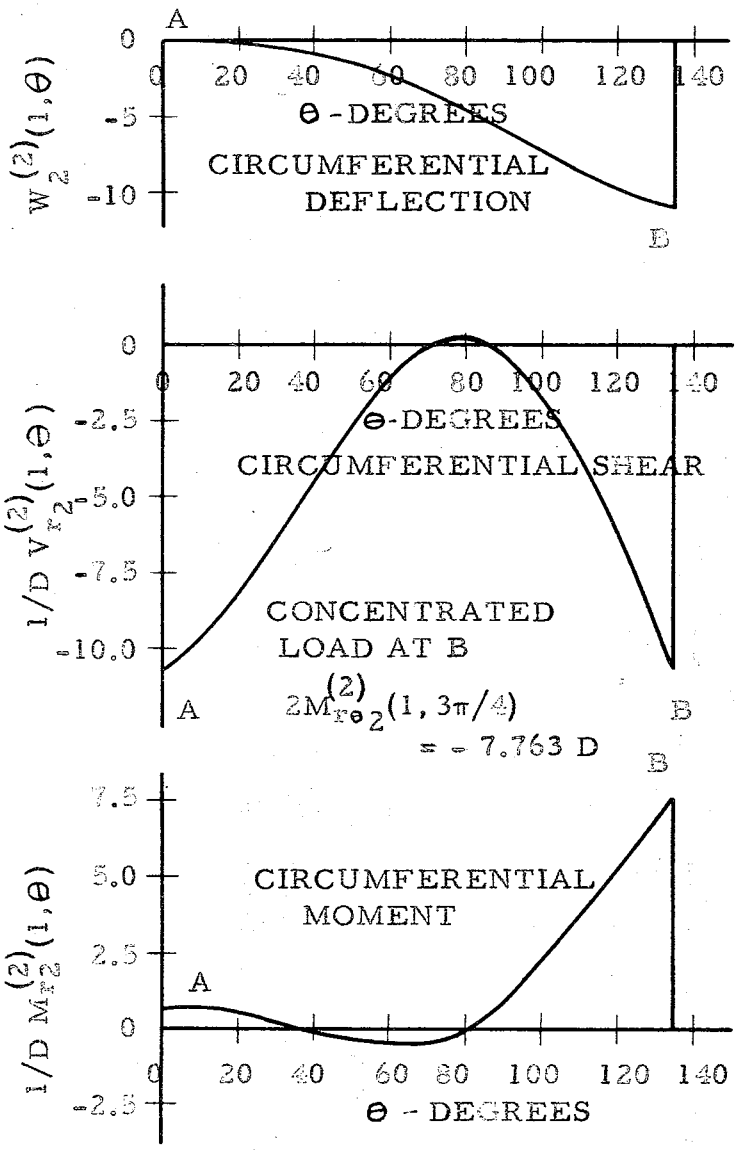

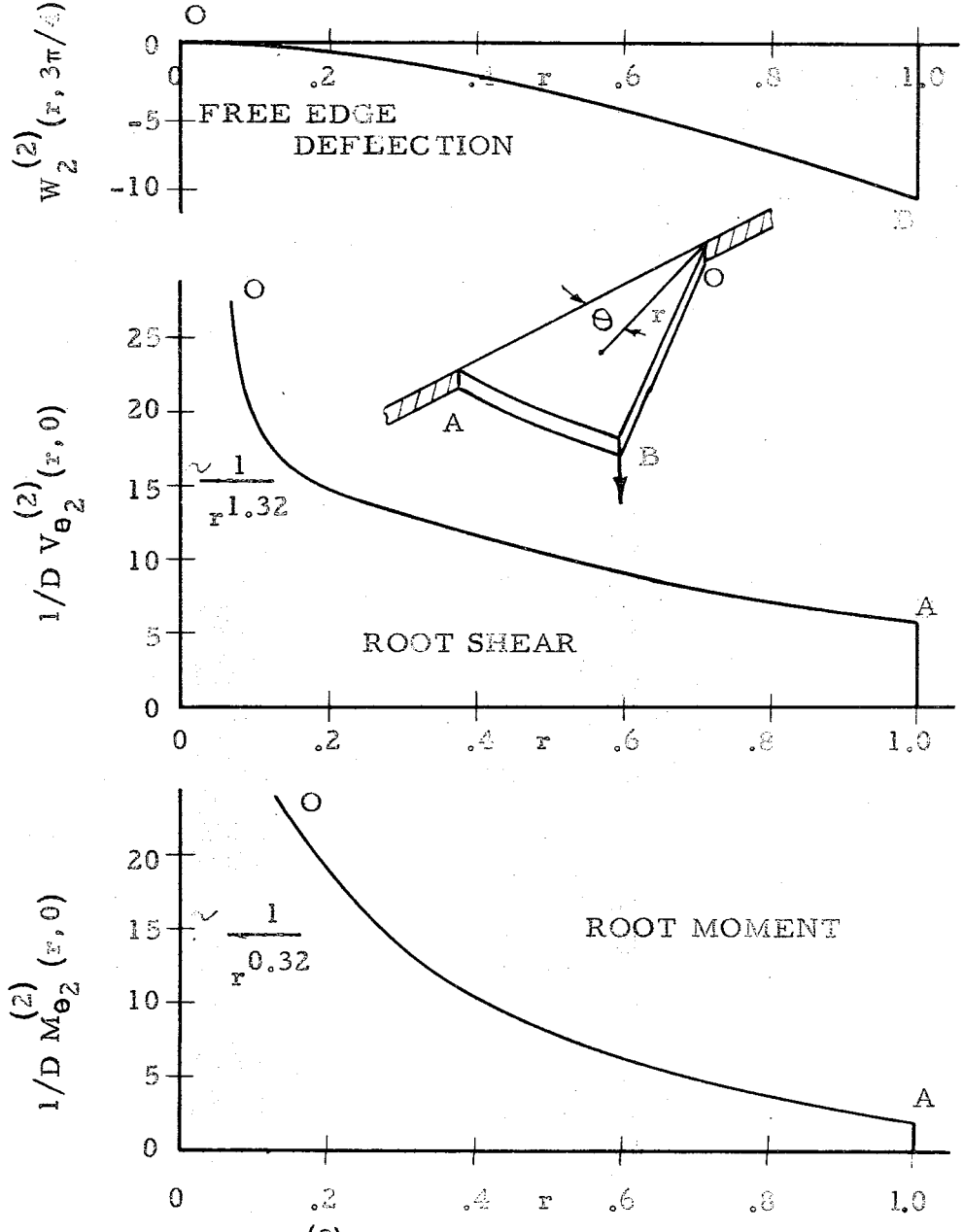

FIGURE 31

LOADING AND DEFLECTION FOR $W_2^{(2)}(r,0)$

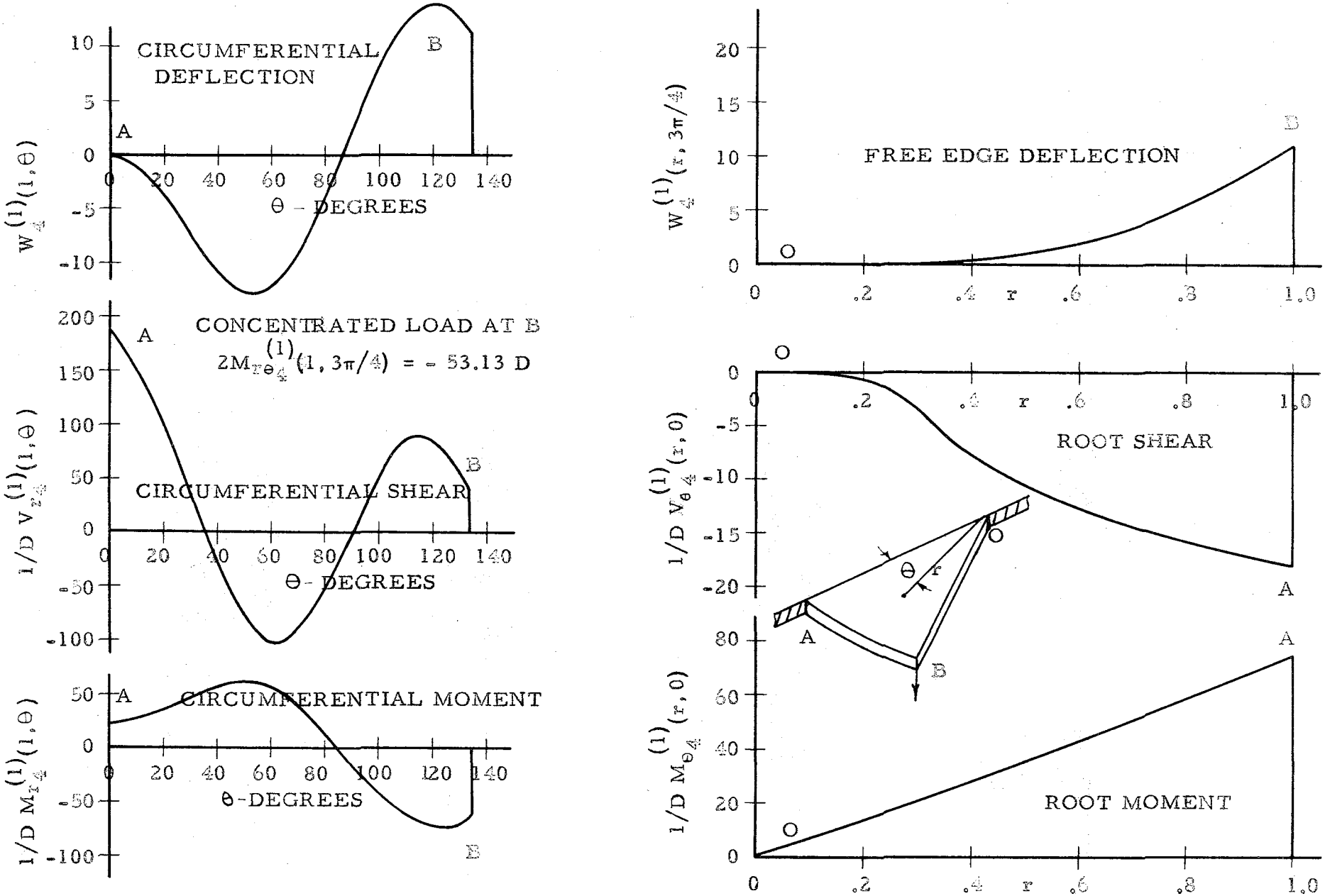

FIGURE 32

LOADING AND DEFLECTION FOR $W_4^{(1)}(r, \theta)$

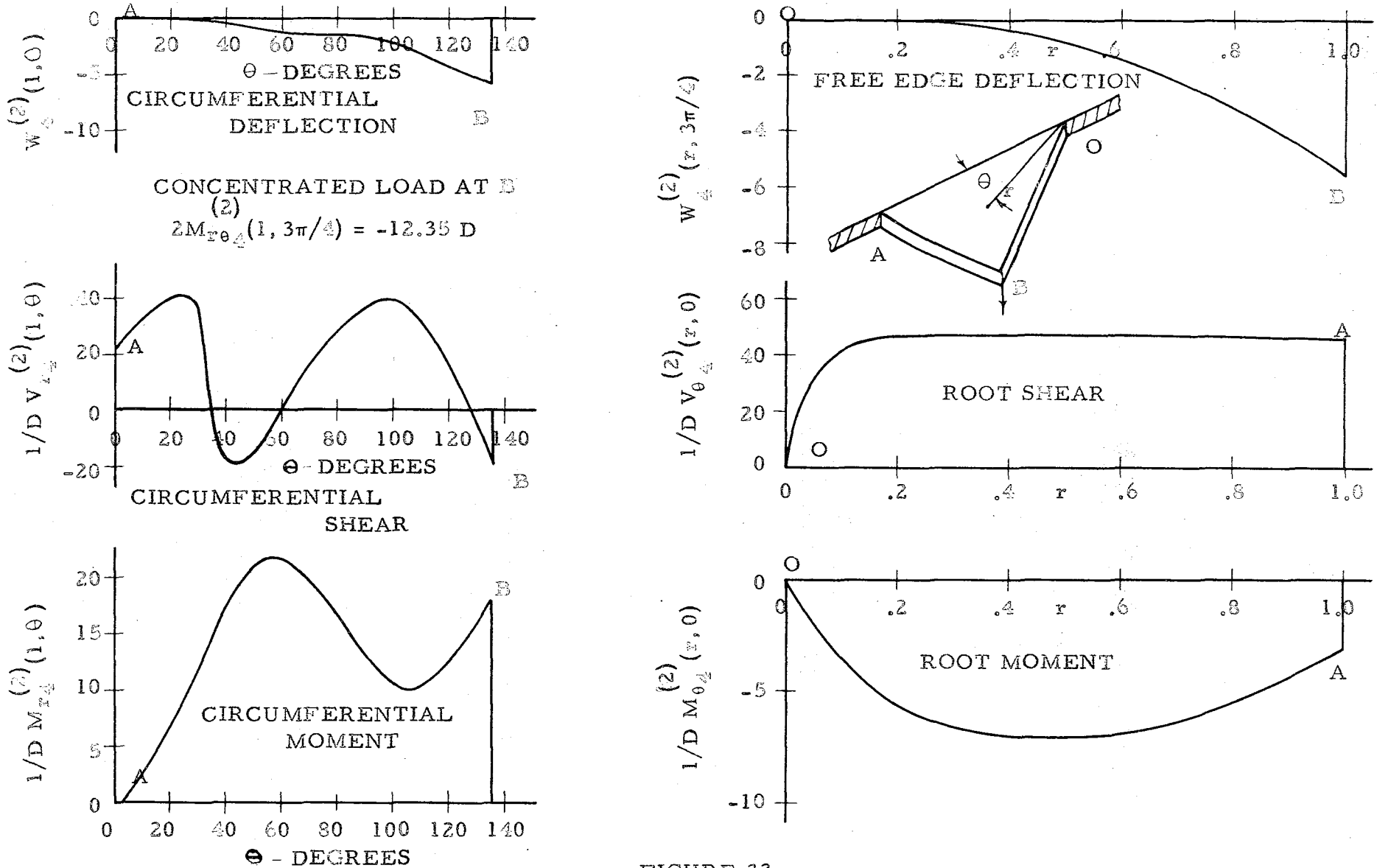

FIGURE 33

LOADING AND DEFLECTION FOR $W^{(2)}_{\pi/4}(r,\theta)$

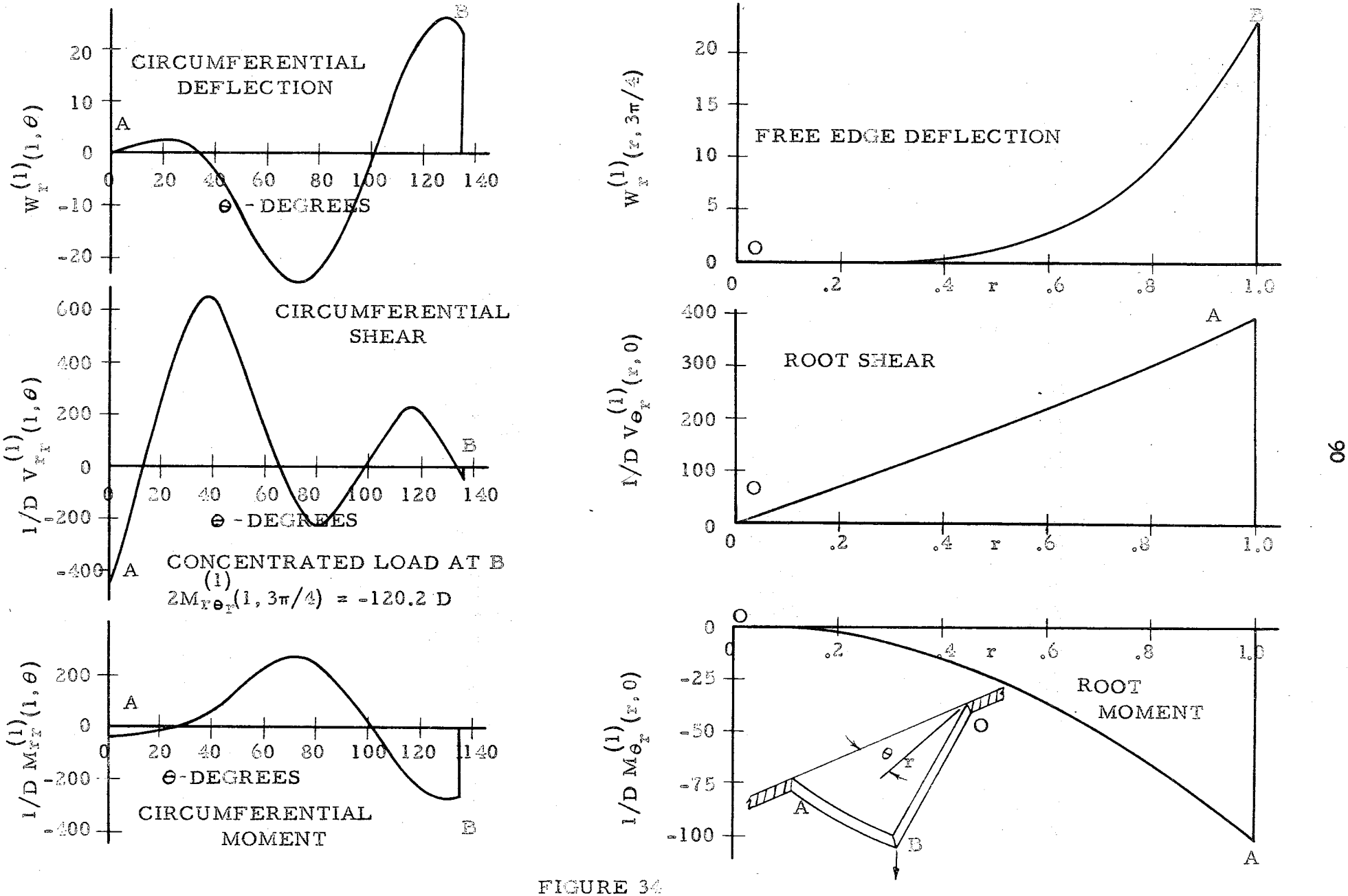

FIGURE 34
LOADING AND DEFLECTION FOR $W_r^{(1)}(r,\theta)$

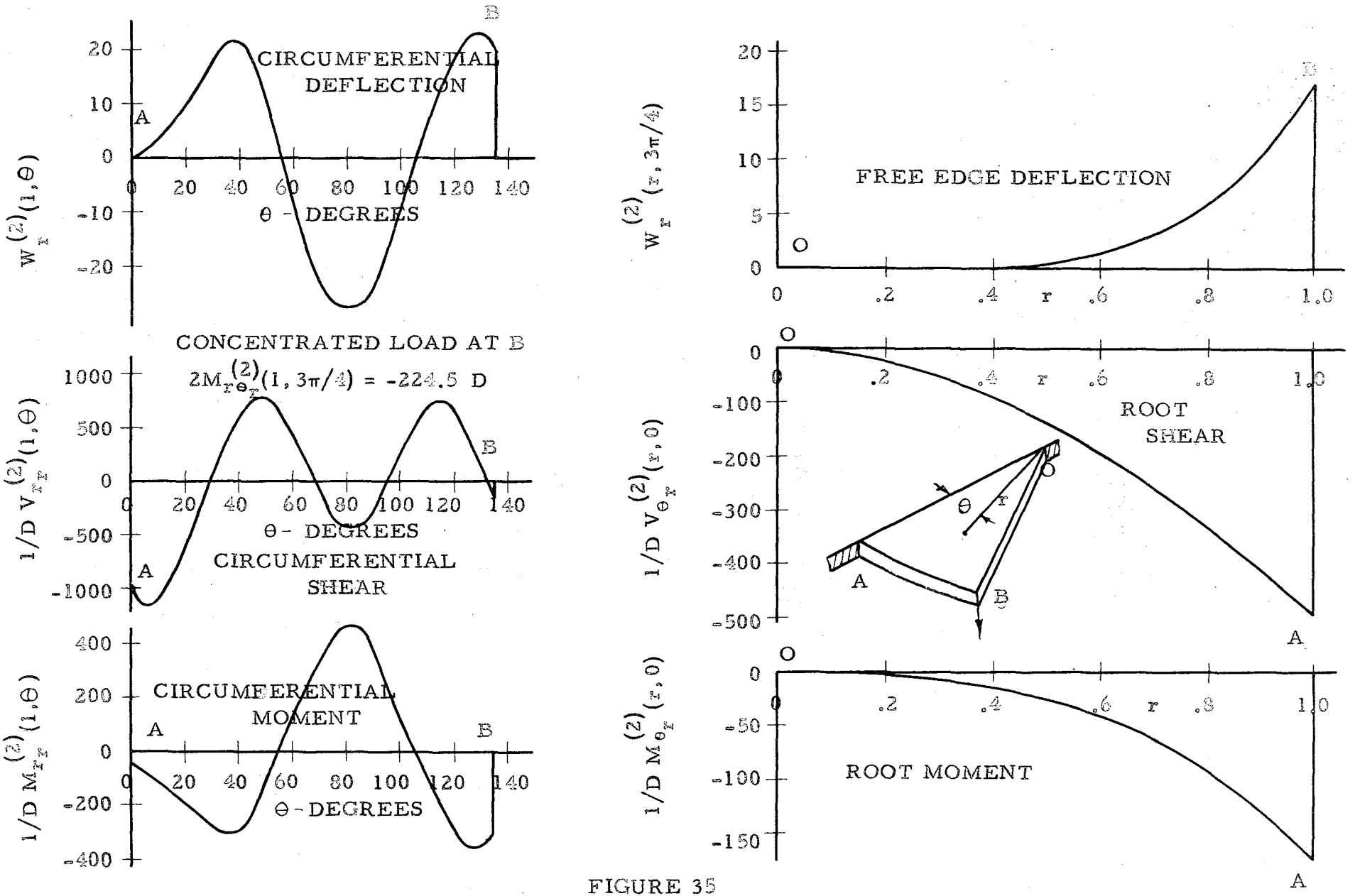

FIGURE 35

LOADING AND DEFLECTION FOR $W_r^{(2)}(r,0)$

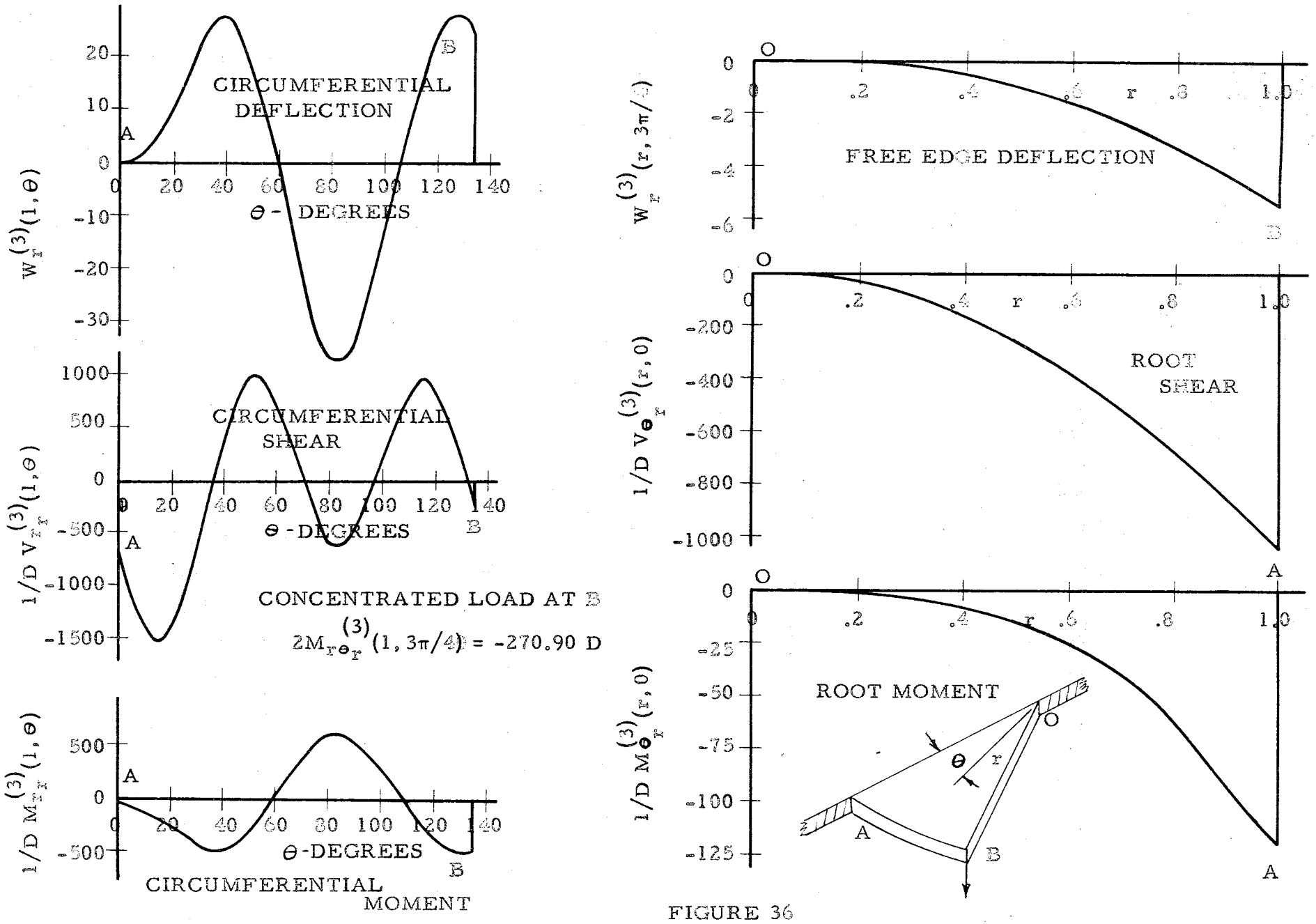

FIGURE 36

LOADING AND DEFLECTION FOR $W_r^{(3)}(r,\theta)$

FIGURES 37-42

DEFLECTIONS AND LOADING CONDITIONS FOR THE EIGEN FUNCTIONS FOR VARIOUS OPENING ANGLES

FOR THE CASE OF $\alpha^{\circ} = \pi$

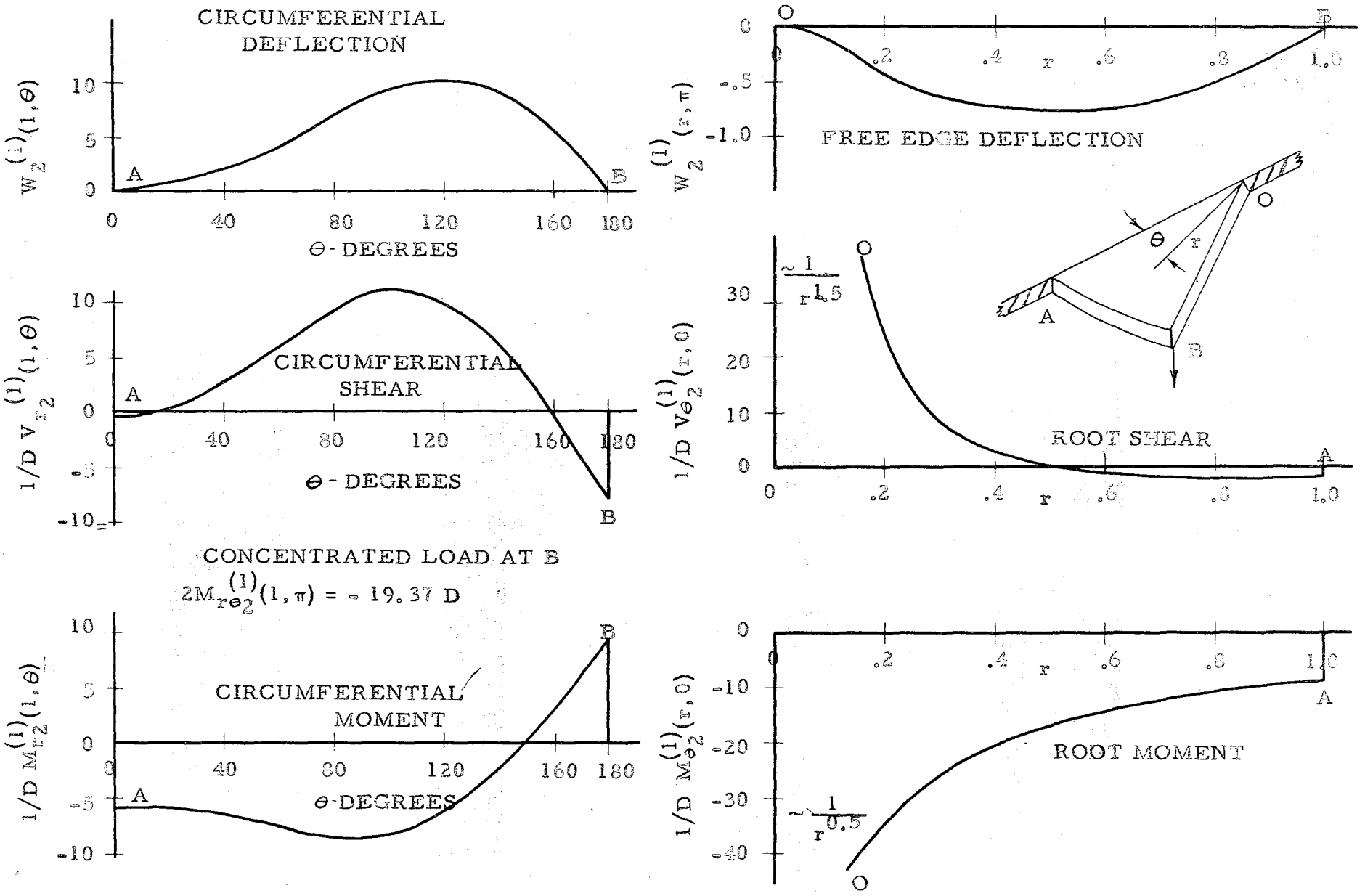

FIGURE 37

LOADING AND DEFLECTION FOR $W_2^{(1)}(r,\theta)$

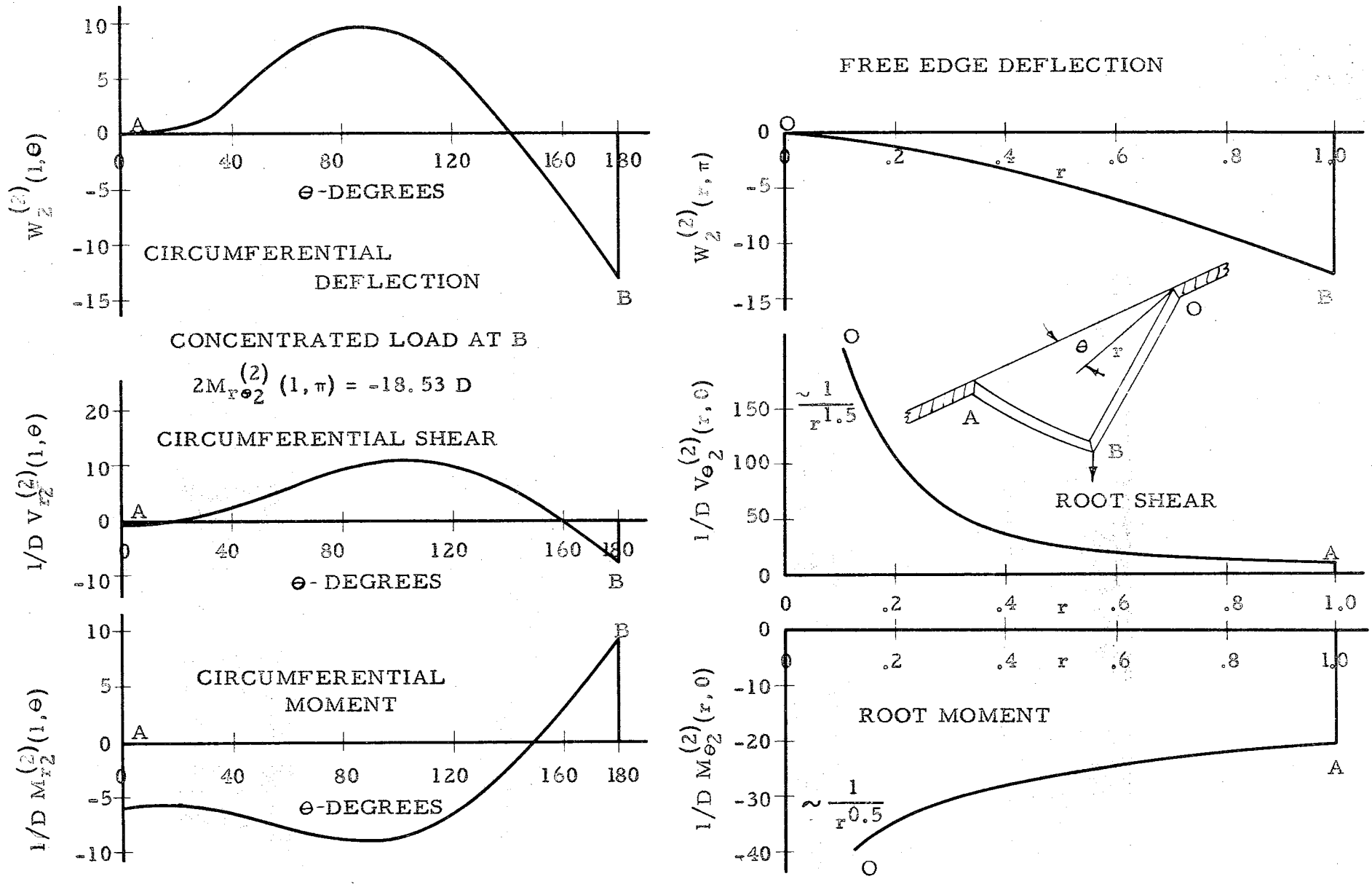

FIGURE 38

LOADING AND DEFLECTION FOR $W_2^{(2)}(r,\theta)$

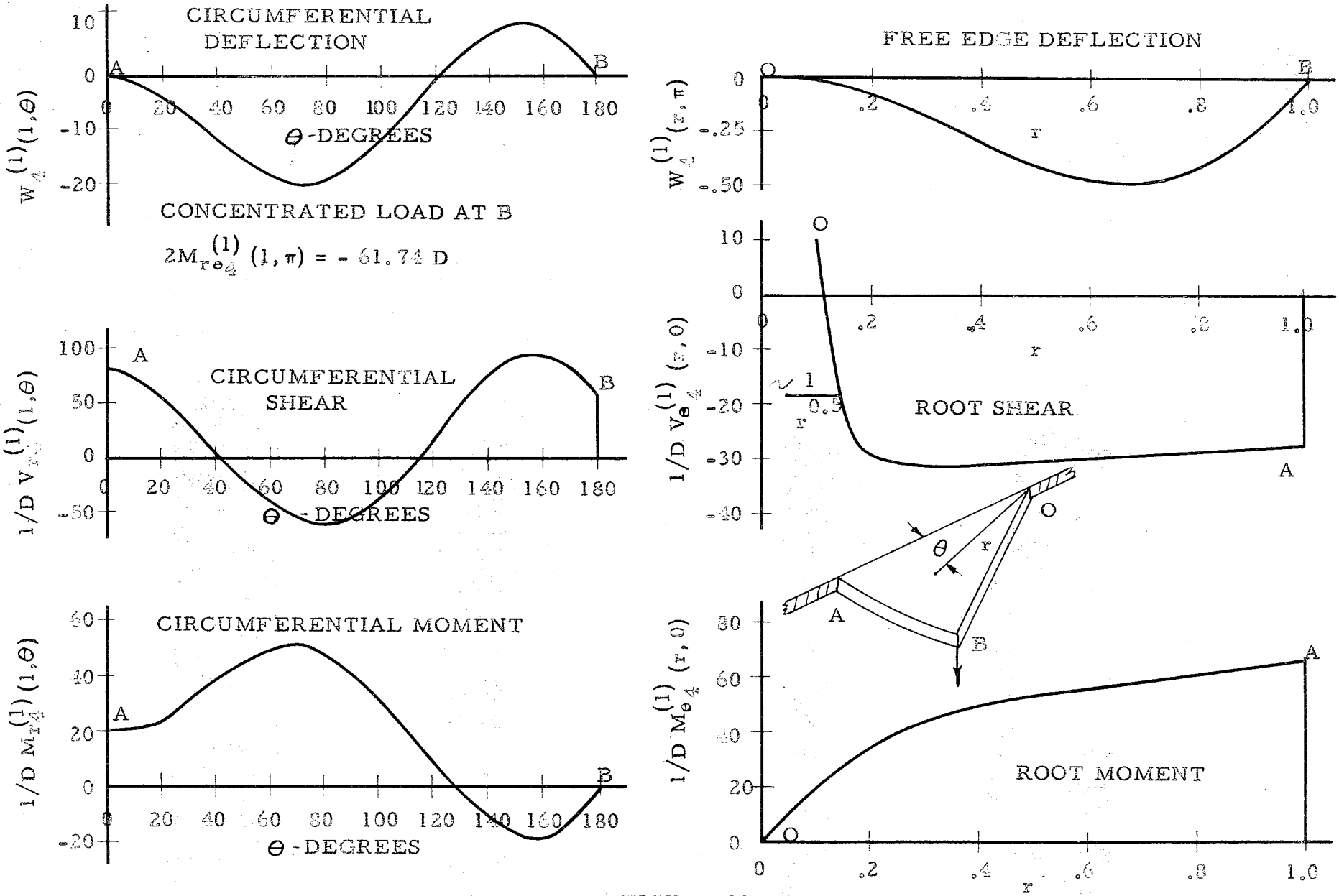

FIGURE 39

LOADING AND DEFLECTION FOR $W_4^{(1)}(r,\theta)$

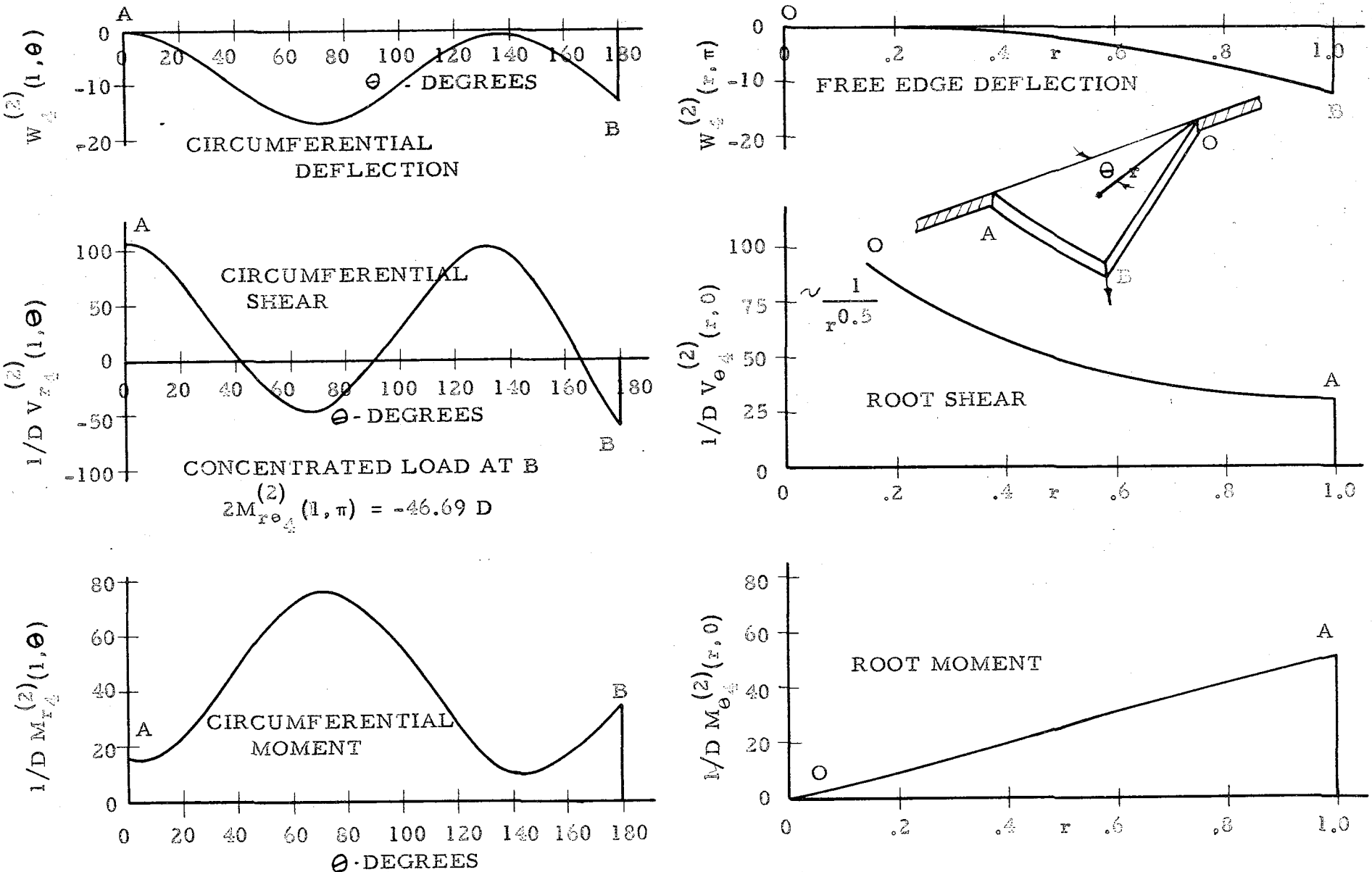

FIGURE 20

LOADING AND DEFLECTION FOR $W_4^{(2)}(r,\theta)$

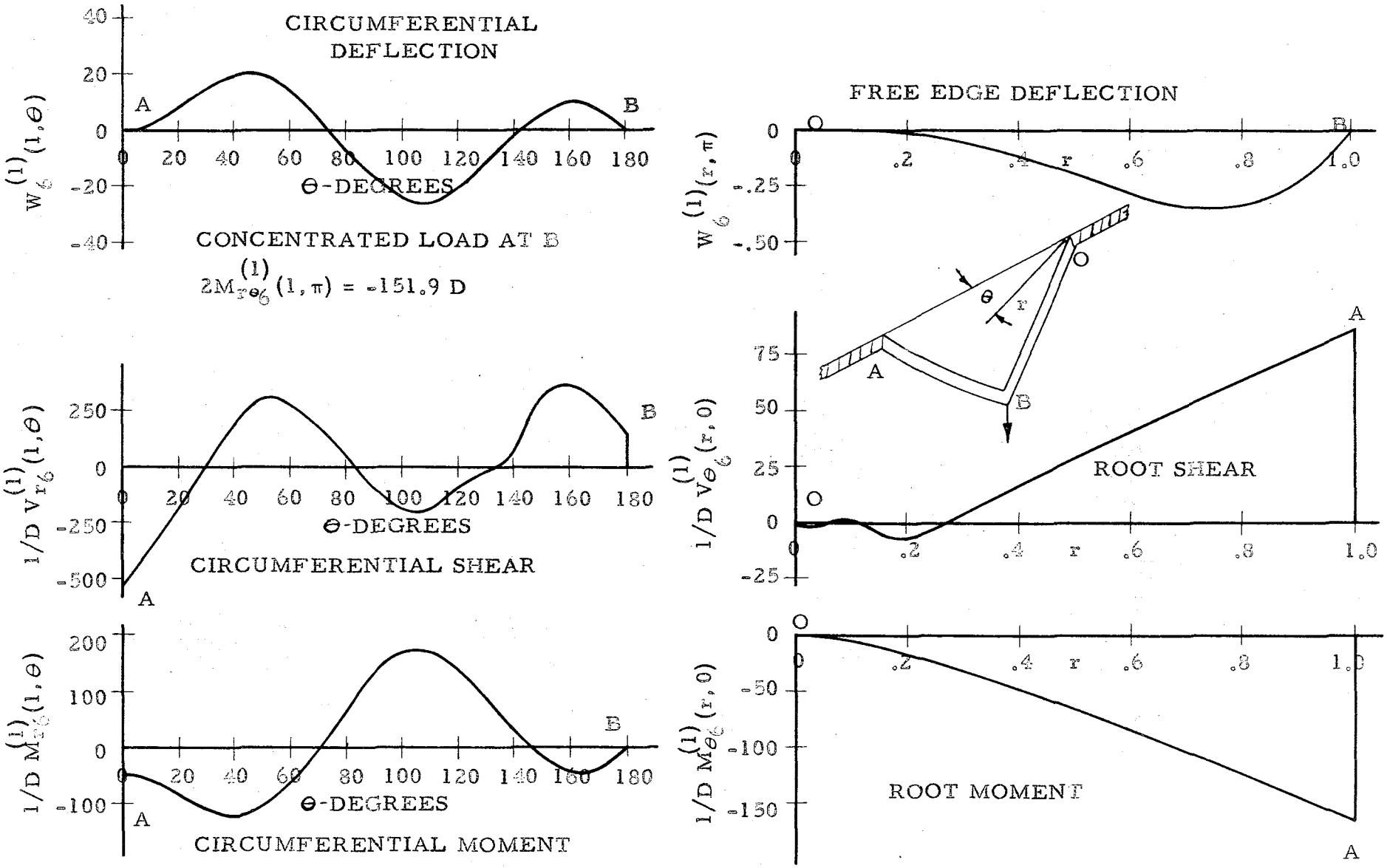

FIGURE 41

LOADING AND DEFLECTION FOR $W_6^{(1)}(r,\theta)$

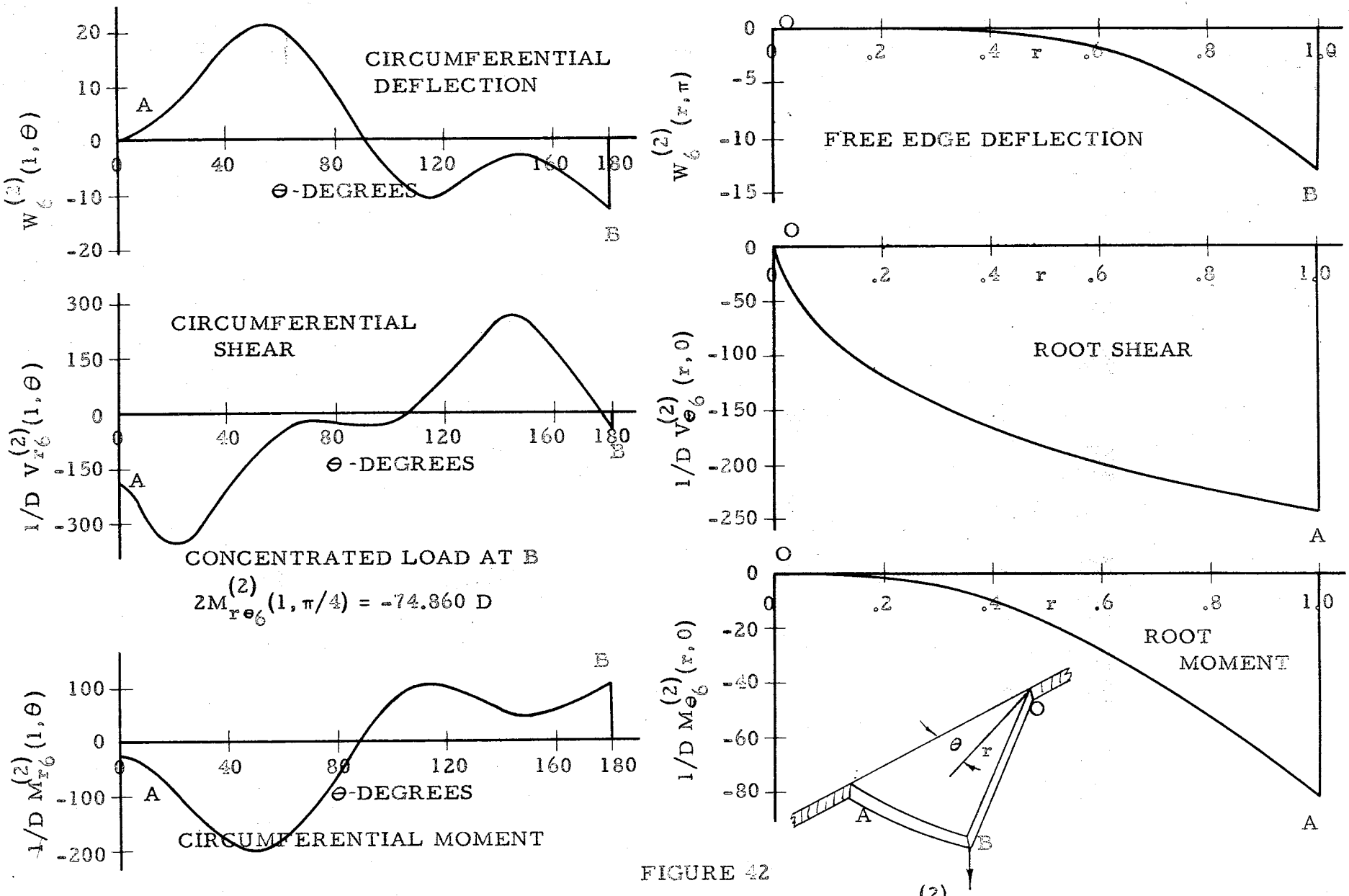

FIGURE 42

LOADING AND DEFLECTION FOR $W_6^{(2)}(r,\theta)$

APPENDIX I

SOLUTION OF THE COMPLEX EIGEN EQUATION

As was indicated in Section III, a detailed description of the method for solving the complex eigen equation

$$1 + \frac{4(1+\nu)}{(1-\nu)^2} + \frac{3+\nu}{1-\nu}\cos 2\lambda\alpha - (1-\cos 2\alpha)\lambda^2 = 0 \qquad (16)$$

is desired. After setting

$$2\lambda\alpha = (\mu + n\pi) + i\omega \qquad ; \; n = 2, 4, 6, \ldots$$

which, as $\lambda = a+ib$ implies that

$$\mu = 2a\alpha - n\pi$$

$$\omega = 2b\alpha$$

The new variables are introduced into (16) and after the real and imaginary parts are separately equated to zero, there result the two simultaneous transcendental equations

$$\sin\mu = -\frac{\left[\frac{2(1-\nu)}{3+\nu}\sin^2\alpha\right]\frac{2(\mu+n\pi)}{(2\alpha)^2}\omega}{\sinh\omega}$$

$$\cosh\omega = \frac{\left[\frac{2(1-\nu)}{3+\nu}\sin^2\alpha\right]\left[\frac{(\mu+n\pi)^2-\omega^2}{(2\alpha)^2}\right] - \frac{5+2\nu+\nu^2}{(3+\nu)(1-\nu)}}{\cos\mu}$$

These equations are most conveniently solved by an iteration procedure, using the following recurrence relation:

$$\sin\mu_{m+1} = -\left\{\left[\frac{2(1-\nu)}{3+\nu}\sin^2\alpha\right]\frac{2(\mu_m+m\pi)}{(2\alpha)^2}\omega_m\right\}\left\{\sinh\omega_m\right\}^{-1}$$

$$\cosh\omega_{m+1} = \left\{\left[\frac{2(1-\nu)}{3+\nu}\sin^2\alpha\right]\frac{(\mu_{m+1}+m\pi)^2-\omega_m^2}{(2\alpha)^2} - \frac{5+2\nu+\nu^2}{(3+\nu)(1-\nu)}\right\}\left\{\cos\mu_{m+1}\right\}^{-1}$$

As an aid to selecting the first trial values, one may consider the asymptotic behavior at large values of n for which it is found that

$$\cos\mu\cosh\omega \sim \left[\frac{2\pi^2(1-\nu)\sin^2\alpha}{(2\alpha)^2(3+\nu)}\right]\left[n^2-\left(\frac{\omega}{\pi}\right)^2\right]$$

$$\sin\mu\sinh\omega \sim -\left[\frac{2\pi^2(1-\nu)\sin^2\alpha}{(2\alpha)^2(3+\nu)}\right]\left[2n\,\frac{\omega}{\pi}\right]$$

Squaring and adding the two, observing that for large values of ω, $\sinh\omega \doteq \cosh\omega$

$$\left[\frac{1}{2}e^{\omega}\right]^2 \sim \left[\frac{2\pi(1-\nu)\sin^2\alpha}{(2\alpha)^2(3+\nu)}\right]^2\left[n^2+\left(\frac{\omega}{\pi}\right)^2\right]^2$$

from which it is found that, asymptotically,

$$\omega \sim \log\left\{2\left[\frac{2\pi^2(1-\nu)\sin^2\alpha}{(2\alpha)^2(3+\nu)}\right]\left[n^2+\left(\frac{\omega}{\pi}\right)^2\right]\right\} \approx \log\left\{2\left[\frac{2\pi^2(1-\nu)\sin^2\alpha}{(2\alpha)^2(3+\nu)}\right]n^2\right\}$$

It also follows that

$$\mu \sim -\tan^{-1}\left[\frac{2n\,\frac{\omega}{\pi}}{n^2-\left(\frac{\omega}{\pi}\right)^2}\right] \approx -\tan^{-1}\left(\frac{2\omega}{n\pi}\right)$$

Using this iterative process, it is found that the convergence

is quite rapid except for the lowest eigenvalues corresponding to $n = 2, 4, 6, \ldots$ which is to be expected. The asymptotic representation is fairly accurate in itself for the larger values of n, say of the order of 20.

For the smaller values of n, λ is very sensitive and it has proved necessary to consider the case more carefully, particularly with respect to obtaining upper and lower bounds on its value.

The iterative forms of the complex eigen equation may be written

$$\frac{\sin\mu}{n\pi+\mu}\cdot\frac{\sinh\omega}{\omega} = -K_1^2 \quad ; \; K_1^2 = \frac{(1-\nu)\sin^2\alpha}{(3+\nu)\alpha^2} \tag{A}$$

$$\cosh\omega = \frac{\frac{1}{2}K_1^2\left[(\mu+n\pi)^2-\omega^2\right]-K_2^2}{\cos\mu} \quad ; \; K_2^2 = \frac{5+2\nu+\nu^2}{(3+\nu)(1-\nu)} \tag{B}$$

Next recall the boundary conditions peculiar to this problem, namely, that the deflection and slope at $r = 0$ be finite. Then as $\lambda = a + ib$ and $w \sim r^{\lambda+1}$, this requires $a \geq 0$ or

$$a = \frac{\mu+n\pi}{2\alpha} \geq 0 \Rightarrow \mu+n\pi \geq 0 \tag{C}$$

(It should be remarked in passing that the negative integers -2, -4, -6, ... , making $n\pi+\mu < 0$ correspond to an outside solution where the aforementioned boundary condition is not imposed.)

In order to restrict the value of μ further, turn to a consideration of (A). As $\frac{\sinh\omega}{\omega}$ is never negative, it must follow that $\frac{\sin\mu}{n\pi+\mu}$ is never positive. But then as a consequence of (C), $\sin\mu \leq 0$. This deduction leads to the conclusion that $-\pi \leq \mu \leq 0$ for $n \geq 2$; and that if $n = 0$, $\frac{\sin\mu}{\mu} \leq 0$, which is of course impossible

unless μ assumes the particular values $\pm\pi$ (which could actually be considered under the $n = \pm 2$ case). Finally, $\sin\mu \neq 0$ for finite ω.

It may therefore be concluded that for these particular boundary conditions the roots in the finite complex plane have been restricted to $n \geq 2$, $-\pi < \mu < 0$.

As an aid to the actual calculation of these lower roots, which are somewhat elusive, several inequalities can be established which are necessary conditions for the existence of roots, or sufficient conditions for non-existence.

First, as $\frac{\omega}{\sinh\omega} \leq 1$, from (A)

$$\sin(-\mu) \leq K_1^2(n\pi + \mu) \tag{D}$$

Second, as $\cosh\omega \geq 1$, it is evident from (B) that

$$\tfrac{1}{2} K_1^2\left[(\mu + n\pi)^2 - \omega^2\right] - K_2^2 > \cos\mu$$

or

$$\left(n + \frac{\mu}{\pi}\right)^2 - \left(\frac{\omega}{\pi}\right)^2 - \frac{2}{\pi^2}\frac{K_2^2}{K_1^2} > \frac{2}{\pi^2 K_1^2}\cos\mu$$

So for $-\frac{\pi}{2} \leq \mu < 0$

$$\left(n + \frac{\mu}{\pi}\right)^2 - \frac{2}{\pi^2 K_1^2}\left|\cos\mu\right| \geq \frac{2}{\pi^2}\frac{K_2^2}{K_1^2} + \left(\frac{\omega}{\pi}\right)^2 \tag{E}$$

and for $-\pi < \mu \leq -\frac{\pi}{2}$

$$\left(n + \frac{\mu}{\pi}\right)^2 + \frac{2}{\pi^2 K_1^2}\left|\cos\mu\right| \leq \frac{2}{\pi^2}\frac{K_2^2}{K_1^2} + \left(\frac{\omega}{\pi}\right)^2 \tag{F}$$

As an example of the use of these equalities, consider the case of $\alpha = 3\pi/4$ for n = 6.

$$\cosh \omega = \frac{0.0943\,(6+\frac{\mu}{\pi})^2 - (\frac{\omega}{\pi})^2 - 2.462}{\cos \mu}$$

$$\sin \mu = -\frac{0.1886(6+\frac{\mu}{\pi})\frac{\omega}{\pi}}{\sinh \omega} \quad ; \quad \omega = 2b\alpha$$

From (A) with $\frac{\omega}{\sinh \omega} \leq 1$

$$\sin(-\mu) \leq \frac{0.1886}{\pi}(6+\frac{\mu}{\pi}) < \frac{6(0.1886)}{\pi} \quad as\ \mu < 0$$

$$\therefore (-\mu) \leq 0.3690$$

which implies

$$-0.1175 < \frac{\mu}{\pi} < 0 \quad ; \quad -1 < \frac{\mu}{\pi} < -0.8825$$

From (E), which is applicable $-0.1175 < \frac{\mu}{\pi} < 0$

$$(6+\frac{\mu}{\pi})^2 - 10.60\,|\cos\mu| \geq 26.10 + (\frac{\omega}{\pi})^2$$

which is impossible for any ω.

Proceeding to (F) which is valid in $-1 < \frac{\mu}{\pi} < -0.8825$, obtain

$$(6+\frac{\mu}{\pi})^2 + 10.60\,|\cos\mu| \leq 26.10 + (\frac{\omega}{\pi})^2$$

which implies that at least $\omega \geq 9.68$, and $\cosh \omega \geq \cosh 9.68$. Now from (B)

$$|\cos \mu| \cdot \cosh (9.68) \leq 2.462 + 0.0943\left(\frac{\omega}{\pi}\right)^2 - .0943\left(6 + \frac{\mu}{\pi}\right)^2$$

$$< 2.462 + 0.943\left(\frac{\omega}{\pi}\right)^2$$

As both sides are monotonic increasing in ω with the left hand side increasing faster, and as the minimum value $|\cos \mu|$ in the interval is 0.9326, it follows that

$$0.9326 \cosh (9.68) \leq 2.462 + 0.0943 (9.5)$$

which is clearly impossible and hence the conclusion is that there are no complex roots for n = 6. (It develops that there is an extra pair of real roots.)

The eigenvalues are then ordered according to their absolute values, including the real roots of (16) in their proper places. This information is summarized in Table I.

APPENDIX II

EXTENSION OF THE EXPERIMENTAL DATA OF REFERENCE 13 TO THE ROOT LINE

Inasmuch as it is physically impossible to place strain gages exactly along the root line while at the same time providing ample support rigidity for the case of a clamped edge, the test data of Reference 13 was taken along a line parallel to the root and 1/10 inch outboard from it. Several strain gages (Baldwin-Southwark, type A-8) were distributed along this line and aligned to measure the strain perpendicular to it.

Had the gages been mounted exactly on the root line, they would have measured, directly, the maximum principal strain because it is perpendicular to the root. In certain cases of swept plates, however, the direction of principal strain changes in the 1/10 inch to the gage line, and it becomes necessary to investigate the amount of error introduced in using the gage line data as root line data.

The location of the root and gage lines for the cases where the aforementioned effect is important is indicated in the following sketch, where the obtuse angled corner is expanded greatly.

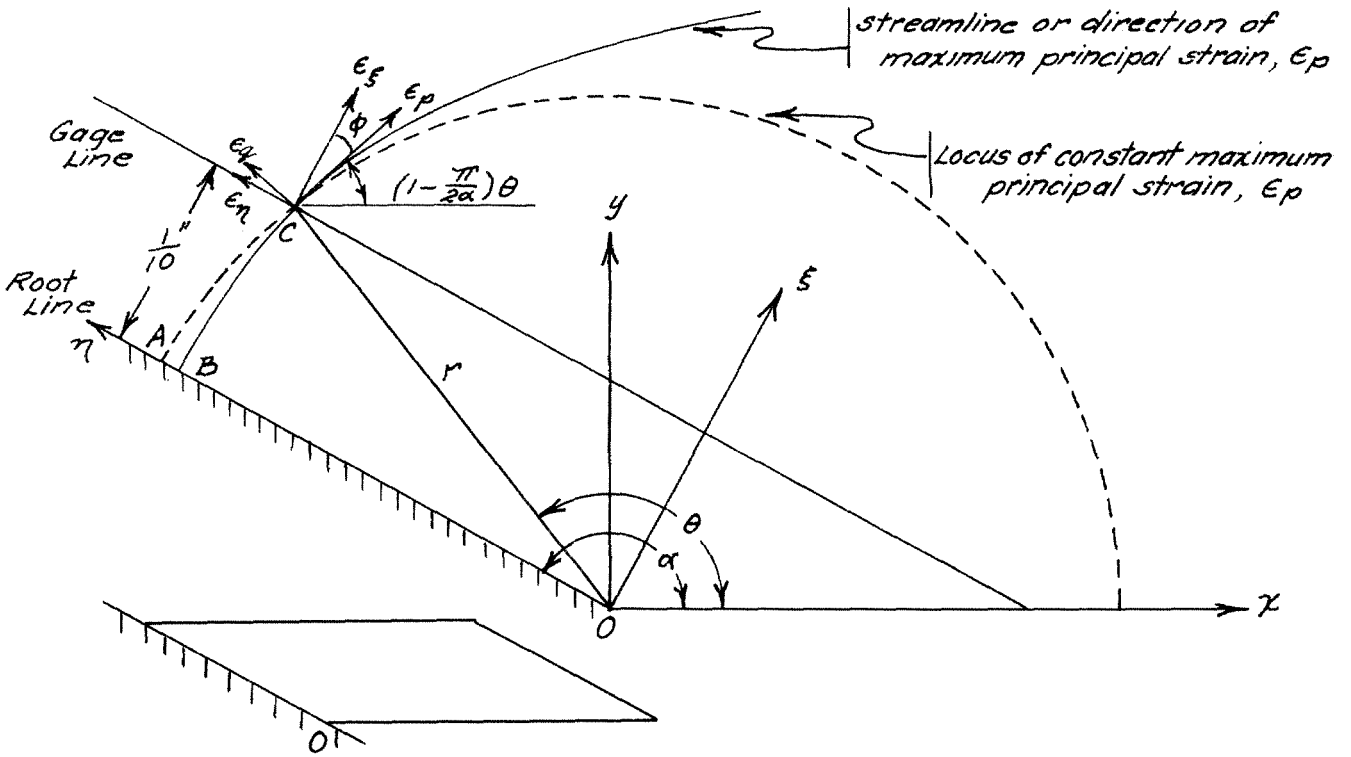

The strain relation at a point is given by

$$\epsilon_\xi = \frac{\epsilon_p + \epsilon_q}{2} + \frac{\epsilon_p - \epsilon_q}{2} \cos 2\phi$$

and thus

$$\epsilon_p = \frac{2\epsilon_\xi}{1+\cos 2\phi}\left[1 - \frac{1-\cos 2\phi}{2}\,\frac{\epsilon_q}{\epsilon_\xi}\right]$$

If, in accordance with the remarks made earlier in this report under the discussion of the hydrodynamic analogy, the direction of maximum principal stress near the corner is given by the streamlines around the corner, the slope of streamlines and hence the direction of the stress may be shown to be

$$\frac{dy}{dx} = \tan\left[\left(1-\frac{\pi}{2\alpha}\right)\theta\right]$$

and hence the inclination of the direction from the horizontal is $(1-\frac{\pi}{2\alpha})\theta$.

It may further be shown that for OA $\geq \frac{1}{4}$ inch, the angle between ϵ_ξ and ϵ_p, ϕ, is of the order of 10 degrees or less and hence may be considered a small angle so that

$$\frac{\epsilon_p}{\epsilon_\xi} = (1+\phi^2)(1-\phi^2\frac{\epsilon_q}{\epsilon_\xi})$$

Then as $\epsilon_\xi + \epsilon_\eta = \epsilon_p + \epsilon_q$, it may be shown that to the same order in ϕ

$$\frac{\epsilon_p}{\epsilon_\xi} = (1+\phi^2)(1-\phi^2\frac{\epsilon_\eta}{\epsilon_\xi})$$

where

$$\phi = (1-\frac{\pi}{2\alpha})(\alpha-\theta)$$

It is now assumed that the loci of maximum principal stress or strain lines are circles about point O. It might be remarked that this assumption is supported by test data from Reference 15 and the solution for stress presented in this report. Also it may be noted that deviations from a circle are not too important in any event because of the small distances of the gage from the root, to which the data is to be extrapolated.

Finally, the ratio $\frac{\epsilon_\eta}{\epsilon_\xi} \geq 0$ with the equality holding only along the root line, hence

$$\frac{\epsilon_p}{\epsilon_\xi} \leq (1+\phi^2)$$

and if the principal strain ϵ_p is the same at A

$$\epsilon_p \doteq \epsilon_{\xi_o} \leq (1+\phi^2)\epsilon_\xi$$

and hence the root stress, σ_{ξ_o}

$$\sigma_{\xi_o} \leq \frac{E\epsilon_\xi}{1-\nu^2}\left[1+\left(1-\frac{\pi}{2\alpha}\right)^2(\alpha-\theta)^2\right]$$

In the case of a trailing edge swept 60 degrees for example, the principal strain at the root and $\frac{1}{4}$ inch from the origin may be of the order of 3 per cent more than the strain measured at the gage line, with the percentage decreasing as the distance from the origin is increased.

For most purposes, this deviation may be neglected and the gage line strain may be considered the actual root line strain.